TO MY SON

DESIGN, CONSTRUCTION AND TESTING OF A MODEL BLOWER TYPE WIND TUNNEL

A MASTER'S THESIS

in

Mechanical Engineering
University of Gaziantep

By
Fatma USKANER
September 1991

Approval of the Graduate School of Natural and Applied Sciences

Prof. Dr. Mazhar Unsal
Director

I certify that I have read this thesis and that in my opinion it is fully adequate, in scope and quality, as a thesis for the degree of Master of Science in Mechanical Engineering Department.

Assoc. Prof. Dr. Sedat Bayseç
Chairman of the Department

I certify that I have read this thesis and that in my opinion it is fully adequate, in scope and quality, as a thesis for the degree of Master of Science in Mechanical Engineering Department.

Prof. Dr. Ömer T. Göksel
Major Supervisor

Examining Commitee in Charge

Prof. Dr. Mazhar Unsal .....

Prof. Dr. Ömer T. Göksel .....

Assoc. Prof. Dr. Sedat Bayseç .....

Prof. Dr. Mazhar Unsal
Commitee Chairman

ABSTRACT

DESIGN, CONSTRUCTION AND TESTING OF A MODEL BLOWER TYPE WIND TUNNEL

USKANER, Fatma.
M.S. in M.E.
Supervisor: Prof. Dr. Ömer T. GÖKSEL
September 1991, 165 pages.

In the work presented in this thesis, a prototype blower wind tunnel and 1/7 model of it were designed by developing a similarity analysis for the similar tunnels. The model tunnel was constructed and instrumented. The flow quality in the test section and in other tunnel components were investigated. Additionally, the test results of the model tunnel were compared with the theoretical results.

Key words: Prototype, Model, Similitude, Blower Wind Tunnel, Wind Tunnel Design.

Scientific Code: 625.04.03

ÖZET

UFLEMELİ TİP BİR RÜZGAR TÜNELİ MODELİNİN TASARIMI, İMALATI VE DENENMESİ

USKANER, Fatma
Yüksek Lisans Tezi,Mak. Müh. Bl.
Tez Yöneticisi: Prof. Dr. Ömer T. GÖKSEL
Eylül 1991, 165 sayfa

Bu tezde sunulan çalışmada, bir prototip üflemeli rüzgar tüneli ve onun 1/7 oranında küçültülmüş modeli, benzer tüneller için bir benzerlik analizi geliştirilerek tasarlandı. Model tünel imal edildi ve deneyler için gerekli teçhizatı ile donatıldı. Deney bölgesindeki ve diger tünel bölgelerindeki akımın davranışı araştırıldı. Ilave olarak, model tünelin deney sonuçları, teorik tasarımıyla karşılaştırıldı.

Anahtar kelimeler: Prototip, Model, Benzerlik, Üflemeli rüzgar tüneli, Rüzgar Tüneli tasarımı

BİLİM DALI SAYISAL KODU: 625.04.03

ACKNOWLEDGEMENTS

I am very grateful to Prof. Dr. Ömer T. Göksel for the supervision of this thesis, his continuous suggestions, guidance and encouragements.

I wish to thank to my husband, Mr. Uskaner for his valuable supports and helps. My very special thanks are due to my parents for their moral supports and continuous helps.

I thank to Mr. Bircan Yılmaz, Mr. Durmuş Büyüktuncel and to Mr. Murat Gültekin for their incredible assistance during the preperation of the thesis.

I thank to Mr. Yaşar Akşit and Mr. Mehmet Abuş Aksoy for their continuous helps during the laboratory work of this study.

I thank to the stuff of Metal and Wood workshops for their helps in the construction of the tunnel.

I wish to acknowledge the support received from the Research Fund of the University of Gaziantep.

CONTENTS

LIST OF TABLES

LIST OF FIGURES

NOMENCLATURE

A Crossection of tunnel components, m^2

AR Area ratio of diffuser

AS Aspect ratio of the contraction crossection

a Height of crossection, m

b Width of crossection, m

C System resistance coefficient

Cp Pressure coefficient

CR Contraction ratio

D Hydraulic diameter of tunnel crossection, m

d Diameter, mm

E Euler number

f Friction factor

f_n Fineness ratio

g Gravitational acceleration, m/s^2

H Head, m

K Hydraulic loss coefficient

k Roughness height, mm

L Length, m

l_y, l_z Developed contour lengths of contraction, mm

l Mesh length, mm

M Dimensionless spanwise coordinate of tunnel crossection

N Dimensionless pitchwise coordinate of tunnel crossection, fan speed, RPM

N_h Honeycomb cell number

n Number of screen in diffuser

P Pressure, Pa

Q Volume flowrate, m^3/s

q_o Dynamic head, m

Re Reynolds number based on hydraulic diameter

S Micrometer distance, mm

t Thickness, mm

V Mean velocity, m/s

U Local velocity, m/s

u Velocity in the boundary layer, m/s

u' Mean velocity fluctuation

Δu Variation of velocity at tunnel crossection

W Fan power, W

w Complex conjugate velocity; u-iv

x, y, z Cartesian coordinates

α Yaw angle

Υ Corner fillet divergence angle

β Open area ratio of screen

ζ Open area ratio of honeycomb

θ Boundary layer momentum thickness

2θ Included angle of diffuser

ρ Density

μ Dynamic viscosity

ν Kinematic viscosity

ε Relative roughness

η Fan efficiency

λ Power factor

Δ Difference

Ψ Pressure coefficient, stream function

ϕ Flow coefficient, velocity potential

δ Boundary layer thickness

δ^* Boundary layer displacement thickness

δ_f Diameter coefficient

σ Specific speed

Subscripts

c Settling chamber

d Diffuser

ds Diffuser screen

f Fan, friction

h Honeycomb

l Lenght, local

m Model

max Maximum

n Nacelle

p Prototype

Re Reynolds number

s Screen

T Total

o Test section

v Straightener vane

Superscripts

' Model

* Boundary layer displacement thicness

CHAPTER 1

INTRODUCTION

Despite the recent developments in theoretical and computational fluid dynamics, many problems in this field have been investigated experimentally. The aim of this study is to design a prototype blower wind tunnel and to design, construct and test the model of this prototype tunnel.

In chapter 2, a survey of available literature on the wind tunnels and its components are presented. Required dimensionless parameters and similarity analysis for the design of prototype and model tunnels are given in chapter 3.

In chapter 4, the specifications of the prototype tunnel and the factors effecting the design of the tunnels are presented. Aerodynamic design of the prototype and model tunnels are accomplished. Additionally, the similarity analysis which was developed in chapter 3 are applied to the designed tunnels.

In chapter 5, the construction of the model tunnel is described and the traversing mechanisms which were constructed are presented.

The calibration of the model tunnel is given in chapter 6. The flow quality of the tunnel components were investigated and the test results of the model tunnel were compared with the theoretical results.The test results are discussed and conclusions drawn from the test results are also given in this chapter.

The conclusions that are reached from this study with recommendations for future work are presented in chapter 7.

CHAPTER 2

LITERATURE SURVEY

2.1 INTRODUCTION

For many fluid dynamic problems, a wind tunnel is an essential tool for verification of the results of the theoretical studies and determination of the aerodynamic forces on a model. Although a great number of low speed wind tunnels were constructed in the last decade and some design rules were evolved from the experimental results with the aid of theoretical considerations, there is little knowledge about the similitude of a wind tunnel model with the prototype.

The available literature about the design of a low-speed wind tunnel and its components were surveyed giving emphasis on the effect of the tunnel components on the flow parameters in the test section such as turbulence level, flow nonuniformity, shear stress variation in the boundary layer and unsteadiness. These are presented in this chapter as a basis for the design of the model and the prototype of a blower type open-circuit wind tunnel.

2.2 GENERAL TYPES OF LOW-SPEED WIND TUNNELS

In the existing literature, low-speed wind tunnels are generally placed in two main categories

1- Open-circuit wind tunnels which may be suction type or blower type.

2- Closed-circuit type tunnels with an open test section or a closed test section.

Most high performance wind tunnels were designed as closed circuit type to ensure a controlled return flow and low power factor.

However, open-circuit tunnels are advantageous due to their low constructional cost and space requirement. It is also possible to obtain high flow quality in the test section of open-circuit tunnels.

The room at which the open circuit tunnel is placed acts as the return circuit for the air discharged from the tunnel. Open-circuit tunnels can be driven by a fan which is placed to the upstream or downstream side of the test section and are called blower type or suction type of wind tunnel respectivelly. An example for suction and blower type wind tunnels are shown in figure 2.1.

A blower tunnel consists of the following parts:

1- Test section
2- Contraction
3- Settling chamber
4- Screens and honeycomb
5- Wide angle diffuser
6- Fan section with driving unit and straightener.

The older blower wind tunnels were employed in 1899, by H. Maxim and Col. Renard and in 1909-10 by M. Rateau according to reference [1]. In this type of tunnel the entire structure operates as a retarder of the airflow delivered by the fan. Therefore, it was accepted inefficient and expensive as compared with the suction tunnel for a long time. After the need of strong wind energy to test some models such as transportation vehicles, buildings, propellers, ducts which creates highly disturbed flow behind them, the blower tunnels were prefered rather than the suction type tunnels.

In a low-speed wind tunnel, the predominant forces effecting the flow are inertial, viscous and pressure forces. The influence of the compressive forces are negligible which means that there is no compressibility effect on the flow. Therefore, the aerodynamic design procedure based on the predominant factors which are yielded from the above forces determines the contraction ratio, discharge capacity, pressure losses and power requirement of the fan to obtain the desired

flow in the test section.

2.3 WIND TUNNEL DESIGN

The know how deduced from the previous theoretical and experimental studies about the wind tunnels and experimentation techniques used on wind tunnels were firstly collected by Pankhurst and Holder [2] in 1952. They gave an approximate approach for the calculation of hydraulic losses throughout the tunnel to determine the geometry and required power for the tunnel.

In 1966, Pope and Harper [3] published a new book on the low-speed wind tunnel design and testing. They followed a similar approach as reference [2] to calculate the hydraulic losses throughout the tunnel. In addition to this, they proposed a fan-straightener system design and also they estimated the hydraulic losses in the exit diffuser and in the contraction section of the tunnel in a different manner from that of reference [2].

In 1966, Gorlin and Slezinger [4] published another book on the wind tunnels and their instrumentation. In the relevant chapters of this book, a design procedure for a wind tunnel was suggested more systematically than references [2] and [3]. The suction type tunnel which was build at the Gaziantep University, Fluid Mechanics Laboratory in 1982 [5] was mainly designed according to the design procedure of reference [4]. The performance of this wind tunnel is satisfactory with very uniform and steady test section flow and with a turbulence level around 0.2 % at maximum tunnel speed. Reference[4] gives a general design procedure for all low-speed wind tunnels, however there is no guidance for the design of wide angle diffuser which is a part of the blower tunnel.

In 1977, Mehta [6] suggested a design procedure for wide angle diffuser using collected data for wide angle diffusers with satisfactory efficiencies. In addition to this he proposed a general design procedure for blower wind tunnels.

After reference [6], in 1979, Mehta published a new paper with his supervisor Bradshaw [7] in the same subject as a guide for wind tunnel designers.

In all of the references covered up to this point the methods for determining the power requirement of a wind tunnel are the same. However, many empirical relations were suggested for the design of the tunnel elements. Besides references [8] and [9], there appears to be no significant information in the available literature on the design of a prototype wind tunnel and its model.

In 1979, Greenway and Wood [8] published about a 4m x 2m suction tunnel of Oxford University that was built for the purpose of conducting experiments on industrial aerodynamics. They mentioned that a model of this tunnel was constructed at a scale of 1/13.6. This model scale was choosen in order to use an existing contraction model. Then, the flow quality in the twin diffusers and in the test section were tested.

In 1981, a 0.186 scale model of a pressurized cryogenic wind tunnel with a 2.5 m square test section [9] was designed and constructed to simulate the aerodynamic behaviour of the components of the prototype and to estimate the power requirements of the prototype. Although the model was not geometrically similar to the prototype , it was predicted that if the hydraulic losses along the tunnel components of the prototype were equated to the hydraulic losses of the model components, the Euler number similarity criteria could be achieved.

2.4 DESIGN OF THE TUNNEL COMPONENTS

A survey of available literature about the design of the tunnel components are given below:

2.4.1 Test Section

The crossection size, shape and length of the test section depends on the test requirements. For a general purpose wind tunnel,

references [6] and [7] suggested a rectangular geometry for the crossection of the test section. It was proposed that the width to height ratio of the test section should approximately be $\sqrt{2}/1$. Reference [3] stated this ratio might be about 10/7. According to reference [4] this might be between 0.6-1.7 depending on the models which would have been tested. It is seen that all of the aforementioned width to heigth ratios are in agreement with each other.

To compansate the blockage effect resulted from the boundary layer in the test section, reference [2] suggested that the crossectional area of the test section should be gradually increased according to the calculated boundary layer displacement in the test section. On the other hand in references [3] and [4], approximate range of divergence angles of the test section walls were given according to the test section Reynolds number based on test section length, Re_l.

$0.1° - 0.25°$ for $Re_l = 10^7 - 10^8$

$0.25° - 0.5°$ for $Re_l = 10^5 - 10^6$

2.4.2 Contraction

Many analytical and numerical solutions of the contraction shape have been proposed for both axisymetric and two dimensional contractions.

The solutions for the axisymetric contractions are based on a series solution of either Laplace equation for the velocity potential or Stokes- Beltrami equation for the stream function using a given velocity distribution along the centerline.

In 1946, Thwaites [10] solved the Laplace equation with variable-separable solution for the potential function. For axisymetric potential flow he assumed the ends of the contraction to be equipotential planes. In 1980, Tulapurkara [11] worked on Thwaites' method, and extended his solution for N terms of the series.

Tulapurkara tried the theoretically determined contours experimentally. He concluded that there was a well agreement between the experimental velocity distribution and the analytical solution when first 10 terms of the series was used.

In 1962, Cohen [12] developed a design method which was basically similar to Tsien's [13] approach. It was based on a radial expansion from an adapted centerline velocity distribution, of a series solution of the Beltrami differential equation written in terms of Stokes stream function. After Cohen, some designers solved the Stokes-Beltrami equation for different centerline velocity distributions [14], [15] and axisymetric solution was satisfactorily modified for the test section having square crossection geometry.

In 1974, Chemielewski [16] solved the Strokes-Beltrami equation numerically using the finite difference method with the assumption of an acceleration function at the centerline.

In 1979, Mikhail [17] worked on the solution of the same equation by the method of lines, utilizing the coordinate transformation such that the calculation domain is rectangular with fixed boundaries.

In 1975, Morel [18] came up with a practical solution to the axisymetric wind tunnel contraction design. He formed the design charts where the maximum value of the wall pressure coefficient, Cp_i, at inlet to the contraction and the maximum value of the wall pressure coefficient, Cp_e, at exit to the contraction were related to one parameter family of wall shapes formed of two smoothly joined cubical equations. Cp_i is used to avoid the danger of seperation which caused by the adverse pressure gradient at inlet Cp_e is related with the exit velocity nonuniformity.

In 1986, Batill and Hoffman [19] presented mentioned design charts with the same parameters as in reference [18] for contractions having square and rectangular crossectional geometries. In 1988, Tulapurkara [20] investigated the Morel's contraction design method experimentally and he showed that the method satisfied the design requirements.

There were no seperation at inlet and exit of the contraction and thin boundary layer thickness at the exit of the contraction.

Another approximation method for the contraction design is the electrical analogy which was described by Alston in 1968 [21]. The conduction between the electrodes in an electrolytic tank was used as an analogy to find the potential field distribution. The tank was used for plotting the equipotential lines and from these the velocities at any point could be determined. A similar method was applied by Gibson in 1959 [22] to test a model of a wide angle diffuser which was designed for 4'x 2' blower tunnel of Liverpool University. He found a satisfactory solution with an insignificant error.

The two dimensional contractions are usually designed by using conformal transformation technique. A path is choosen in the hodograph plane describing the velocity along the wall of the contraction. The corresponding wall shape to the velocity distribution is then obtained by transformation into the physical plane. Libby and Reiss [23], in 1951 proposed this method for two dimensional contraction design. In 1982, Yegen [24] and in 1984, Albayrak [5] used this method to design the contraction section of the wind tunnels which they designed.

There is no wholly satisfactory method for theoretical contraction designs. Most of the methods are only mathematical tools to be used for anlysis of the flow. The application of them to an existing contraction require the existence of criteria assumed in the particular contraction design method.

2.4.3 Screens

There is no wholly satisfactory method for the determination of pressure drop coefficient, K_s, for wind tunnel screens. In 1939 Collar [25] and in 1953 Weighardt [26] suggested the relationships for K_s in terms of screen Reynolds number, Re_s, and screen open area ratio, β:

$$K_s = 0.9\,\frac{1-\beta}{\beta^2} \qquad \text{for } Re_s > 600 \tag{2.1}$$

$$K_s = 6.5\,\left(\frac{1-\beta}{\beta^2}\right)\,(Re_s)^{-1/3} \qquad \text{for } Re_s < 600 \tag{2.2}$$

where

$$Re_s = \frac{V_c d_s}{\beta\,\nu}$$

V_c, d_s and ν are the free stream velocity, screen wire diameter and the kinematic viscosity of the fluid respectivelly.

In references [2], [6], [7] and [27] the above expressions were recommended for evaluating the value of K_s. Reference [4] proposed a different approach to determine the pressure drop coefficient of the screen, but the result is in agreement with the approach used by Collar and Weighardt.

For steady non-uniform flow Collar [25], in 1939 analysed and confirmed with experiments that the flow non-uniformity was removed by a screen with an amount of,

$$\frac{\Delta u_2}{\Delta u_1} = \frac{2 - K_s}{2 + K_s} \tag{2.3}$$

where Δu_1 and Δu_2 were the mean velocity variation before and after the screen respectivelly.

In 1950, Schubauer et al [28] conducted a series of experiments on the reduction of level of turbulence created by screens. They compared the test results with the suggested approaches by Prandtl, Collar, Dryden and Schubauer, Taylor and Batchelor mentioned in the same reference. They found that reduction of the turbulence intensity was in agreement with Dryden and Schubauer theory which was expressed as,

$$\frac{u_2'}{u_1'} = \frac{1}{\sqrt{1+K_s}} \tag{2.4}$$

where subscripts 1 and 2 refer to the streamwise component of the fluctuating velocity just before and after the screen respectively.

Many research workers observed a spanwise variation of boundary layer thickness and surface shear stress in the test sections of wind tunnels fitted with screens. In 1960, Morgan found that the flow behind a uniform screen was unstable with both spatial and temporal velocity variation. In 1965, Bradshaw [27] suggested that the spanwise variations of boundary layer thickness and surface shear stress in the test section were caused by screens having improper open area ratios. According to Bradshaw's test results, screens with open area ratio less than 0.57 produce instabilities in the flow resulting from the random coalition of the jets forming the the longitutional vortices which are very effective at producing spanwise variation of boundary layer thickness and surface shear stress in a nominally two dimensional boundary layer [2], [3] and [27]. However, if too large values of open-area ratio for the screen was selected, the reduction of the pre-existing variations in the flow direction becomes difficult [27]. Bradshaw suggested that use of screens with open area ratios greater than 0.57 gave good results providing that this value is not significantly increased.

2.4.4 Honeycomb

According to references [2], [4], [6], [7] and [29] the crossectional size and shape of the honeycomb was not critical and often determined by availability of honeycomb material. Recommended cell length to diameter ratio was given between 5 to 10. In references [6] and [7] the cell size was suggested to be smaller than the smallest lateral wavelength of the velocity variation. It was suggested that there should be roughly 150 cells per settling chamber diameter.

References [5], [6] and [7] were in agreement about the yaw angles at the entrance to honeycomb. They proposed that the yaw angles should be less than 10°-15°. Higher yaw angles inceased the stalling possibilty of the honeycomb cells which in turn increased the pressure

loss across the honeycomb and reduced their effectiveness in straightening the flow.

The dependence of pressure loss coefficient, K_h, of honeycomb of different lengths on free stream velocity was investigated by Loehrke and Nagib [29] and is given in figure 2.2.

In 1967, Lumley and McMahon [30] studied the effect of honeycomb on a laminar and turbulent stream, and they also studied the level of turbulence produced by the honeycomb in a water tunnel. They found that for equal pressure drops the honeycomb is more efficient in reducing turbulence intensity than screens.

In 1976, Loehrke and Nagib [29] studied on the effect of honeycomb of different lengths on the flow which were either followed by a screen or without it. They also investigated the level of free stream turbulence at the downstream side of the honeycomb with hot-wire anemometry, and investigated, this flow in a water tunnel using hydrogen buble technique for flow visualization. Although the honeycomb itself generate new turbulence, a net suppression of the free stream turbulence was achieved by all the honeycombs tested in reference [29]. They concluded that the level, structure and decay of the generated turbulence partly depended on the instabilities of the shear layers and these instabilities could be modified by placing a fine mesh screen to the back of the honeycomb. Loehrke and Nagib visualised the flow downstream of the honeycomb with and without screen in a water tunnel with hydrogen buble technique. Their findings are shown in figure 2.3.

2.4.5 Wide Angle Diffuser

In this type of diffuser the crossectional area increases so rapidly that seperation which usually causes the unsteadiness [1], [7], [31] in test section flow can be avoided only by boundary layer control methods. Most popular method to avoid the seperation is to install gauze screens which the flow behaves like a manner as shown in figure 2.4. [6], [7], [22]

In references [6] and [7] some design charts were constructed for the diffuser parameters such as diffuser area ratio, AR, included diffuser angle, 2θ, pressure drop coefficient of screens placed in the diffuser, K_{ds}, and number of installed screens in the diffuser, n, from the collected data about wide angle diffusers. The design rules are in well agreement with previously proposed rules and with some experiments which used the above mentioned design charts [6], [7].

In references [2], [3] and [4], calculation of pressure loss coefficients of diffusers with small divergence angle were given, but there is no information in the available literature for determining the wide-angle diffuser loss coefficient, K_d, except figure 2.5 from reference [32].

2.5 EFFECT OF WIND TUNNEL COMPONENTS ON THE FLOW

In 1976, Hussain and Ramjee [33] stuied four axisymetric contraction shapes with the same contraction ratio and found that cubic equation contour evaluated from third order polynomial with boundary conditions gave the best results in velocity nonuniformity and exit boundary layer thickness. They showed that the turbulence intensity was not affected from the contraction shape.

In 1976, Ramjee and Hussain [34] investigated the effect of axisymmetric contraction ratio on the free stream turbulence. They firstly tested the influence of the upstream turbulence level on the test section flow. The different levels of turbulence was generated for a wide range of screen Reynolds number by placing upstream screens having different mesh size and wire diameter. They observed that for wide variations in screen mesh Reynolds number and screen wire diameter Reynolds number the exit value of turbulence intensity did not change. After a series of experiments they concluded that, lateral and longitudinal turbulence intensity decreased if the contraction ratio increased up to 45. For greater values of contraction ratio, lateral turbulence intensity kept on decreasing

while longitutional turbulence intensity slightly increased.

Results of Ramjee and Hussain [34] about the effect of contraction ratio on the turbulence intensity were confirmed by Tulapurkara and Ramjee [35] in 1980. In reference [36], Winter and Boyd compared the test results of reference [35] with the theoretical results given by Batchelor and Prandtl. This comparison is shown in figure 2.6 [36].

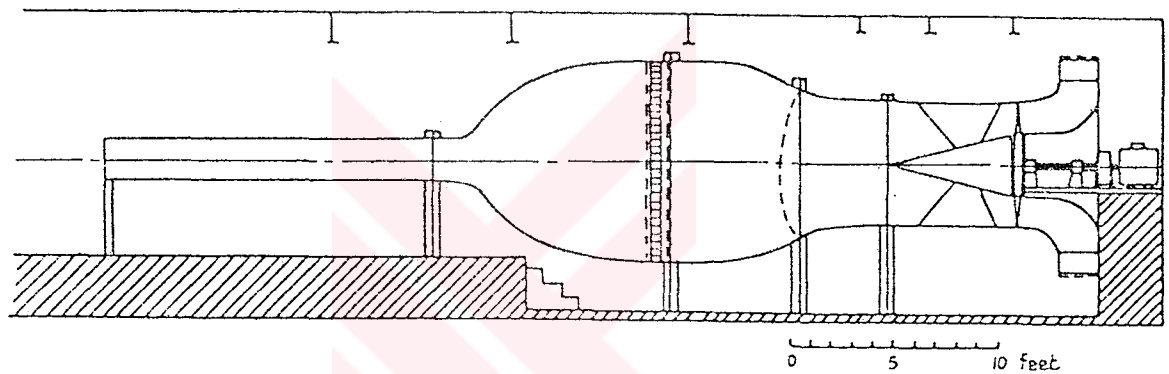

(a) 4'X 2' Blower Tunnel of Liverpool University, 1959

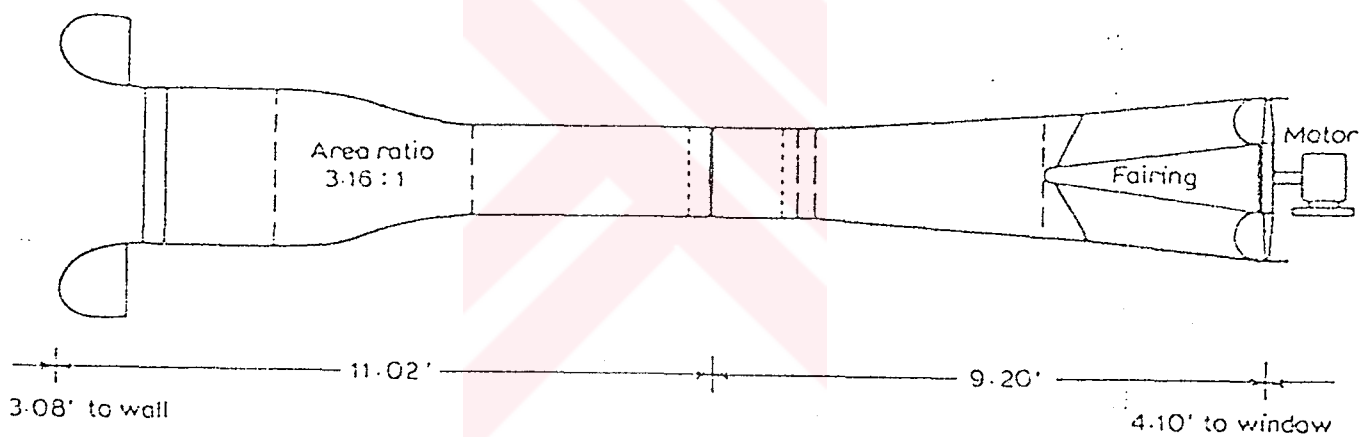

(b) NPL. 18" Suction Tunnel, 1947

Figure 2.1. Open-Circuit Blower and Suction Tunnels

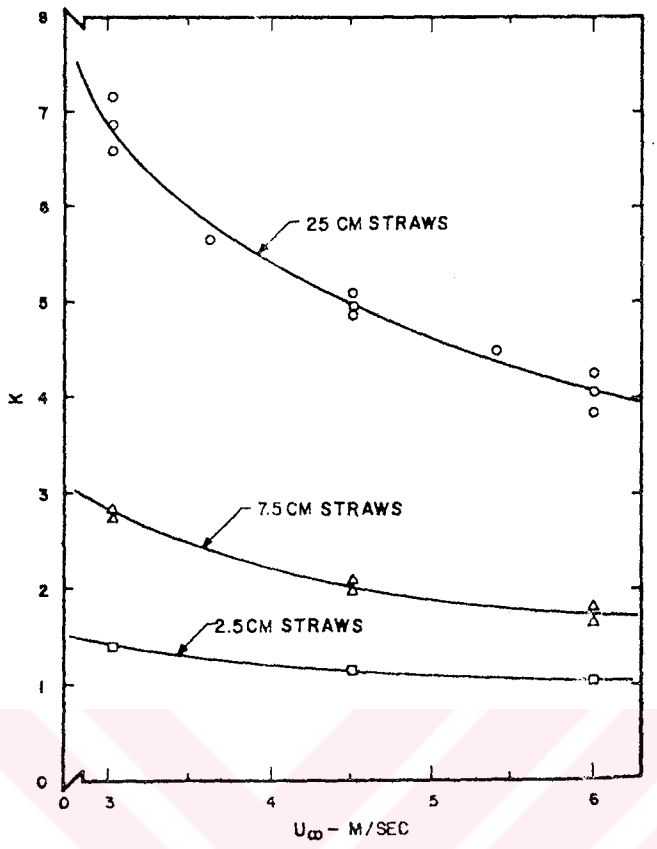

Figure 2.2. Dependance of Pressure Loss Coefficient of Honeycombs of Different Lengths on Free-Stream Velocity [29]

Table 2.1. Properties of Honeycombs and Screen used in Reference [29]

	M (cm)	σ	$K^{(a)}$	l (cm)	$Re_M{}^{(a)}$
Screens:					
0.013-cm Dacron thread	0.084	0.28	0.86	0.013	245
Straws:					
Plastic					
0.445-cm OD					
0.015-cm wall					
2.5 cm	0.445	0.20	1.2	2.5	1290
7.5 cm	0.445	0.20	2.1	7.5	1290
25 cm	0.445	0.20	5.0	25	1290
Straws and screen:					
2.5 cm			2.0	2.5	
7.5 cm			2.9	7.5	
25 cm			5.9	25	

(a) At U_∞ = 4.6 m/s

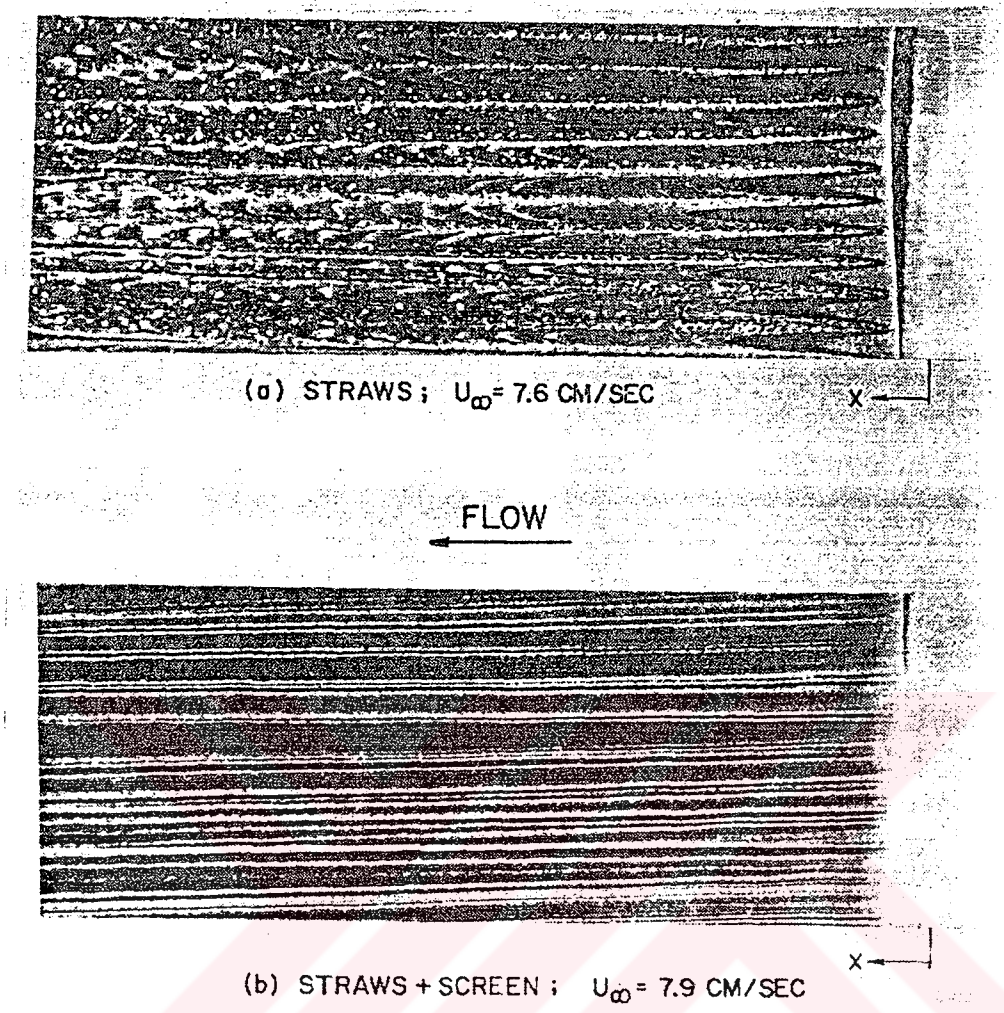

Figure 2.3. Visualisation of Flow Downstream of Honeycomb without (a) and with (b) screen [29]

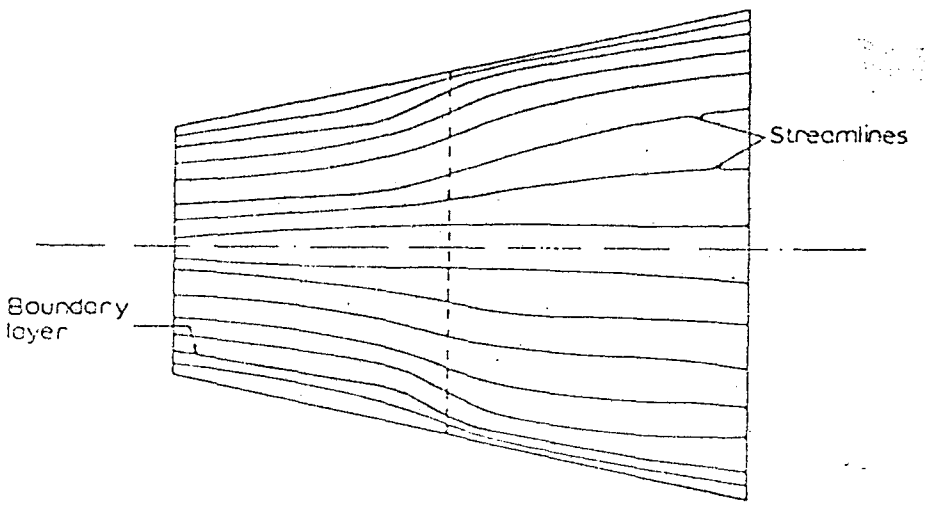

Figure 2.4. Flow Through a Plane Screen in a Wide Angle Diffuser [6]

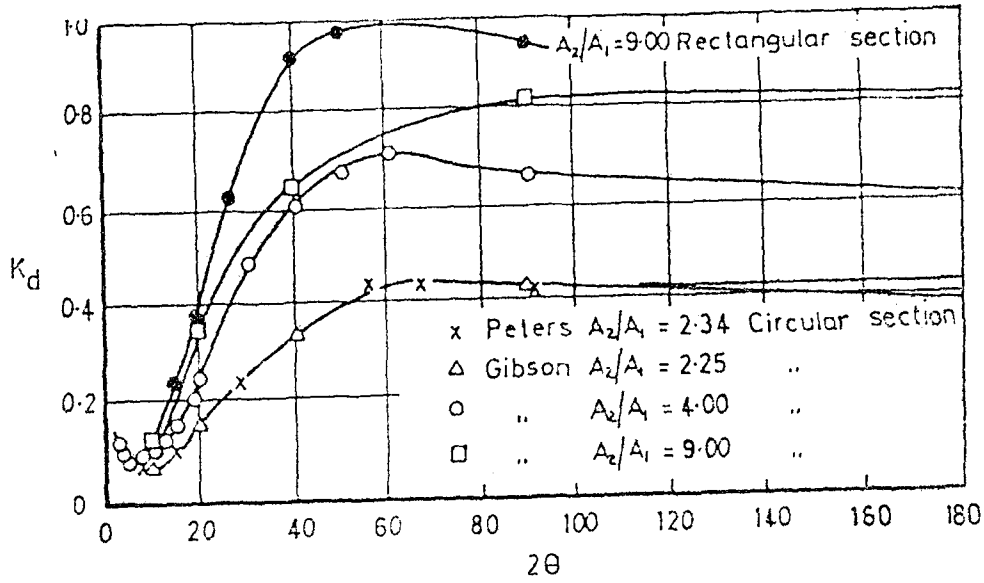

Figure 2.5. Diffuser Loss Coefficients w.r.t. the Diffuser Angle [32]

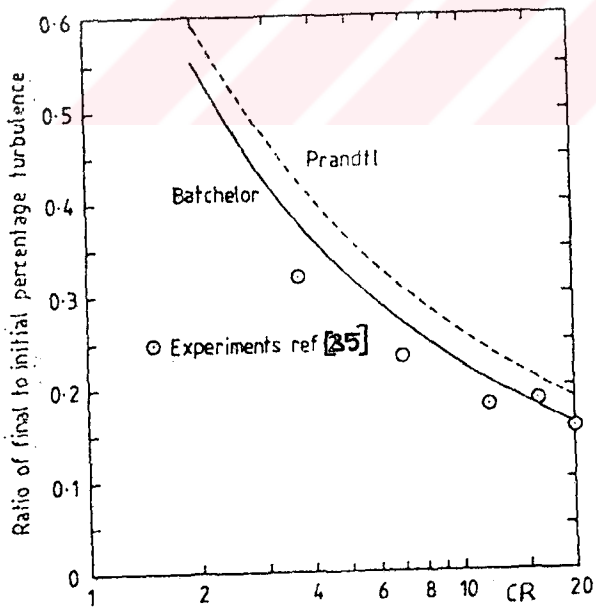

Figure 2.6. Turbulence Reduction through a Contraction in Incompressible Flow [36]

CHAPTER 3

DIMENSIONAL ANALYSIS AND SIMILARITY

3.1 INTRODUCTION

Since there is no analytical solution of many fluid mechanic problems, especially in turbulent flow media, an experimental evaluation and empirical relation is required to approach this type of problem. Dimensionless parameters are essential tools for analyzing model studies and for correlating experimental results. The technique is not as precise as the mathematical analysis which may provide exact solutions, but the solutions become impossible if the functional relationships between the parameters are not known [37].

In the absence of complete similitude, it is impossible to obtain similar motions in the same medium for two bodies with different sizes [4].

A model of a wind tunnel may be designed to predict the actual behaviour of the flow, such as turbulence level, flow uniformity, wall interference effects, and the estimation of the power factor of the prototype.

3.2 DIMENSIONAL ANALYSIS

Dimensional analysis and similarity concept is a powerful tool in determining the functional relationships between the parameters with the aid of experimental data.

In order to find the dimensionless parameters Buckingham's π-theorem is applied to the following flow parameters of the tunnel. Reference [38] describes the application of this theorem.

As it is shown below, the pressure difference along the tunnel may be expressed as a function of flow parameters, geometrical parameters

of the tunnel and the properties of the fluid flowing in the tunnel.

$$\Delta P = f(V, D, L, \rho, \mu, k, N) \qquad (3.1)$$

where

ΔP ($\frac{M}{LT^2}$) = Pressure difference between the two points

V ($\frac{L}{T}$) = Mean velocity of the crossection

D (L) = Hydraulic diameter of the crossection

L (L) = Length of the considered part

ρ ($\frac{M}{L^3}$) = Density of the fluid

μ ($\frac{M}{LT}$) = Dynamic viscosity of the fluid

k (L) = Roughness height on tunnel surfaces which are in contact with the fluid

N ($\frac{1}{T}$) = Rotational speed of the fan

For the above parameers (M,L,T) system of units are selected. There are 8 parameters so that 8 - 3 = 5 independent dimensionless groups may be formed.

As the repeating parameters V, D and ρ are selected, the following dimensionless "π" terms are constructed as described in reference [38]

$$\pi_1 = V^a D^b \rho^c \Delta P$$

$$\pi_2 = V^a D^b \rho^c \mu$$

$$\pi_3 = V^a D^b \rho^c N$$

$$\pi_4 = V^a D^b \rho^c k$$

$$\pi_5 = V^a D^b \rho^c L$$

The superscripts a, b and c are calculated in the following way;

π_1:

$$\left(\frac{L}{T}\right)^a (L)^b \left(\frac{M}{L^3}\right)^c \left(\frac{M}{LT^3}\right) = M^0 L^0 T^0$$

$$L : a + b - 3c - 1 = 0$$

$$M : c + 1 = 0$$

$$T : -a - 2 = 0$$

which gives, a = -2, b = 0, c = -1

$$\pi_1 = \frac{\Delta P}{\rho V^2} = E \qquad (3.2)$$

Similarly the other "π" terms are determined and they are stated below:

$$\pi_2 = \frac{\mu}{VD\rho} = \frac{1}{Re} \qquad (3.3)$$

$$\pi_3 = \frac{DN}{V} \qquad (3.4)$$

$$\pi_4 = \frac{k}{D} = \varepsilon \qquad (3.5)$$

$$\pi_5 = \frac{L}{D} \qquad (3.6)$$

When the dimensional analysis is made on these variables using V, D and ρ as repeating variables, the following functional relationship between the dimensionless parameters could be obtained;

$$\frac{\Delta P}{\rho V^2} = f\left(\frac{\mu}{VD\rho}, \frac{ND}{V}, \frac{k}{D}, \frac{L}{D}\right) \qquad (3.7)$$

Using the continuity equation, the flowrate may be written as:

$$Q \propto VD^2 \tag{3.8}$$

Inserting π_3 into equation 3. 8, it is found that:

$$Q \propto ND^3 \tag{3.9}$$

Systematic combination of π_1 and π_3 reduces the number of "π" terms,

$$\pi_{1,3} = \frac{\pi_1}{\pi_3^2} = \frac{\Delta P/\rho V^2}{N^2D^2/V^2} = \frac{\Delta P}{\rho N^2 D^2} = E \tag{3.10}$$

where E is the Euler number. If π_3 is divided by π_2, $\pi_{2,3}$ is found as,

$$\pi_{2,3} = \frac{ND/V}{\mu/VD\rho} = \frac{ND^2\rho}{\mu} = Re \tag{3.11}$$

which gives the Reynolds number.

3.3 SIMILITUDE

Similitude is the theory of predicting the protoype performance from its model observations and involves the application of dimensionless numbers.

In similarity criteria all parameters, geometric, kinematic and dynamic must be the same both in model and prototype. [37]

Geometric similarity is fundamental to aerodynamic experimentation including scale reproduction of all small design details and the surface roughness. If the two bodies are geometrically similar, the ratio of all corresponding linear dimensions of them are equal and

this can be expressed as the scale ratio, $L_r = L_p/L_m$.

For dynamic similarity, however, the forces on the model and prototype must be in the same ratio throughout the entire flow field and can be expressed as, $F_r = F_p / F_m$.

The flow patterns will be the same in the model as in the prototype (i.e. kinematic similarity is achieved) if the geometric similarity is satisfied and if the relative forces acting on the fluid are the same both in the model as in the prototype.

The requirements for the similarity of the flow between model and prototype are that the significant dimensionless parameters must be equal both for model and prototype [37]. However, in practice, this is often impossible to achieve. Consequently, some of the independent dimensionless variables which are believed to have secondary influences are allowed to deviate from their correct values. So the important thing is to compansate the allowed deviations by some corrections for complete similarity [39], [40]. Since the similarity requirements are not totally satisfied, this method is named as partial similarity.

3.3.1 Similitude According To Reynolds Number Criteria

If the model and prototype are produced at the same scale ratio with the same relative roughness and similitude is achieved at the same Reynolds number, $Re_p = Re_m$, at design point of the prototype it follows that Euler number, E, will also be the same for both of them. However, for the same fluid, if it is desired to apply Reynolds number similarity at the design point of the prototype, the required tunnel power, W, in terms of Reynolds number may be expressed as;

$$W \propto Q\Delta P \qquad (3.12)$$

from equation 3.8

$$Q \propto VD^2 \text{ and } \Delta P \propto \rho V^2$$

the power, W, can be written as,

$$W \propto \rho V^3 D^2 \tag{3.13}$$

since, $Re = \frac{\rho VD}{\mu}$

$$W \propto \frac{Re^3 \mu^3}{\rho^2 D} \tag{3.14}$$

Consequently, to achieve the same Reynolds number in the model as in the prototype:

1- Flow velocity must be increased as the size of the model decreases. This will eventually cause significant change in fluid density and will violate the incompressible fluid flow assumption.

2- The tunnel size is inversely proportional to the required power which increases the cost of operation of model tunnels.

Therefore, at the design point of the prototype tunnel, the Reynolds number similarity could not be applied to the model tunnel.

3.3.2 Similitude According To Euler Number Criteria

To apply Euler number similarity, $E_P = E_M$, to the tunnels that will be designed, the following conditions must be satisfied:

i. Relative roughness must be the same both in model and prototype,

ii. Friction factor must be independent of the Reynolds number.

Hydraulic losses in a blower tunnel are due to the following causes:

1- Pressure drop due to friction along the tunnel walls, ΔP_f

2- Pressure drop due to variation of crossection areas, ΔP_l

3- Exit energy from the test section (in the absence of the exit diffuser), q_o

So, the total tunnel loss coefficient both in model and prototype in terms of their exit energy, $q_o = \rho V_o^2/2$, are:

$$K_T = \sum_{i=1}^{n} K_i + 1 = \sum_{i=1}^{n} K_{fi} + \sum_{i=1}^{n} K_{li} + 1 \qquad (3.15)$$

where $K_f = f\frac{L}{D}$ is the frictional resistance coefficient which depends on the friction factor, f, and K_l is the local resistance coefficient of corresponding tunnel component.

If the geometrical similarity is fully achieved, the local resistance coefficients are nearly equal for Re $>$ $1x10^5$ [4]. Therefore, the local resistance coefficient, K_l and exit energy loss coefficient, 1, are constant at the operation range of the model and prototype tunnels. However frictional resistance coefficient which is directly proportional to friction factor, f, varries with the Reynolds number.

The design parameters that are to be taken into account when designing a tunnel may be expressed as:

$$\frac{\Delta P_T}{q_o} = E = f\left(Re, \frac{Q}{ND^3}, \frac{ND}{V}, \varepsilon, \frac{L}{D}\right) \qquad (3.16)$$

Total loss coefficient which results from surface friction and crossectional area variations gives the overall tunnel Euler number.

Since,

$$\Delta P_T = \Delta P_f + \Delta P_l + q_o = (K_f + K_l + 1)\, q_o = K_T q_o \qquad (3.17)$$

where ΔP_T is the total pressure loss along the tunnel, ΔP_f is the

pressure loss due to frictional resistance which depens on the Reynolds number and relative roughness of the wall, and ΔP_l is the pressure loss due to local resistance caused by local flow seperation and turbulent mixing which depends on the crossectional geometry of the tunnel.

Since the Euler number is directly proportional to friction factor, to achieve the same Euler number in both prototype and model tunnels which have different design Reynolds numbers, the Euler number should be independent of Reynolds number. As shown in figure 3.1, at the turbulent region of the flow Euler number similarity is satisfied, but in laminar and transitional regions of the flow, the independance of Euler number on Reynolds number can not be satisfied.

Therefore, a reference Reynolds number in the operation range of the prototype and model tunnel is selected. Then the variation of E with Re for the model are determined up to the reference Reynolds number. After this point obtained E vs. Re curve is extrapolated up to the design point of the prototype as shown in figure 3.2. This will secure the partial similarity in the operation of the prototype tunnel.

3.3.3 Similitude of the System Characteristics of the Tunnels

A more convenient way to express the similitude of the model and prototype is to construct the system (H-Q) characteristic curves of both tunnels. Therefore, equation 3.17 can be written in the form of,

$$H = \frac{K_T}{2g}\left(\frac{Q}{A}\right)^2 = CQ^2 \qquad (3.18)$$

where, $H = \Delta P_T/\rho g$, is the head loss of the tunnel, $C = K_T/2gA^2$, is the system resistance coefficient which depends on the Euler number and, $Q=VA$, is the flowrate through the tunnel.

Since, $K_{T_P} = K_{T_M}$ and $Re_P = Re_M$ for full similarity, neglecting the effect of ε, then from equation 3.18,

$$\frac{H_p}{H_m} = \left(\frac{A_m}{A_p}\right)^2\left(\frac{Q_p}{Q_m}\right)^2 \qquad (3.19)$$

but it is known that from equation 3.9

$$Q \propto ND^3$$

so, we have

$$\frac{H_p}{H_m} = \left(\frac{D_m}{D_p}\right)^2\left[\frac{N_p}{N_m}\left(\frac{D_p}{D_m}\right)^3\right]^2 \qquad (3.20)$$

but equation 3.11 states that,

$$Re \propto ND^2$$

If the Reynolds number similarity is applied, this gives:

$$\frac{N_p}{N_m} = \left(\frac{D_m}{D_p}\right)^2 \qquad (3.21)$$

inserting equation 3.21 into 3.20 and simplifying them,

$$\frac{H_p}{H_m} = \left(\frac{D_m}{D_p}\right)^4 \qquad (3.22)$$

In a similar way,

$$\frac{Q_p}{Q_m} = \frac{N_p}{N_m}\left(\frac{D_p}{D_m}\right)^3$$

$$\frac{Q_p}{Q_m} = \frac{D_p}{D_m} \qquad (3.23)$$

Equation 3.22 shows that for the same Reynolds number H_p is less than H_m by an amount of square of the scale ratio of prototype and model dimensions. According to equation 3.23 discharge ratio, Q_p/Q_m, is equal to the scale ratio of prototype and model for the equality of their Reynols numbers.

Equation 3.19 gives the relationship between the system characteristics of the prototype and model tunnel if the full similarity is achieved (i.e. there is no difference of relative roughness between the model and prototype in any way.)

A design chart for similar tunnels is obtained using the selected reference Reynolds number, Re, in the operation range of prototype and model tunnels. The H-Q charecteristic of the model tunnel is obtained up to the reference Reynolds number using equation 3.18. In the same way, H-Q characteristic of the prototype tunnel is calculated up to its design point. The H-Q characteristics of model and prototype tunnel deviate from each other by an amount of square of the area ratio of the tunnels as found from equation 3.19. The square of the area ratio of the tunnels may be eliminated dividing the equation 3.19 to the equation,

$$\frac{H_{Re}}{H'_{Re}} = \left(\frac{A_m}{A_p}\right)^2 \left(\frac{Q_{Re}}{Q'_{Re}}\right)^2 \qquad (3.24)$$

where H_{Re} and Q_{Re} are the head and volume flowrate of the prototype tunnel at reference Reynolds number. H'_{Re} and Q'_{Re} are the head and volume flowrate of the model tunnel at reference Reynolds number.

Then it is found that,

$$\frac{H_p/H_{Re}}{H_m/H'_{Re}} = \frac{(Q_p/Q_{Re})^2}{(Q_m/Q'_{Re})^2} \qquad (3.25)$$

If we express H/H_{Re} as $\bar{H}$ and Q/Q_{Re} as $\bar{Q}$ both for model and prototype the equation 3.25 may be simplified as,

$$\frac{\bar{H}}{\bar{H}'} = \left(\frac{\bar{Q}}{\bar{Q}'}\right)^2 \qquad (3.26)$$

where $\bar{H}$ and $\bar{Q}$ are the dimensionless head and volume flowrate of the prototype and $\bar{H}'$ and $\bar{Q}'$ are the dimesionless head and volume flowrate of the model respectivelly.

The dimensionless H-Q characteristics of the similar tunnels which were expressed with the equation 3.25 are shown in figure 3.3. The H-Q characteristics of the model and prototype tunnels lie on the same curve.

If the experimentally determined system characteristic of the model tunnel can not reach to the design point of the prototype tunnel, the found curve of the model tunnel is extrapolated to the design point of the prototype.

The above similarity analysis are made by considering,

$$K_T = f\,(\,Re,\ f,\ L/D)$$

but indeed, K_T is also dependent on the relative roughness of the model and prototype. From figure 3.1, as ε increases the friction factor deviates from the fully smooth curve described by Blasius equation,

$$f = \frac{0.3164}{Re^{1/4}}$$

Therefore, the relative roughness, ε, of the prototype must be nearly equal to the relative roughness of the model. In order to achieve this, the model surface should be manifactured very carefully with a high degree of polish. The loss charecteristics of the model and prototype tunnel will be equal to each other up to the begining of

the transition region. After this point the loss characteristics may differ from each other depending upon the value of ε_p and ε_m.

3.4 CONCLUSION

A good model will have a relative roughness which is equal to the relative roughness of the prototype . This will prevent the deviation of the loss characteristics of the model from that of the prototype. However it is seldom possible to construct a model with sufficiently small relative roughness due to the high cost of manifacturing of highly polished surfaces.

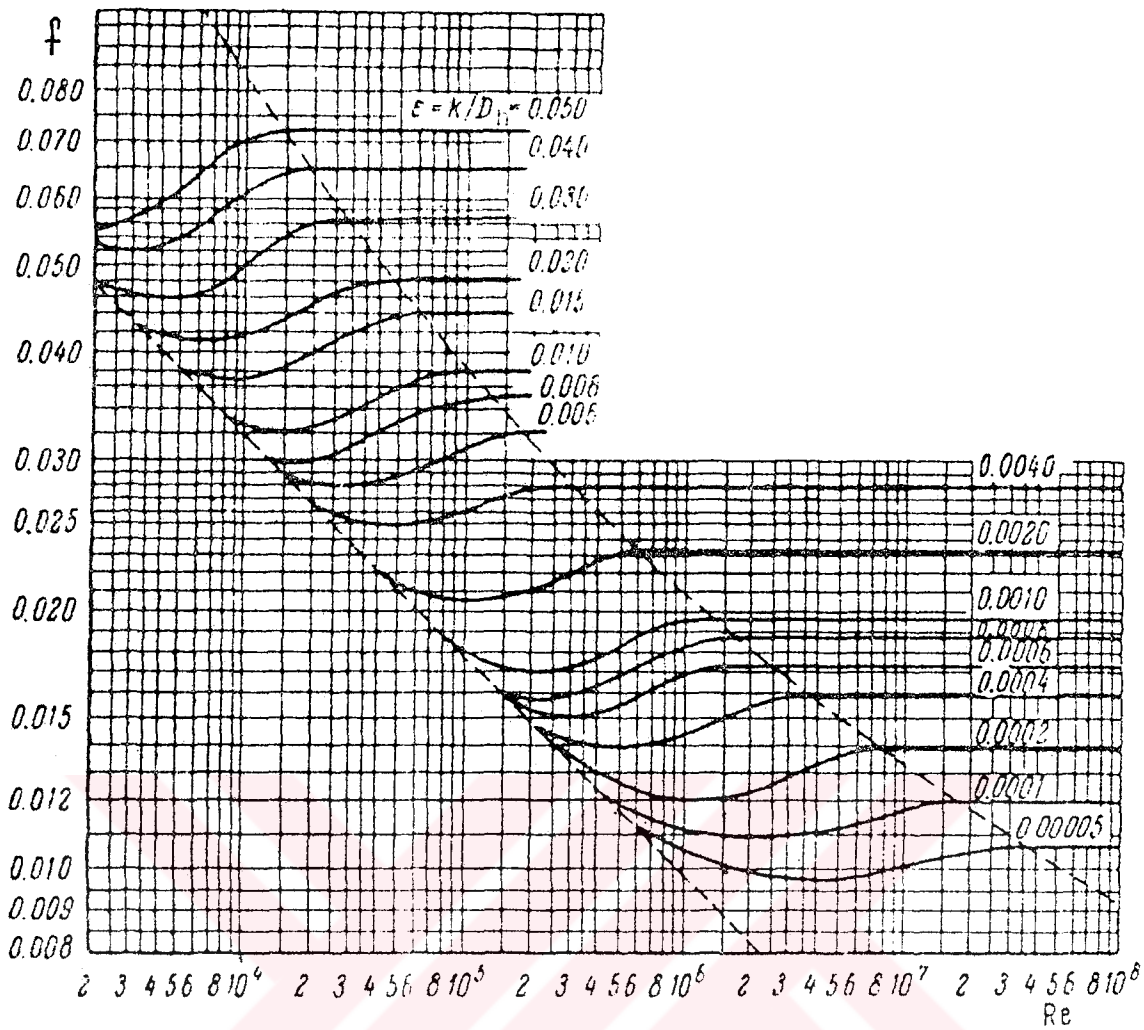

Figure 3.1. Variation of Friction Factor with Reynolds Number for Tunnels of Uniform Wall Roughness; Transitional Regime (Re>2000) [4]

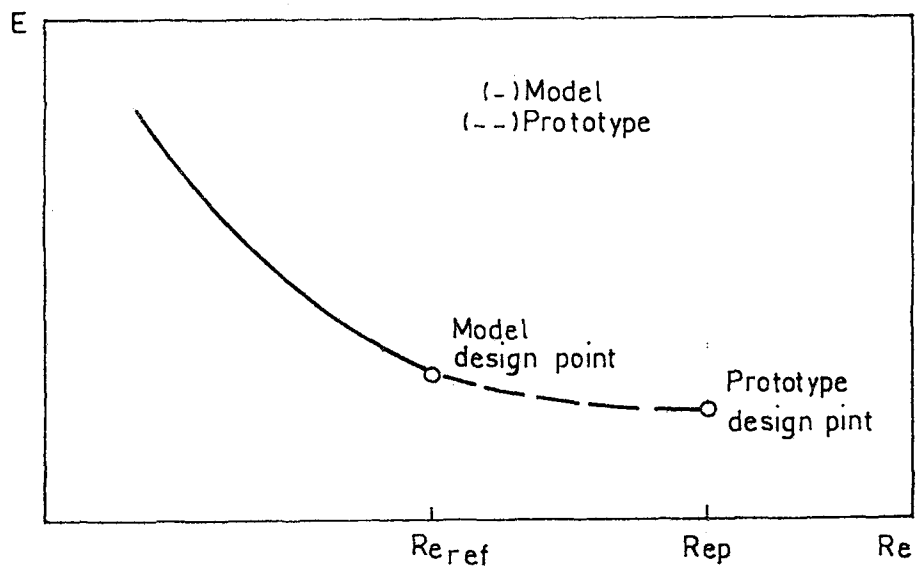

Figure 3.2. Variation of Tunnel Euler Number with Reynolds Number

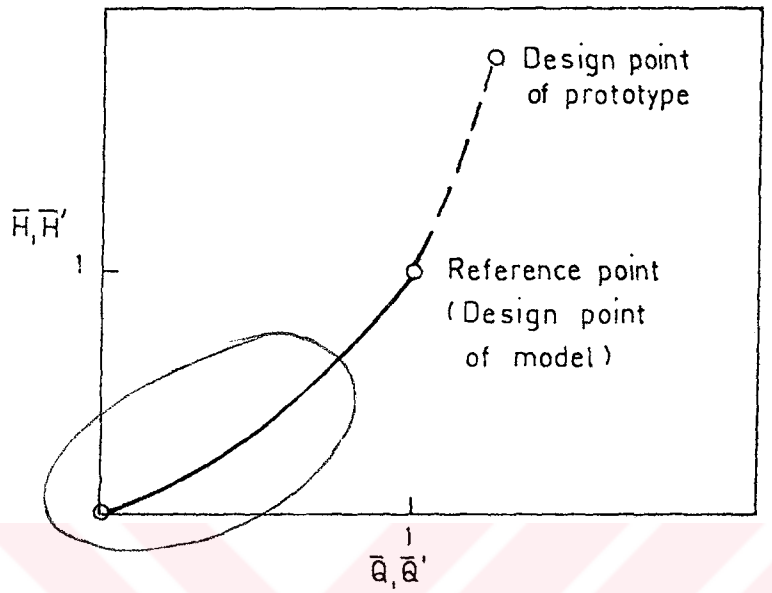

Figure 3.3. Dimensionless H-Q Characteristic of Similar Tunnels

CHAPTER 4

DESIGN OF A PROTOTYPE AND MODEL OF A BLOWER TYPE WIND TUNNEL

4.1 INTRODUCTION

The purpose of designing a wind tunnel is to simulate the free stream flow around the models which need a steady, uniform flow in the test section.

Open-circuit tunnels may be of suction type or blower type. General arrangement of a blower tunnel is similar to that of suction tunnel. However, in a blower tunnel, a diffuser is generally needed between its blower and settling chamber. On the other hand, if the flexibility of the test section arrangement is more important than the pressure recovery, the diffuser downstream of the test section can be excluded. Excluding the exit diffuser makes the power factor greater than unity.

There are advantages and disadvantages of a blower type wind tunnel with respect to the suction type tunnel [6], [7].

1. A blower wind tunnel allowes the operation of complete test section at atmospheric pressure, so the sealing of the test section is not necassary.

2. Different working section arrangements can be used in a blower wind tunnel but in suction wind tunnel this is impossible.

3. Disturbances and blockages created by the model in the test section can greatly affect the flow into a fan which is placed at downstream side of the test section but have little effect on a blower placed at upstream side.

4. In a suction type tunnel, air coming from the tunnel room may be less disturbed than that coming from a blower which may be centrifugal or axial type.

For the investigation of the industrial aerodynamic problems such as aerodynamic optimization of car bodies, determination of wind forces on structures, or propeler tests, a low speed blower wind tunnel is the most suitable type.

In this chapter a prototype and model of a blower type wind tunnel was designed.

4.2. DESIGN CONSIDERATIONS

The type and size of a low-speed wind tunnel is affected by several requirements and restrictions which may be summarized as follows;

1. Type of tests to be performed
2. Model size to be tested
3. The steadiness and uniformity of flow in the test section
4. The upper limit of the free stream turbulence intensity
5. The maximum Reynolds number to be achieved on the model
6. The available space that the wind tunnel is to be installed
7. The manifacturing and running cost
8. The driving system capacity and power supply
9. Available construction material and production facilities.

The design parameters to be decided on were specified in the light of above requirements and restrictions. Since the usage of the wind tunnel is for the architectural and industrial aerodynamics, including vehicle aerodynamics, the design was constrained by the need to provide not only uniform flow without excessive turbulence but also strongly turbulent flow. Therefore, the specifications for determining the above mentioned design requirements should be such that the flow in the test section of the designed tunnel must be uniform, steady and with low free stream turbulence level. The turbulence level may be increased to the desired level by using turbulence grids.

The length, width and height of the space available for the tunnel in the laboratory were 22 m, 9 m and 4.5 m respectivelly. References [3], [6], [7] states that, a rectangular test section that has a width to height ratio of 1.5 is advisable for general purpose wind tunnels. Considering the available space, production cost, required flow conditions, model sizes that could be placed in the test section with the minimum interference effect, a rectangular test section with a 1.5 m width to 1 m height was selected.

Running cost and available power supply has restricted the required power for the tunnel to be less than 60 kW.

References [3], [4] and [7] suggested that, if there is an exit diffuser, overall loss coefficient of a well designed tunnel should be less than 0.3. In the absence of the exit diffuser of the wind tunnel the exit loss coefficient is to be taken as 1. Therefore, to determine the maximum test section velocity roughly, the overall loss coefficient, K_T, of the tunnel was assumed as 1.3.

The relationship between the required power and overall pressure loss coefficient is given as [7]:

$$\lambda = \frac{W}{\frac{1}{2}\rho V_0^3 A_0} = \frac{K_T}{\eta} \qquad (4.1)$$

where λ is the power factor, W is the required shaft power of blower, K_T is the overall loss coefficient of the tunnel, η is the blower efficiency and V_0, A_0 are the test section velocity and crossectional area of the test section respectivelly.

The required velocity at the test section was estimated as 33 m/s from equation 4.1 for the approximate values of: W = 55 kW, A_0= 1.5 m^2, K_T= 1.3, η = 0.75, N = 750 rpm.

Using the above values, the fan diameter was calculated as

2.1 m according to reference [41]. The calculation procedure is given in Appendix 1.

In the design of the model and prototype tunnel air was assumed to be incompressible. For the design calculations the average atmospheric pressure, P , and temperature, T, in Gaziantep where the tunnels are to be built may be taken as 685 mmHg and 20°C respectivelly. At this pressure and temperature, the values of density, ρ, and dynamic viscosity, μ, of air was taken from reference [42].

$$\rho = 1.087 \text{ kg/m}^3$$

$$\mu = 1.79 \times 10^{-5} \text{ kg/ms}$$

and therefore;

$$\nu = \frac{\mu}{\rho} = 1.647 \times 10^{-5} \text{ m}^2/\text{s}$$

4.3 DESIGN OF THE PROTOTYPE

The main components of a blower tunnel, starting from the upstream end are a blower, a wide angle diffuser, a settling chamber, a contraction, a test section and sometimes an exit diffuser. The general arrangement of the tunnel is shown in figure 4.1 with sign conventions of the tunnel components which will be used throughout the design.

4.3.1 Test Section

The design of a wind tunnel is started from the test section which characterizes the tunnel. The other components of the tunnel are to be designed to match the test section and each other.

A wide variety of test section configurations may be used on a blower tunnel that has no exit diffuser.

The flow out of a contraction often takes a distance equivalent

to about 0.5 D_o before the nonuniformities are reduced below an acceptable level. If a turbulence grid is installed, it may take up to 10-15 mesh lengths before a homogenous flow is obtained [6], [7]. Since the hydraulic diameter of the test section is 1.2 m, a length of about 0.75 m was required to obtain a homogenous flow at the test section.

In order to to have a zero streamwise pressure gradient, a grdual increase in crossectional area of the test section is necessary. This increase in crossectional area is accomplished by tapering the corner fillets and walls of the test section in the flow direction. The corner fillets are also intended to reduce the severe secondary flow effects at the corners.

The length for the test section, having a 1.5 m x 1 m rectangular crossection, was taken as 4 m for the prototype tunnel. The angle of divergence for triangular corner fillets and test section walls was taken as 0.25° [4].

4.3.2 Contraction

The main functions of a contraction are:

1. To reduce mean and fluctuating velocity variations in the test section to a smaller fraction of the average velocity.

2. To improve the power factor of the wind tunnel.

The most important parameter in determining these effects is the contraction ratio, CR, defined as:

$$CR = \frac{A_c}{A_o} \qquad (4.2)$$

where A_c and A_o are contraction inlet and exit areas respectivelly.

In the selection of the contraction ratio, the important factor to consider is the effect of contraction on decreasing the velocity variation in the test section.

Let us suppose that, velocity variation at contraction inlet is v_c, average velocity at contraction inlet is V_c ,the velocity variation at test section is v_o and average velocity at test section is V_o. Writing Bernoulli's equation between the contraction and the test section:

$$P_c + \frac{1}{2}\rho(V_c + v_c)^2 = P_o + \frac{1}{2}\rho(V_o + v_o)^2 \qquad (4.3)$$

where P_c and P_o are the static pressures at the contraction inlet and test section inlet respectivelly. In the absence of velocity variations equation 4.3 may be written as:

$$P_c + \frac{1}{2}\rho V_c^2 = P_o + \frac{1}{2}\rho V_o^2 \qquad (4.4)$$

From equations 4.3 and 4.4:

$$v_c^2 + 2v_c V_c = v_o^2 + 2v_o V_o \qquad (4.5)$$

divinding throughout by $V_c^2 V_o^2$ and neglecting the square of the velocity variations, v_c^2 and v_o^2, which are small in comparison to the other terms in equation 4.5. It can be written as,

$$\frac{v_o}{V_o} = (\frac{V_c}{V_o})^2 \frac{v_c}{V_c} \qquad (4.6)$$

but $(V_c/V_o)^2 = 1/CR^2$, then

$$\frac{v_o}{V_o} = \frac{1}{CR^2}\frac{v_c}{V_c} \qquad (4.7)$$

Equation 4.7 shows that as contraction ratio increases, the mean velocity variation in the longitutional direction at the exit of the contraction reduces with an amount of $1/CR^2$.

On the other hand hand, as explained in references [6], [34], [35] and [36] the transverse components of velocity which can be expressed

as a fraction of the mean longitudinal velocity is reduced approximately by $1/CR^{1/2}$. The reduction of velocity variations at the exit of the contraction leads also to a reduced turbulence level in the test section [6]. The reduction of the turbulence intensity across the contraction can be predicted from figure 2.7 on reference [36].

Contraction ratio should be selected as high as possible in order to achieve a large reduction in the flow nonuniformity and free stream turbulence intensity. However, it should be small to avoid the flow seperation problems. On the other hand small contraction ratio decreases the space reguirement and the cost of manufacturing. Although a large contraction ratio was desired, space limitation restricted the selection of the contraction ratio. CR = 9 was used both for the model and the prototype.

The length and shape of the contraction also affect the degree of uniformity and boundary layer thickness at the entrance to the test section.

The design of a contraction requires avoidance of flow seperation. Boundary layer seperation may occur at each end of the contraction where the possibility for obtaining adverse pressure gradient is high. It is possible to avoid seperation by increasing the contraction length sufficiently. However, increasing the length of the contraction increases the boundary layer thickness at the inlet of the test section. This causes an undesirable boundary layer growth and increases the seperation possibility along the test section. A design satisfying all these requirements should be such that the flow seperation in contraction is avoided and at the contraction exit the flow nonuniformity is equal to the maximum tolerable level for a given application.

In designing the contraction contour of the prototype and model blower wind tunnel, the design method for a two dimensional contraction suggested by Libby and Reiss [23] was used. This selection was made after two contraction models were tried in a water channel and found to be unsatisfactory. One of the model contraction was

designed according to Morel's design method [18]. The other contraction model was designed according to reference [33]. It gives a contraction design based on a 3rd order polynominal with appropriate constant which were evaluated from boundary conditions. The models were produced from perspex and tested in the water channel of the Fluid Mechanics Laboratory. Although the models were not satisfactory the following points were observed:

1. The contraction contour should not have a high rate of change of slope.

2. The adverse pressure gradient at the inlet of the contraction should not be too high.

These observations were considered while the contraction contour had been designed. In reference [23] the equations for the two dimensional contraction contour which was solved by conformal transformation technique were given as:

$$\frac{2x}{b_c} = -\frac{1}{\sqrt{CR}\,(\pi-\Psi_0^J)}\{\ln\phi_0 + 1/2(1/\sqrt{CR}-1)\ln(1+\phi_0^2-2\phi_0\cos\Psi_0^J)\} \qquad (4.8)$$

$$\frac{2y}{b_c} = \frac{1}{\sqrt{CR}\,(\pi-\Psi_0^J)}\{(\pi-\Psi_0^J) + (1/\sqrt{CR}-1)\tan^{-1}(\frac{\phi_0\sin\Psi_0^J}{1-\phi_0\cos\Psi_0^J})\} \qquad (4.9)$$

where ϕ_0 and Ψ_0^J represent the potential and stream functions along the contour respectively. The geometry of any streamline contour can be calculated from equations 4.8 and 4.9 by taking Ψ_0^J constant and variying ϕ_0 between zero and infinity.

Due to the selected contour was for an infinitely long contraction, the length was truncated at both ends of the contraction where the velocity peaks are very small.

A three dimensional contraction may also be designed using the method given in reference [23]. Since the crossectional area of the contraction is rectangular in shape, the contraction contours of upper and lower walls are different from contours of side walls. However,

this difference is a function of the aspect ratio which is defined as;

$$AS = z/y \tag{4.10}$$

Therefore, the contraction contour of side surfaces z, were designed according to reference [23]. Then, contours of the upper and lower surfaces y, are calculated from equation 4.10. The contour of the contraction walls are given in table 4.1. Figure 4.2 shows the general view of the contraction with sign conventions.

For construction of the contraction the developed drawings of the contoured surfaces are necassary. Therefore, the length of surfaces bcfe and cdgf as shown in figure 4.2.a should be determined. This may be done with the use of the graphical techniques. The surfaces abeh and adgh may be divided into infinitesimal segments which were called as y and z strips respectivelly. The strips y and z were analized as shown in figure 4.2.b. Assuming that the length of the strip contour, Δl , for infinitesimal Δx increment is approximately a line, it is found that

$$\Delta l = \sqrt{\Delta x^2 + \Delta z^2} \tag{4.11}$$

where $\Delta x = x_{i+1} - x_i$ and $\Delta z = z_{i+1} - z_i$ so that the total length of the dg line, L , is calculated as:

$$L = \sum_{i=1}^{N+1} \Delta l \tag{4.12}$$

Therefore, the total length of the side surfaces are expressed as:

$$L_z = \sum_{i=1}^{N+1} \sqrt{[(x_{i+1} - x_i)^2 + (z_{i+1} - z_i)^2]}$$

In a similar way, the length of the upper and lower surfaces (ie. be line) are determined as:

$$L_y = \sum_{i=1}^{N+1} \sqrt{[(x_{i+1} - x_i)^2 + (y_{i+1} - y_i)^2]}$$

The contours of the surfaces abeh and adgh are given in figure 4.3 and the development of these surfaces; that is the bcfe and dcfg surfaces, are shown in figure 4.4. The coordinates of the developed contours of the surfaces which were non-dimensionalized with the half width of the contraction inlet are also listed in table 4.1.

4.3.3 Screens

Wind tunnel screens are used for the following reasons: It is used to reduce the turbulence intensity in the whole flowfield, and to remove large scale eddies at the expense of introducing a large number of eddies of much smaller scale, so that, they can decay at a shorter distance by the action of viscosity. In addition, screens make the flow velocity profiles more uniform by imposing static pressure drop proportional to V^2. Thus, it reduces the boundary layer thickness so that the ability to withstand to a given pressure gradient is increased in such a manner as shown in figure 2.4 [6].

The effect of a screen on the turbulence and velocity distribution in the test section depends largely on the pressure drop coefficient, K_s, and open area ratio, β, of the screen. Open area ratio is defined as:

$$\beta = (1 - \frac{d_s}{l_s})^2 \qquad (4.13)$$

where d_s is the diameter and l_s is the mesh size of the screen.

Equation 2.3 which was suggested by Collar [25] shows that the screen with pressure drop coefficient about 2 almost entirely eliminates the spatial variations of the mean axial velocity. However, according to equation 2.4, the pressure drop coefficient should be as high as possible for the reduction of turbulence in the flow. The necassary power to drive the tunnel increases with the increase of pressure drop in the screen; therefore screens should be choosen at a

value of K_s to give the low turbulence level at reasonable power requirement for the tunnel.

A screen with d_s = 0.115 mm and l_s = 0.5 mm was used in the model tunnel. The open area ratio of the screen was calculated as 0.6. The pressure drop coefficient of screen was determined from equation 2.1 or 2.2 according to the screen Reynolds number, Re_s, range. For the prototype tunnel, a screen of d_s = 0.8 mm and l_s = 3.5 mm was proposed with an open area ratio of 0.6, same as of the model tunnel screen.

The reduction of velocity nonuniformity and turbulence intensity can be predicted from equations 2.3 and 2.4 as 0.3 and 0.7 respectively.

4.3.4 Honeycomb

Honeycombs are effective for removing swirl and lateral mean velocity variations, as long as the flow yaw angles before honeycomb are not greater than 15° [7].

The honeycomb of model tunnel was produced from plastic drinking straw which had a diameter, d_h, of 3.5 mm. According to the range that was recommended by references [4], [6], [7] and [29] the length to diameter ratio of the straws was taken as 9. By the use of this cell size, the cell number per settling chamber diameter was about 147 as was suggested in reference [7]. The honeycomb structure and determination of cell number per unit area are shown in figure 4.5.

The honeycomb of model tunnel was tested in the water tunnel as shown in figure 4.6. A series of silk treads were placed on 4 raws of the honeycomb. It was observed that in the homogenous part of the honeycomb the flow was uniform.

For the prototype honeycomb cells having a diameter of 24.5 mm and a thickness of 0.8 mm was proposed with the same length to diameter ratio of the model tunnel.

4.3.5 Settling Chamber

The usual arrangement consists of a honeycomb followed by screens. The pressure loss coefficients depends on the geometry of screen and honeycombs. The geometry of these components are selected according to the flow requirements such as flow uniformity, free stream turbulence intensity etc. If severe yaw and swirl are expected in the flow that comes from the wide angle diffuser, reference [7] recommends to install an additional screen upstream of the honeycomb, so that the flow angles are reduced. According to references [6] and [7] a screen with K_s = 1.5 reduces yaw and swirl about 70 percent for swirl angles less than 40°. If a screen is not required before the honeycomb, the honeycomb should be installed near to the wide angle diffuser exit in order to increase the uniformity of static pressure distribution across the crossection and to reduce the flow angularity.

The optimum distance between the last screen and the contraction entry was suggested as at least 0.2 times the hydraulic diameter, D_c, of the settling chamber [18]. On the other hand, the spacing between the screen and the honeycomb was recommended as $0.1D_c$ - $0.2D_c$.

In the designed tunnels both in prototype and model, the space between the honeycomb and the screen was selected as 0.15 D_c. The distance between the screen and the contraction inlet was taken as 0.3 D_c. Honeycomb was placed just downstream of wide angle diffuser.

4.3.6 Wide-Angle Diffuser

The flow uniformity and turbulence in a wind tunnel test section can be greatly improved with a large contraction ratio which requires large settling chamber. To reduce the effect of settling chamber pressure loss on the power factor, λ, a large settling chamber crossectional area is also necassary. On the other hand, references [3] and [6] suggested that the crossectional area of the fan section should be about 2 or 3 times that of the test section for high fan

efficiencies.

Wide angle diffusers which are placed between the blower and the settling chamber are usually preferred in blower type tunnels.

The purpose of the wide angle diffuser is to provide a transmission from blower to settling chamber with a length as short as possible rather than a pressure recovery.

The flow through a wide angle diffuser mostly depends on diffuser area ratio, AR, diffuser angle, 2θ, and pressure loss coefficient, K_d. The diffuser loss coefficient may be expressed as,

$$K_d = 1 - \frac{C_{P_d}}{1-(A_f/A_c)^2} \qquad (4.14)$$

where C_{P_d} is the pressure recovery coefficient. It is expressed as:

$$C_{P_d} = \frac{P_d - P_f}{\frac{1}{2}\rho V_f^2} \qquad (4.15)$$

P, A and V denote pressure, crossectional area and velocity of the related crossections respectivelly. Subscripts f and d refer to the diffuser inlet and outlet respectivelly.

Figure 2.5 shows the variation of the loss coefficient of diffusers with diffuser angle and area ratio.

However, in this type of diffuser there is always danger of seperation which creates unsteady flow in the test section. The most suitable boundary layer control method is to place gauze screens saving production time and cost [6], [7].

Wide angle diffuser of the prototype and model tunnels was designed according to design charts which were given in references [6],

[7]. These charts were resulted from a collection of data obtained from a large number of diffuser tests where boundary layer controls were performed by using screens installed in the diffuser.

Figure 4.7 and 4.8 give the design boundaries and required pressure drop coefficients for a screen [7]. The design parameters are the area ratio of diffuser, AR, included angle of the diffuser, 2θ, number of screens, n, and total pressure drop coefficient of the screens, K_{ds}. The area ratio of the diffuser was calculated as 3.9 for the values of :

$$A_c = 4.5m \times 3m = 13.5\ m^2$$

and

$$A_f = \frac{\pi}{4}(2.1)^2 = 3.46\ m^2$$

Using figure 4.7 and 4.8 the other diffuser parameters were selected as:

$2\theta = 26^\circ$ (maximum)

$K_{ds} = 2.6$

$n = 1$

Both for model and prototype tunnel, the diffuser was designed in 3 parts. First part is to provide a transition from circular to rectangular crossection. Second and third part of the diffuser have a rectangular crossection with corner fillets decreasing in downstream direction. Between second and third part a screen could be placed to prevent seperation. The screen location may be estimated from reference [6] as:

$$\frac{L_{d1}}{L_d} = 0.6$$

where L_{d1} is the distance from diffuser inlet and L_d is the total diffuser length.

4.3.7 The Blower And Straightener

To select a suitable fan and drive unit after deciding on the size and configuration of the tunnel it is essential to estimate the power factor. Reference [7] states that while estimating the power factor of the fan, adequate extra power should be added to the required power to cope with a variety of model and test section configuration.

In a tunnel design, fan crossectional area is also an important parameter that should be considered. Since the fan diameter was determined as 2.1 m in Appendix 1, the area ratio of fan section to test section was calculated as 2.3. This ratio was in the recommrnded range given by reference [6], [3].

Straightener vanes are necassary at the downstream of the fan to remove produced swirl by the fan. A nacelle which is supported by straightener vanes is placed at the center of the fan section. Nacelle diameter should be equal to boss diameter which was determined in Appendix 1 as 0.4 D_f. References [3], [7] states that number of straightener vanes should not be equal to the number of fan blades to avoid periodic interference between them.

For the nacelle shape, any sufficient streamlined body of revolution may be used [41]. In the design of streamlined body of revolution, fineness ratio, f_n , is an important parameter in deciding the length of the body. It may be defined as,

$$f_n = \frac{l_n}{d_n} \tag{4.16}$$

where l_n is the length of the nacelle. d_n is the maximum diameter of the nacelle which is equal to the boss diameter of the fan. According to reference [43], a suitable fineness ratio for nacelle is given as 1.2. However, a large fineness ratio is more desirable for the fan which discharge into a diffuser [41].

A streamlined body was designed for nacelle shape and straightener vanes. The design was based on the potential flow theory

[38] and is given in Appendix 3. For the nacelle shape, the revolution of streamlined body was used with a fineness ratio of 2.5 and boss diameter of 0.4 D_f. For the straightener vanes, the same streamlined body was used with a fineness ratio of 5 and with a thickness of 0.04 D_f. The contour of the streamlined body in cartesian coordinates to ease the drawing for production are given in Table 4.2 as the percentage of the body length, L, and thickness, b_s.

4. 4 CALCULATION OF HYDRAULIC LOSSES OF THE PROTOTYPE TUNNEL

To estimate the required power to drive the tunnel, the hydraulic resistance of different components of the wind tunnel in terms of the dynamic pressure in the test section should be determined.

The pressure losses, ΔP_i, for each tunnel component can be written as:

$$\Delta P_i = K_i \tfrac{1}{2}\rho V_i^2 \qquad (4.17)$$

where K_i is the sum of the loss coefficients which are due to form and viscous resistance, and V_i is the velocity of the fluid in the corresponding tunnel component. Equation 4.12 can be written in terms of test section dynamic pressure, $q_0 = \tfrac{1}{2}\rho V^2$, as:

$$\Delta P_i = K_i \frac{\tfrac{1}{2}\rho V_i^2}{\tfrac{1}{2}\rho V_0^2} q_0 \qquad (4.18)$$

Since, velocity is inversely proportional to crossectional area at any section, equation 4.13 may be expressed as:

$$\Delta P_i = K_i \left(\frac{A_0}{A_i}\right)^2 q_0 \qquad (4.19)$$

where A_0 and A_i is the crossectional area of the test section and the tunnel section under consideration respectivelly.

The calculation of the hydraulic resistance of the tunnel components are mainly based on the empirical results of the experiments performed on previously built wind tunnels. The design procedure that was suggested in reference [4] was mainly followed for the calculation of hydraulic loss coefficients of the tunnel components.

4.4.1 Test Section

The test section velocity was selected as 33 m/s. Since the crossection throughout the tunnel is rectangular all calculations were based on hydraulic diameter of the related parts.

The hydraulic diameter for rectangular crossection may be given as:

$$D = \frac{2ab}{a+b} \qquad (4.20)$$

where a and b correspond to heigth and width of the crossection respectivelly.

The test section hydraulic diameter, D_0, and the test section Reynolds number based on D_0 were calculated as 1.2 and 2.4×10^6 respectivelly.

The hydraulic loss in the test section is due to the frictional resistance. It may be determined by using the following relation:

$$K_0 = f \frac{L_0}{D_0} \qquad (4.21)$$

where f is the friction factor and L_0 is the length of the test section which was determined as 4 m for the prototype.

To find the friction factor, the average hight of the surface roughness, k, for plywood was taken as 0.1 mm [4]. The relative roughnees, ε, was determined as:

$$\varepsilon = \frac{k}{D_o} = 0.000083$$

and f corresponding to the test section Reynolds number was found from figure 3.1 as:

$$f = 0.011$$

K_o can be calculated as:

$$K_o = 0.0367$$

4.4.2 The Contraction

The hydraulic losses in the contraction was calculated by using the expression [4]:

$$K_c = \frac{4}{9} f \frac{L_c}{D_o} \frac{CR^{9/2} - 1}{CR^{5/2}(CR - 1)} \qquad (4.22)$$

since CR = 9 (contraction ratio)

$$f = 0.011 \text{ (friction factor)}$$

$$L_c = 4.5 \text{ m (total length of the contraction)}$$

$$D_o = 1.2 \text{ m (hydraulic diameter of the contraction outlet)}$$

Therefore, the hydraulic loss coefficient of the contraction for $Re = 2.4 \times 10^6$ was found as:

$$K_c = 0.1856$$

4.4.3 Settling Chamber

Because of the low flow velocities and small length to diameter ratio, the frictional losses in the settling chamber were found to be negligible.

4.4.4 The Screen

To determine the hydraulic loss of the screen, K_s,equation 2.1 or 2.2 may be used for the previously mentioned Re_s range.

The screen that was proposed for the prototype tunnel has a 0.8 mm wire diameter and 3.5 mm mesh length. The open area ratio of the screen was determined by using equation 4.8:

$$\beta = 0.6$$

The screen Reynolds number, Re_s, was determined as, Re_s =297. Since this value of Re_s is smaller than 600, equation 2.2 was used to calculate the value of, K_s. Therefore,

$$K_s = 1.083$$

4.4.5 Honeycomb

To determine the honeycomb loss coefficients, K_h,there is no appriaceable knowlege in the literature. Therefore, produced honeycomb cells for the model tunnel was tested in the air rig that was shown in figure 4.9. Air rig pipe diameter was 0.121 m. Outside diameter of honeycomb cell, d_h, its thickness, t_h,and length, l_h,were 3.5 mm, 0.11 mm and 32 mm respectivelly. The pressure differences were taken from 17 mesh lengths upstream and downstream of the honeycomb.

The honeycomb loss coefficient was calculated from,

$$K_h = \frac{\Delta P}{\frac{1}{2}\rho V_\infty^2} \qquad (4.23)$$

where ΔP is the measured pressure drop across the honeycomb and V_∞ is the free stream velocity in the duct.

The test results are in well agreement with the results which was given by Loehrke and Nagib [29] in table 2.1. For example, at honeycomb mesh Reynolds number, Re_h =1290, they found that the pressure drop coefficients as [29]:

$$K_h = 1.2 \quad \text{for} \quad \frac{l_h}{d_h} = 5.62$$

$$K_h = 2.1 \quad \text{for} \quad \frac{l_h}{d_h} = 16.85$$

On the other hand, our test results for the same Re_h gives:

$$K_h = 1.975 \quad \text{for} \quad \frac{l_h}{d_h} = 9$$

The value of the pressure drop coefficient of the honeycomb for a length to diameter ratio of 9 is between the results of Loehrke and Nagib [29] for the given l_h/d_h ratios at the same Reynolds numbers, Re_h. This shows that K_h is a function of length to the diameter ratio of honeycomb, l_h/d_h, as well as the honeycomb mesh Reynolds number, Re_h.

The honeycomb Reynolds number, Re_h,is

$$Re_h = \frac{V_h \, d_{hi}}{\nu} \tag{4.24}$$

where V_h and $d_{hi} = d_h - 2t_h$, are the velocity and inside diameter of the honeycomb cell respectivelly.

The free stream Reynolds number, Re_∞, is

$$Re_\infty = \frac{V_\infty \, D_h}{\nu} \tag{4.25}$$

where V_∞ and D_h are the free stream velocity and the hydraulic diameter of the honeycomb chamber. The relation between Re_h and Re_∞ may be found from

$$V_h A_h = V_\infty A_\infty$$

where A_h and A_∞ are honeycomb flow area and honeycomb chamber area respectivelly.

Assuming the area outside the circular cells were filled with glue as shown in figure 4.5, the flow area of the honeycomb could be given as:

$$A_h = N\frac{\pi}{4}d_{hi}^2 \qquad (4.26)$$

where N is the number of cells in the tested duct. The number of cells per unit area, n, was found from

$$n = \frac{1}{d_h^2} \qquad (4.27)$$

as shown in figure 4.5. Then, the total number of cells in the honeycomb chamber was calculated from

$$N = nA_\infty = \frac{A_\infty}{d_h^2} \qquad (4.28)$$

The open area ratio of the honeycomb, ς, was determined as:

$$\varsigma = \frac{A_h}{A_\infty} = n\frac{\pi}{4}d_{hi}^2 = \frac{\pi}{4}\left(\frac{d_{hi}}{d_h}\right)^2 = N\left(\frac{d_{hi}}{D_h}\right)^2 \qquad (4.29)$$

then, the velocity in the honeycomb cells could be given as:

$$V_h = V_\infty \frac{1}{\varsigma} \qquad (4.30)$$

By using equation 4.24 and 4.30

$$Re_h = \frac{V_\infty}{\varsigma}\,\frac{d_{hi}}{\nu} \qquad (4.31)$$

multiplying and dividing the equation 4.31 with D_h and rearranging, it was found that

$$Re_h = \frac{Re_\infty}{(\sqrt{N})^{0.5}} \qquad (4.32)$$

Therefore,

$$Re_h = f\,(Re_\infty,\ N,\ \varphi) \qquad (4.33)$$

Since, the open area ratio of honeycomb is depended upon the honeycomb cell, for the same open area ratio of honeycomb, φ,

$$Re_h = f\,(Re_\infty,\ N) \qquad (4.34)$$

Therefore, the pressure drop coefficient of the honeycomb, K_h,was plotted for a range of honeycomb Reynolds number, Re_h, as shown in figure 4.10. For the figure 4.10, a curve was fitted with the aim of a computer program that was given in [44]. The equation of the curve was found as:

$$K_h = 4.424 - 0.3586\times10^{-2}Re_h + 0.1756\times10^{-5}Re_h^2 - 0.3841\times10^{-9}Re_h^3 + 0.3103\times10^{-13}Re_h^4$$

for $Re_h < 4000$ (4.35)

$K_h = 1.52$ for $Re_h > 4000$

Since, the proposed honeycomb cell for the prototype tunnel has a d_h = 24.5 mm, t_h = 0.8 mm and l_h = 225 mm, the number of cells in 13.5 m^2 settling chamber crossectional area was found from equation 4.28 as:

$$N = 22490$$

the open area ratio, φ, was calculated from equation 4.29 as:

$$\varphi = \frac{\pi}{4}\left(\frac{d_{hi}}{d_h}\right)^2 = 0.6862$$

Equation 4.31 gives

$$Re_h = \frac{V}{CR\acute{e}} \frac{d_{hi}}{V} = 7429.6$$

Using equation 4.35 the pressure drop coefficient of the honeycomb was determined as:

$$K_h = 1.52$$

4.4.6 The Wide Angle Diffuser

If no boundary layer control method is applied on the wide angle diffuser, its hydraulic loss coefficient may be predicted from figure 2.5. For the selected wide angle diffuser which has a 26° maximum included angle with an area ratio of 3.9 from figure 2.5 the hydraulic loss coefficient was determined as 0.3.

Acording to reference [7], if the boundary layer control was provided by installing screen to the wide angle diffuser the pressure loss coefficient is insignificant as compared with the screen loss coefficient. For the determined diffuser parameters a screen which has a pressure loss coefficient of 2.4 was recommended by references [6], [7].

Hydraulic loss coefficient of the fan section was very small due to its small length to diameter ratio. Therefore it was neglected. To compansate the miscelleneous losses and model losses a 15 % of total hydraulic loss throughout the prototype tunnel was added to the sum of hydraulic loss of each tunnel component.

The hydraulic losses of the tunnel components of prototype are listed in table 4.3. The required fan total pressure was calculated from,

$$\Delta P_T = q_o \left[\sum_{i=1}^{n} K_i \left(\frac{A_o}{A_i}\right)^2 + 1\right] \qquad (4.36)$$

Therefore:

ΔP_T = 678.55 Pa

where q_0 = 591.87 Pa

Since $Q = A_0 V_0$, the required fan capacity was

$Q = 49.5\ m^3/s$

The shaft power was estimated from

$$W = \frac{\Delta P_T Q}{\eta} \qquad (4.37)$$

for an assumed 75 % fan efficiency

W = 44.784 kW

The power factor of fan from equation 4.1 is found to be as:

λ = 1.5286

The total length of the prototype is found to be

L_T = 16.82 m

4.5 DESIGN OF A MODEL OF THE PROTOTYPE TUNNEL

After the prototype tunnel had been designed, a 1/7 model of it was designed according to the same design procedure. The design Reynolds number of the model was choosen as 2.18×10^5 from figure 3.1 in a way so as to nullify the effect of relative roughness. In this way it is possible to make a sound similarity analysis between the prototype and the model. Using $Re' = 2.18 \times 10^5$, the test section velocity of the model tunnel was determined as 21 m/s.

The hydraulic losses of components of the model tunnel is listed in Table 4.4. The following parameters for the model were determined by

using equations 4.21, 4.36, 4.37 as:

$\Delta P_T' = 286.67$ Pa

$Q' = 0.64264$ m^3/s

$W' = 245.64$ W

$\lambda' = 1.5947$

A computer program was prepared in order to determine the total hydraulic loss coefficients and the system characteristics of the model and prototype for a range of Reynolds numbers covering the operation range of both tunnels. The computer program is given in Appendix 4.

The variation of total hydraulic loss coefficient K_T, with Reynolds number or in other words the variation of Euler number with respect to Reynolds number, both for prototype and model are presented in figure 4.11. From this figure, the hydraulic loss coefficients of the model and the prototype were same at the operation points where Re = Re'. However, at respective design points of the model and the prototype Re ≠ Re'; therefore, their loss coefficients were not equal to each other. This does not imply that the tunnels were not similar.

The relative roughness of the prototype tunnel which would be constructed from pine plywood was determined as 0.000083. As is seen from figure 3.1, there is no effect of relative roughness on the friction factor up to Re = $5x10^5$. Since E = $f'(f)$, after this value of f, the Euler number of prototype tunnel deviate from the curve that was obtained from the computer program evaluated for fully smooth turbulent flow. This deviation is shown in figure 4.11.

4.6 SYSTEM CHARECTERISTICS OF DESIGNED TUNNELS

The calculated system charecteristics of the prototype and the model are given in figure 4.12 and 4.13 respectivelly. The trends of these curves were similar which showed that it is possible to reduce

these curves into a nondimensional curve.

To nondimensionalize the system charecteristic curves both for the model and prototype, the design Reynolds number of the model tunnel was selected as the reference Reynolds number. The system parameters, H and Q were nondimensionalized according to H_{Re} and Q_{Re} values corresponding to the reference Reynolds number both for the model and the prototype tunnels. Therefore, nondimensional relations which were obtained from equation 3.26 were used for the model as:

$$\overline{H}' = K_r \overline{Q}'^2 \tag{4.38}$$

and for the prototype:

$$\overline{H} = K_r \overline{Q}^2 \tag{4.39}$$

The calculated results are tabulated in Table 4.4. The dimensionless H-Q charecteristics of both tunnels were plotted on a log-log paper as shown in figure 4.14. The system charecteristics of both the model and the prototype tunnels fall on the same line. This means that the proportionality constant, K_r have the same value for both tunnels at the same Reynolds number.

If we consider the effect of the relative roughness on the dimensionless H-Q characteristic of the tunnels at Re $> 5x10^5$ the characteristic line deviates from fully smooth curve as shown in figure 4.14.

4.7 CONCLUSIONS

In this chapter a prototype blower wind tunnel and its model were designed using similarity analysis which was derived in chapter 3

The technical drawings of the prototype and model tunnels are presented in Drawings section of this thesis. Pine wood was selected as the construction material for the framework of both tunnels. For the

prototype tunnel walls plywood was proposed. Since the model tunnel must be as smooth as possible to obtain the same relative roughness in the model and prototype for full similarity, the walls of the model tunnel were constructed from formica covered plywood and perspex except the contraction walls where plywood was used.

Table 4.1. Contour of the Contraction Walls and Their Developments

x/b_c	z/b_c	y/b_c	l_y/b_c	l_z/b_c
0	1	0.668	0	0
0.1	0.998	0.667	0.100	0.100
0.2	0.993	0.662	0.200	0.205
0.3	0.983	0.655	0.300	0.315
0.4	0.970	0.646	0.400	0.420
0.5	0.954	0.636	0.500	0.530
0.6	0.933	0.622	0.600	0.642
0.7	0.908	0.605	0.700	0.750
0.8	0.877	0.584	0.802	0.862
0.9	0.837	0.558	0.905	0.970
1.0	0.788	0.525	1.010	1.082
1.1	0.730	0.487	1.122	1.200
1.2	0.660	0.440	1.230	1.330
1.3	0.583	0.388	1.345	1.450
1.4	0.502	0.335	1.460	1.580
1.5	0.435	0.290	1.565	1.700
1.6	0.389	0.260	1.665	1.810
1.7	0.363	0.242	1.765	1.920
1.8	0.349	0.233	1.870	2.025
1.9	0.341	0.228	1.965	2.125
2.0	0.334	0.224	2.060	2.230

Table 4.2. Section Coordinates of the Streamlined body

$\frac{x}{L} * 100$	$\frac{2y}{b_s} * 100$
0	0
1.25	27.0
3.0	40.0
5.0	50.2
10.0	66.8
20.0	84.4
30.0	93.4
40.0	99.0
42.0	100.0
50.0	97.7
60.0	90.5
70.0	78.2
80.0	60.0
90.0	34.7
95.0	18.7
100.0	0

Table 4.3. Hydraulic Losses of Prototype Tunnel Components at Design Point

TUNNEL COMPONENTS	K_i	$\frac{A_0}{A_i}$	$K_i(\frac{A_0}{A_i})^2$
Test section	0.0367	1	0.0367
Contraction	0.1856	1/9	0.00229
Screen	1.0830	1/9	0.01337
Honeycomb	1.5200	1/9	0.01876
Wide angle diffuser	0.3000	1/2.31	0.05622
SUM			0.12734
Miscelleneous losses	0.15*SUM		0.019101
Exit energy loss	1.0	1	1.0
TOTAL, K_T			1.14644

Table 4.4. Hydraulic Losses of Model Tunnel Components at Design Point

TUNNEL COMPONENTS	K'_i	$(\frac{A_0}{A_i})'$	$K'_i(\frac{A_0}{A_i})'^2$
Test section	0.05124	1	0.05124
Contraction	0.2396	1/9	0.00296
Screen	2.2078	1/9	0.02726
Honeycomb	2.65	1/9	0.03271
Wide angle diffuser	0.3	1/2.31	0.0562
SUM			0.1704
Miscelleneous losses	0.15*SUM		0.02555
Exit energy loss	1.0	1	1.0
TOTAL, K'_T			1.1959

Table 4.5. Nondimensionalized System Characteristics

PROTOTYPE			MODEL		
V_o (m/s)	$\overline{Q}$	$\overline{H}$	V_o' (m/s)	$\overline{Q}'$	$\overline{H}'$
1	0.333	0.115	3	0.143	0.0218
2	0.667	0.450	5	0.238	0.0595
3	1.000	1.000	7	0.333	0.115
4	1.333	1.761	8	0.381	0.150
5	1.667	2.734	10	0.476	0.232
6	2.000	3.916	12	0.571	0.333
7	2.333	5.311	14	0.667	0.450
8	2.667	6.916	16	0.762	0.586
9	3.000	8.733	18	0.857	0.738
10	3.333	10.761	19	0.904	0.821
11	3.667	13.000	20	0.952	0.909
12	4.000	15.452	21	1.000	1.000
$Re = 2.186 \times 10^5$ $Q_{Re} = 4.5\ m^3/s$ $H_{Re} = 0.54872\ m$			$Re' = 2.186 \times 10^5$ $Q'_{Re} = 0.64264\ m^3/s$ $H'_{Re} = 26.8839\ m$		

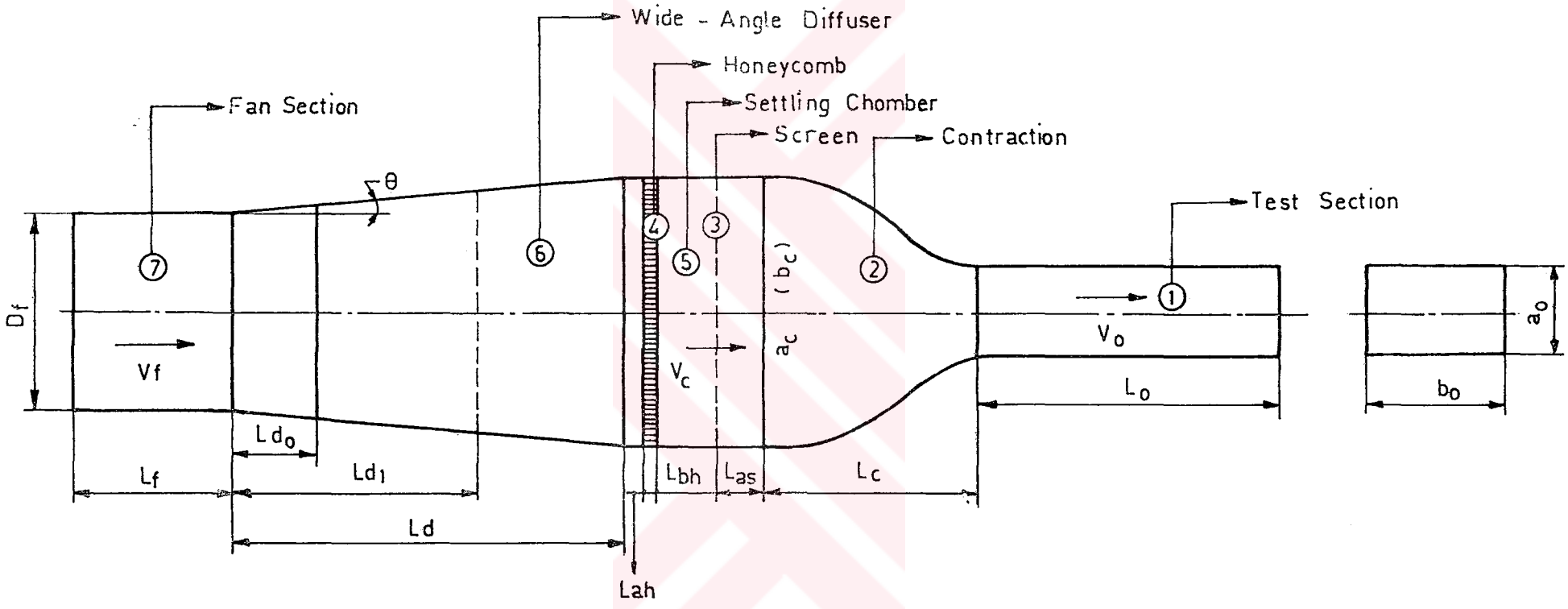

Figure 4.1. The Main Components of a Typical Blower Wind Tunnel

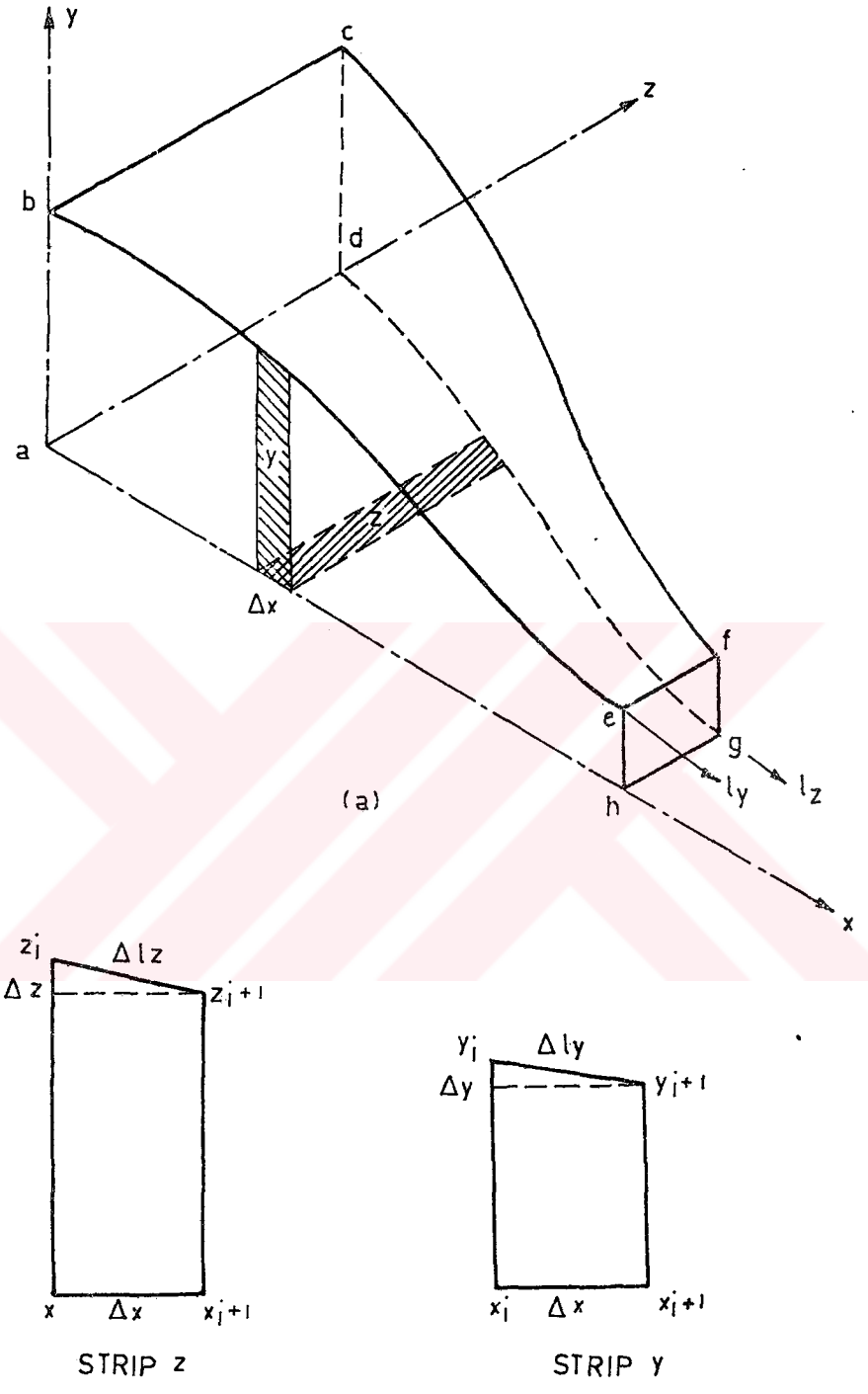

Figure 4.2. General View of one Quadrant of the Contraction

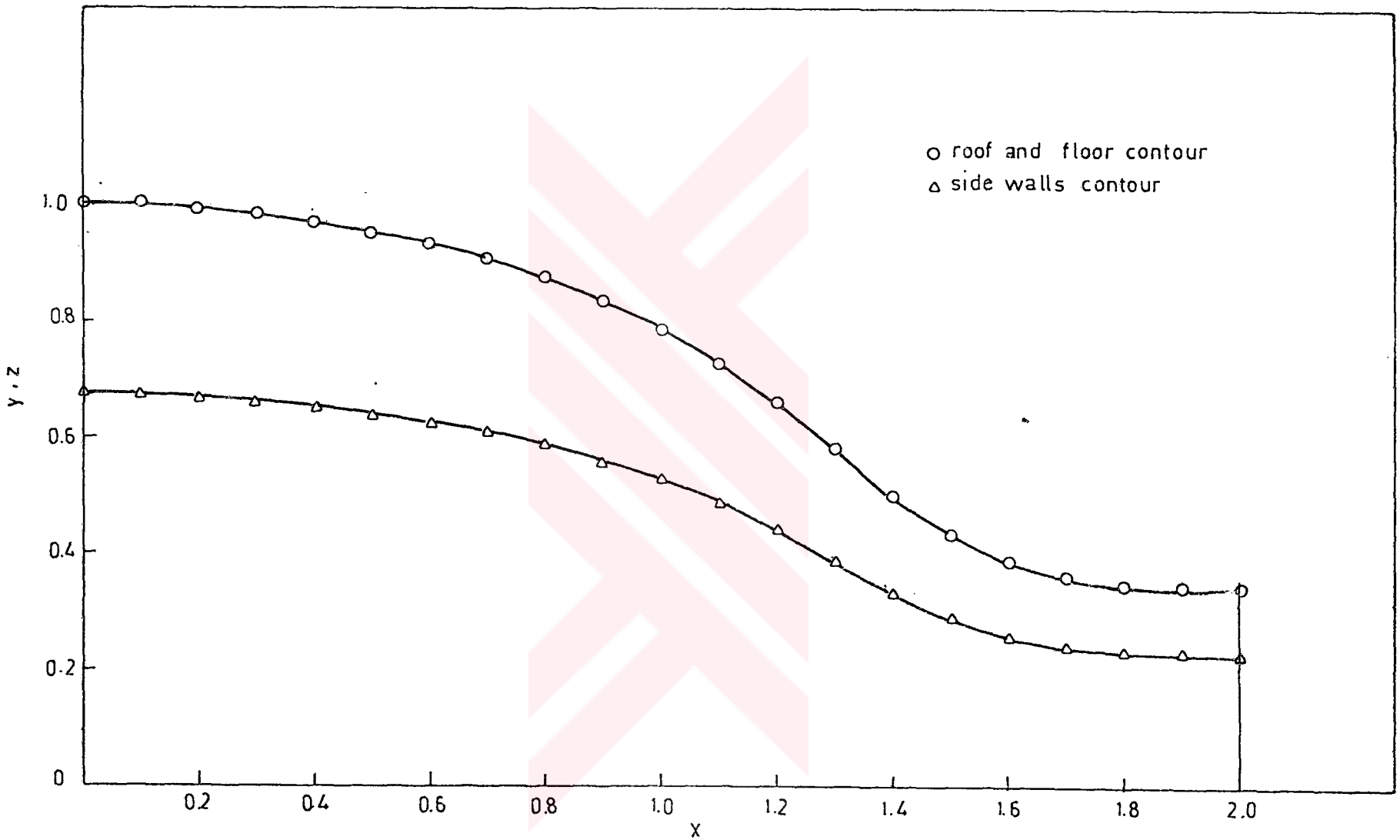

Figure 4.3. The Contraction Contours

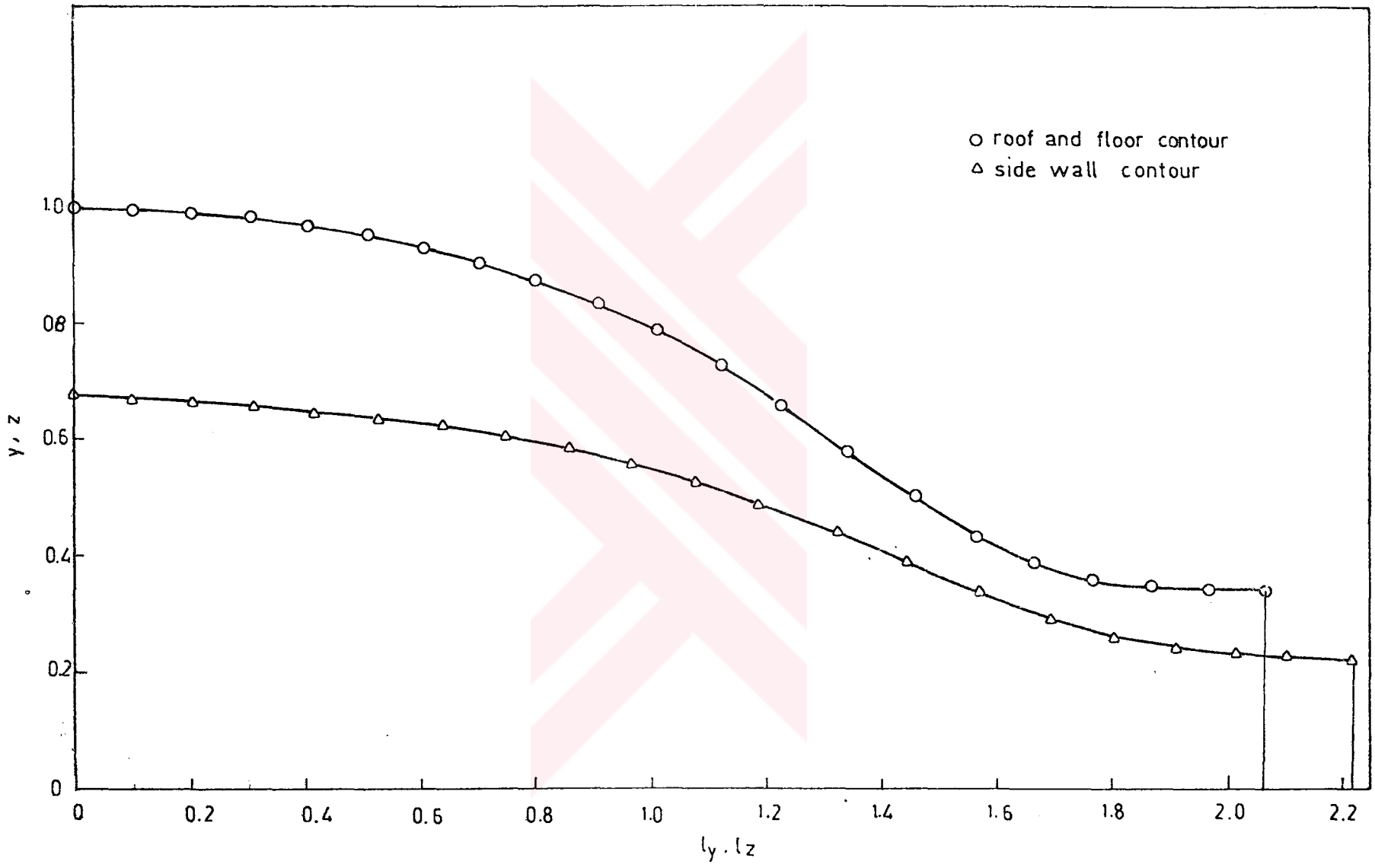

Figure 4.4. Developments of the Contraction Surfaces

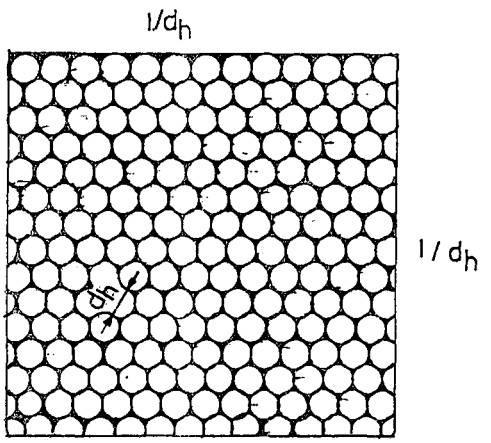

Figure 4.5. Honeycomb Cell

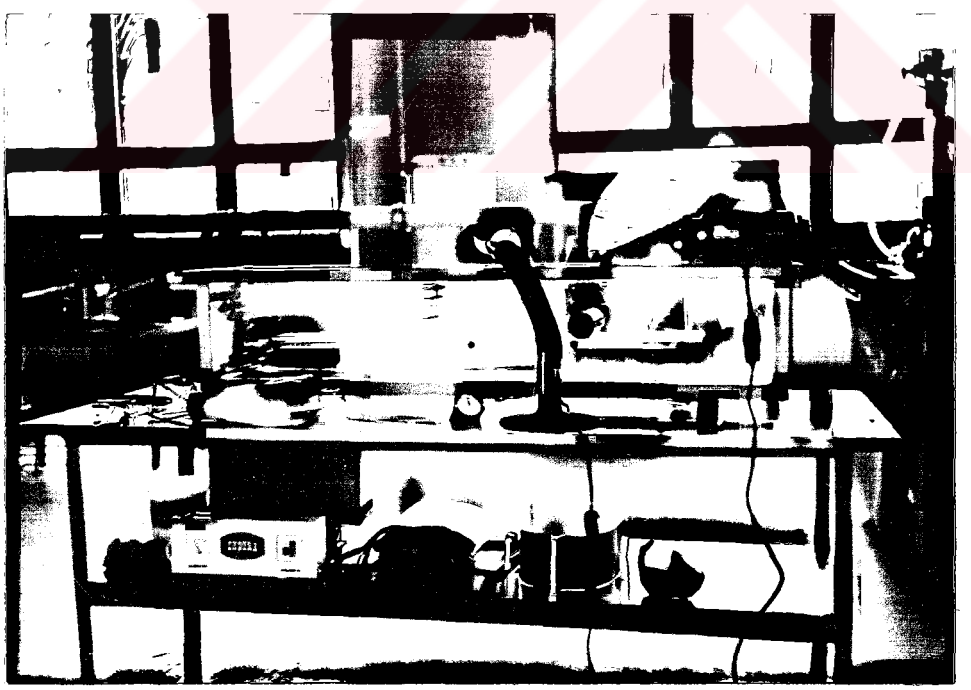

Figure 4.6. Tested Honeycomb in the Water Channel

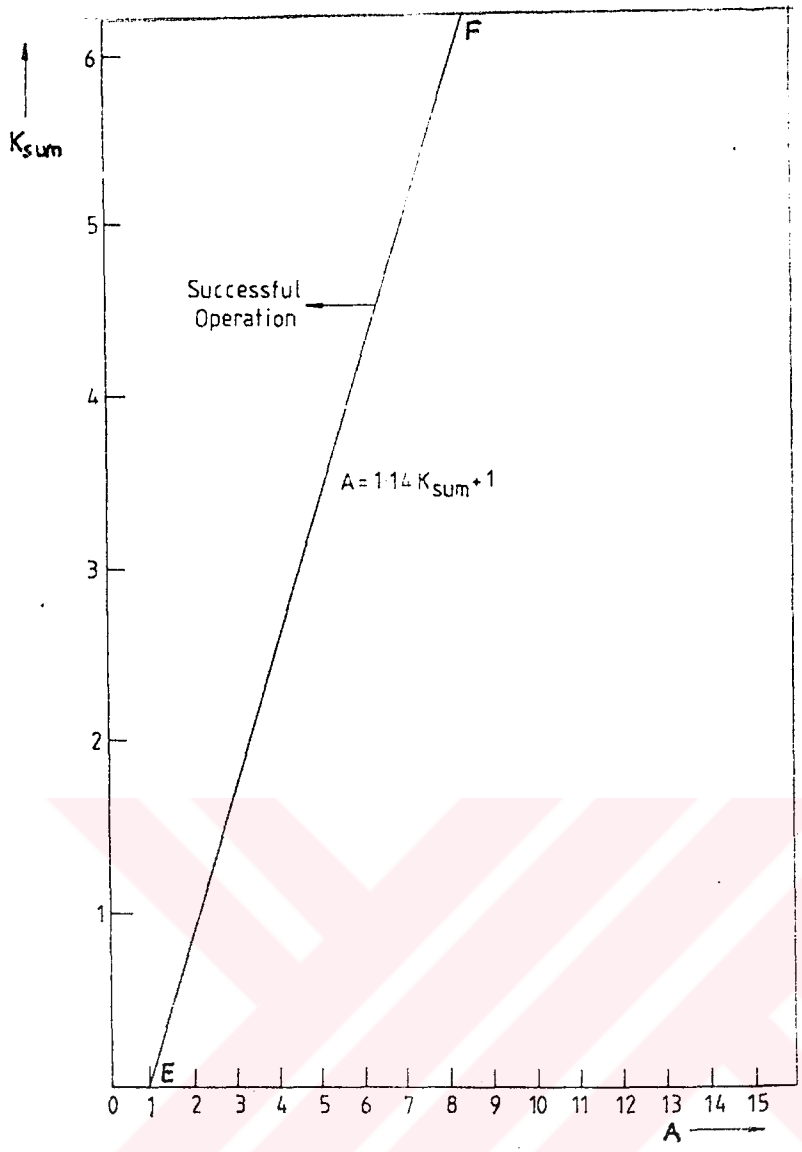

Figure 4.7. Overall Pressure Drop Coefficient Requirements for a Diffuser with Screens [6], [7]

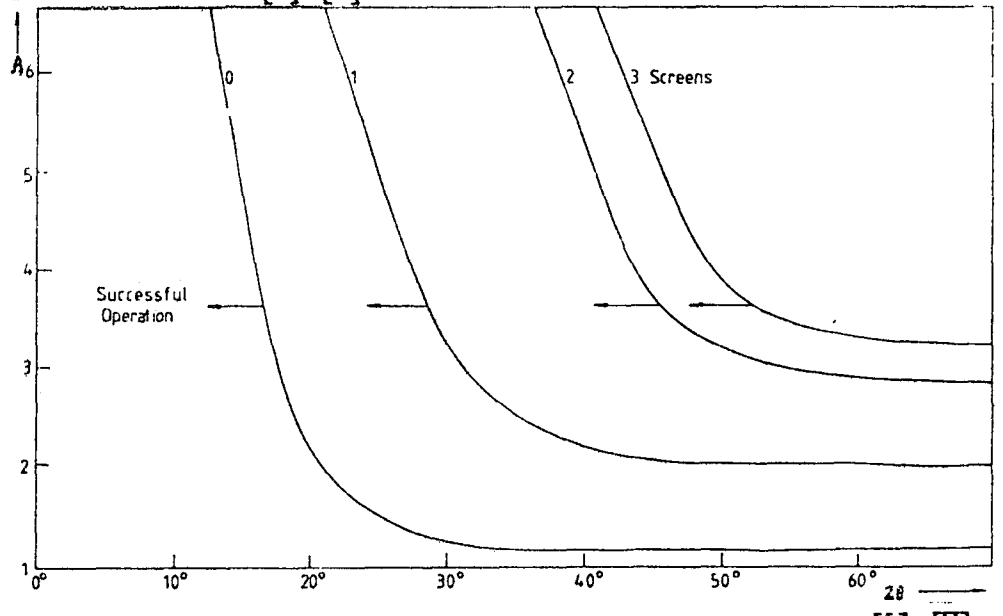

Figure 4.8. Design Boundaries for Diffusers with Screens [6], [7]

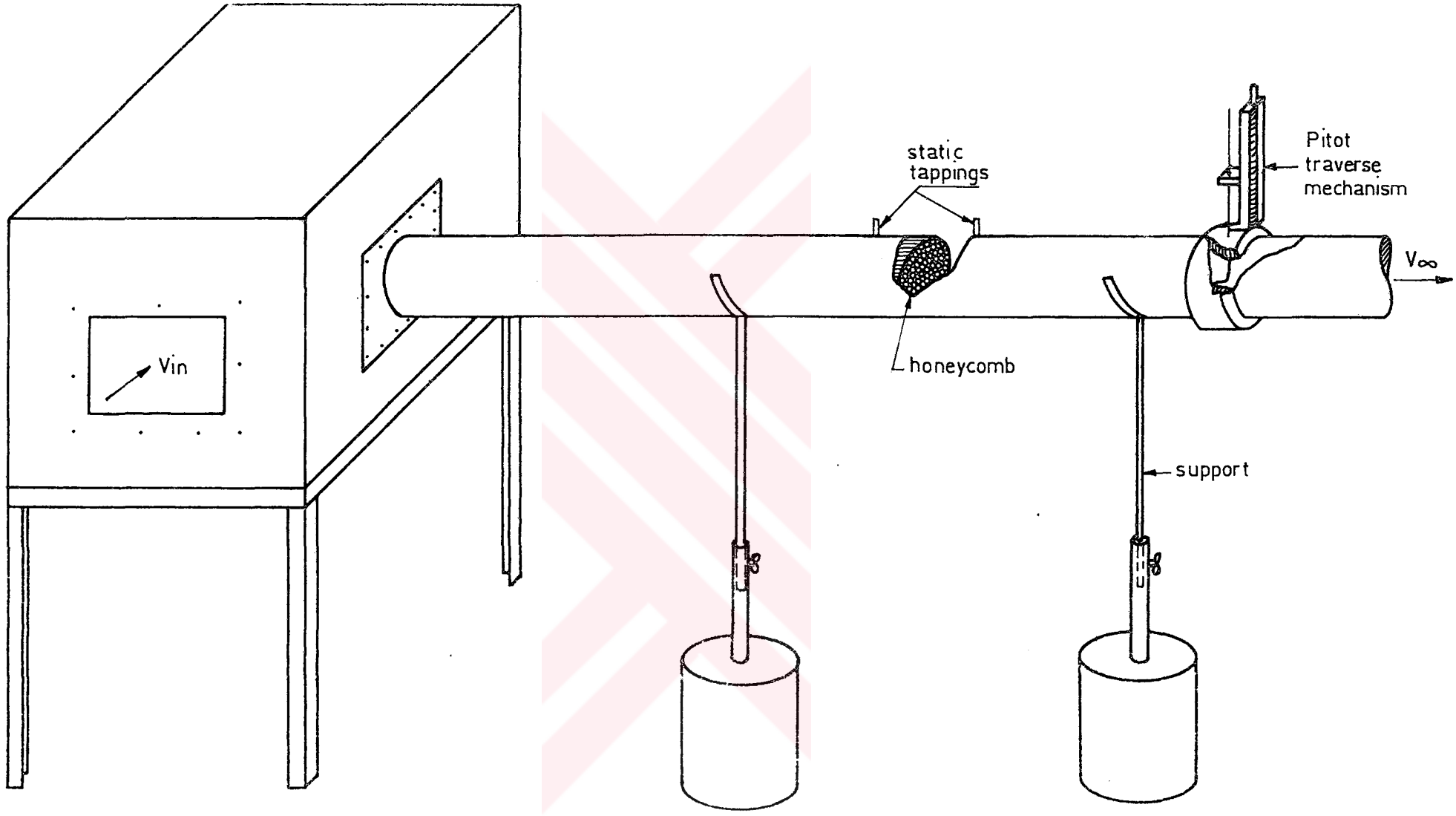

Figure 4.9. Air Rig for Honeycomb Testing

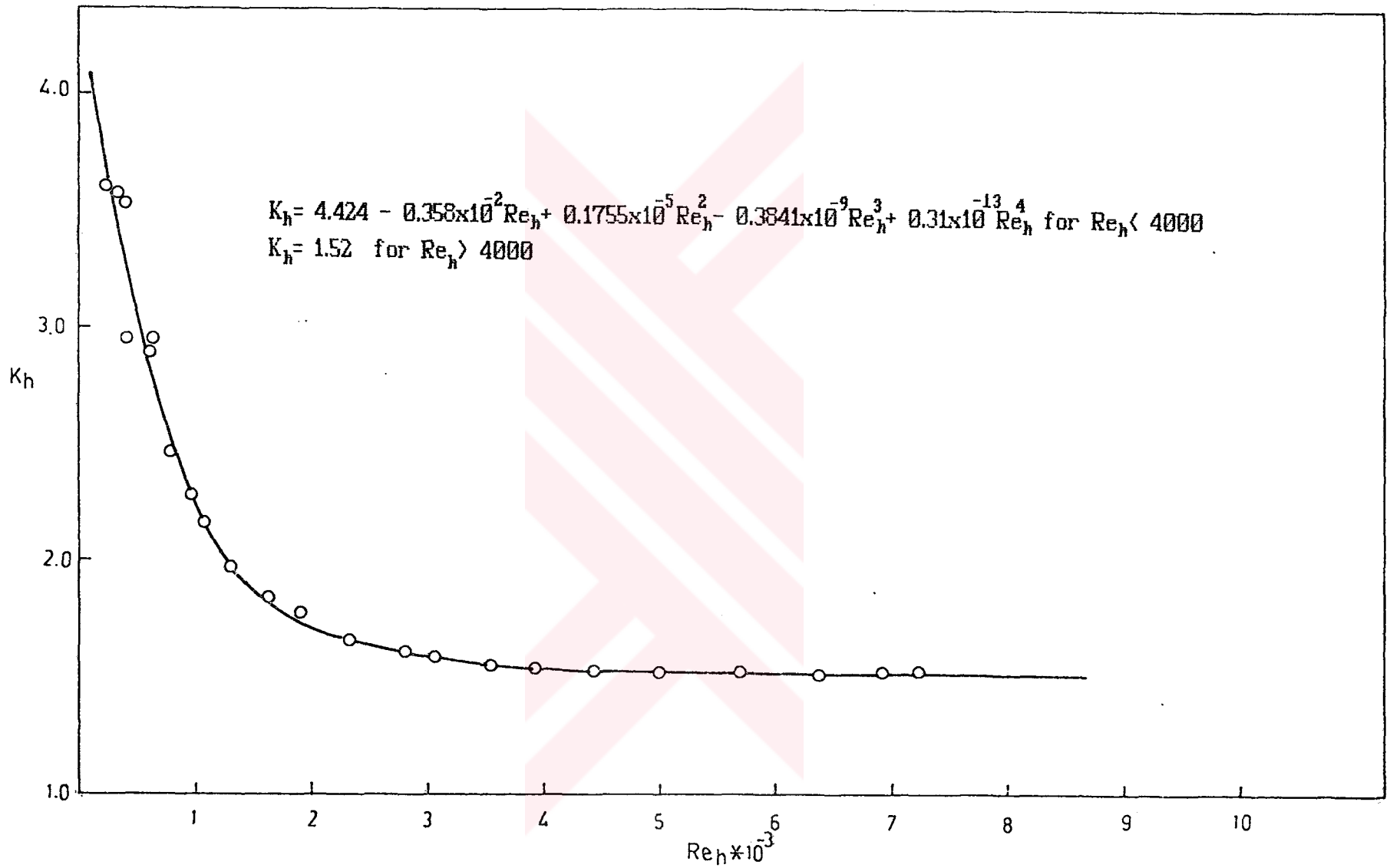

Figure 4.10. Variation of Pressure Loss Coefficient of Honeycomb with Honeycomb Reynolds Number

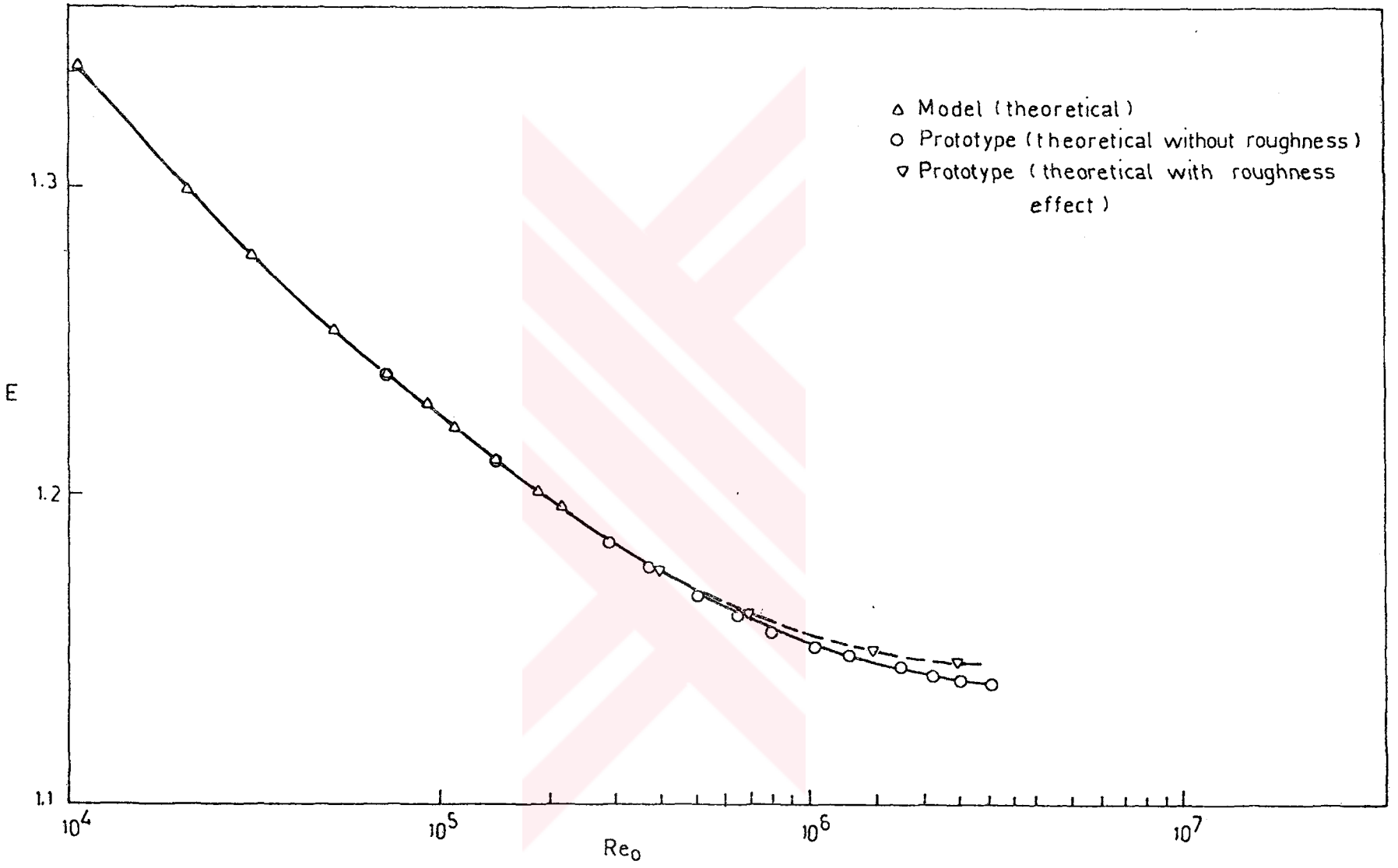

Figure 4.11. Variation of Euler Number with Reynolds Number for Designed Model and Prototype Tunnels

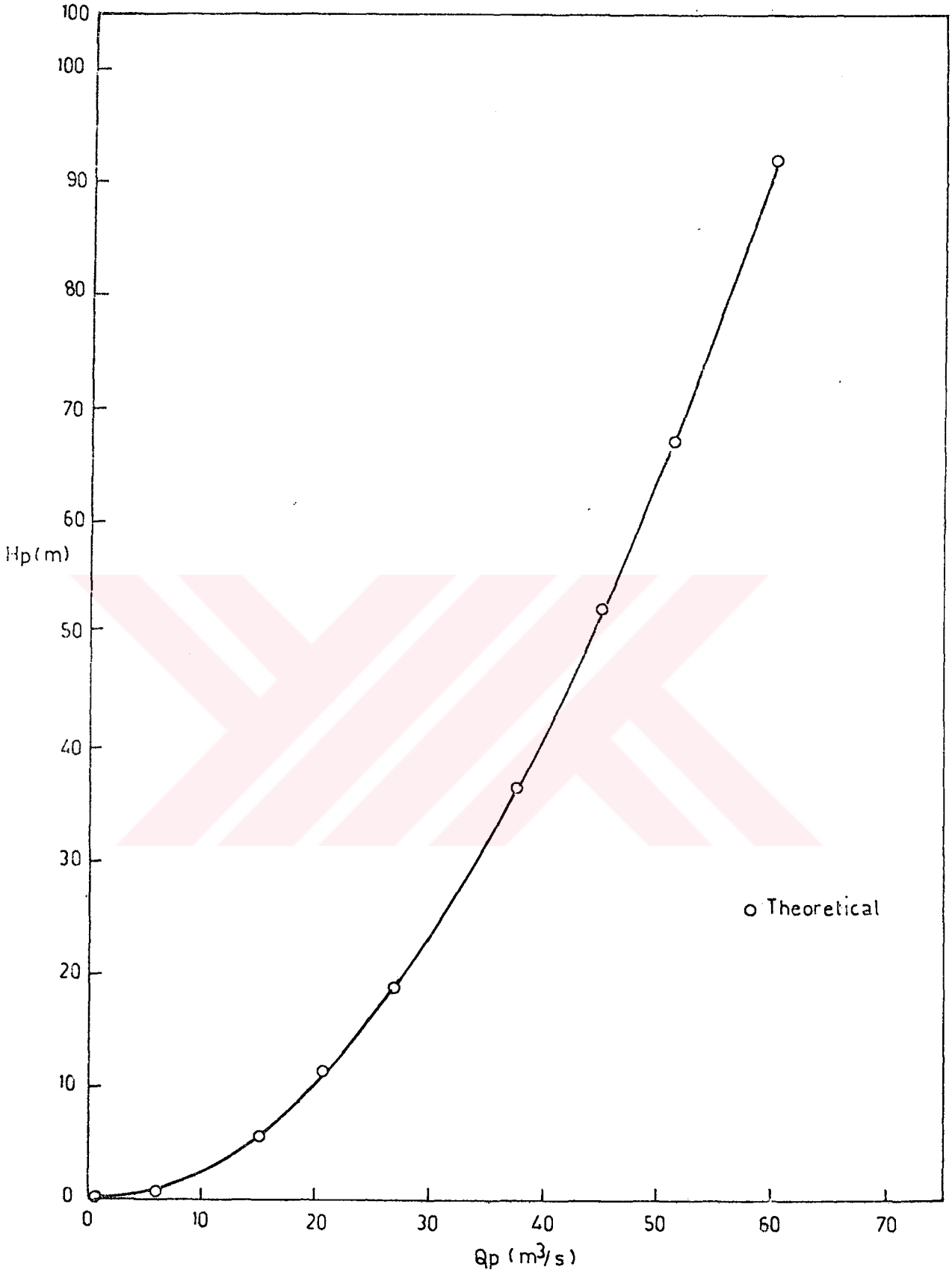

Figure 4.12. System Characteristic of the Prototype Tunnel

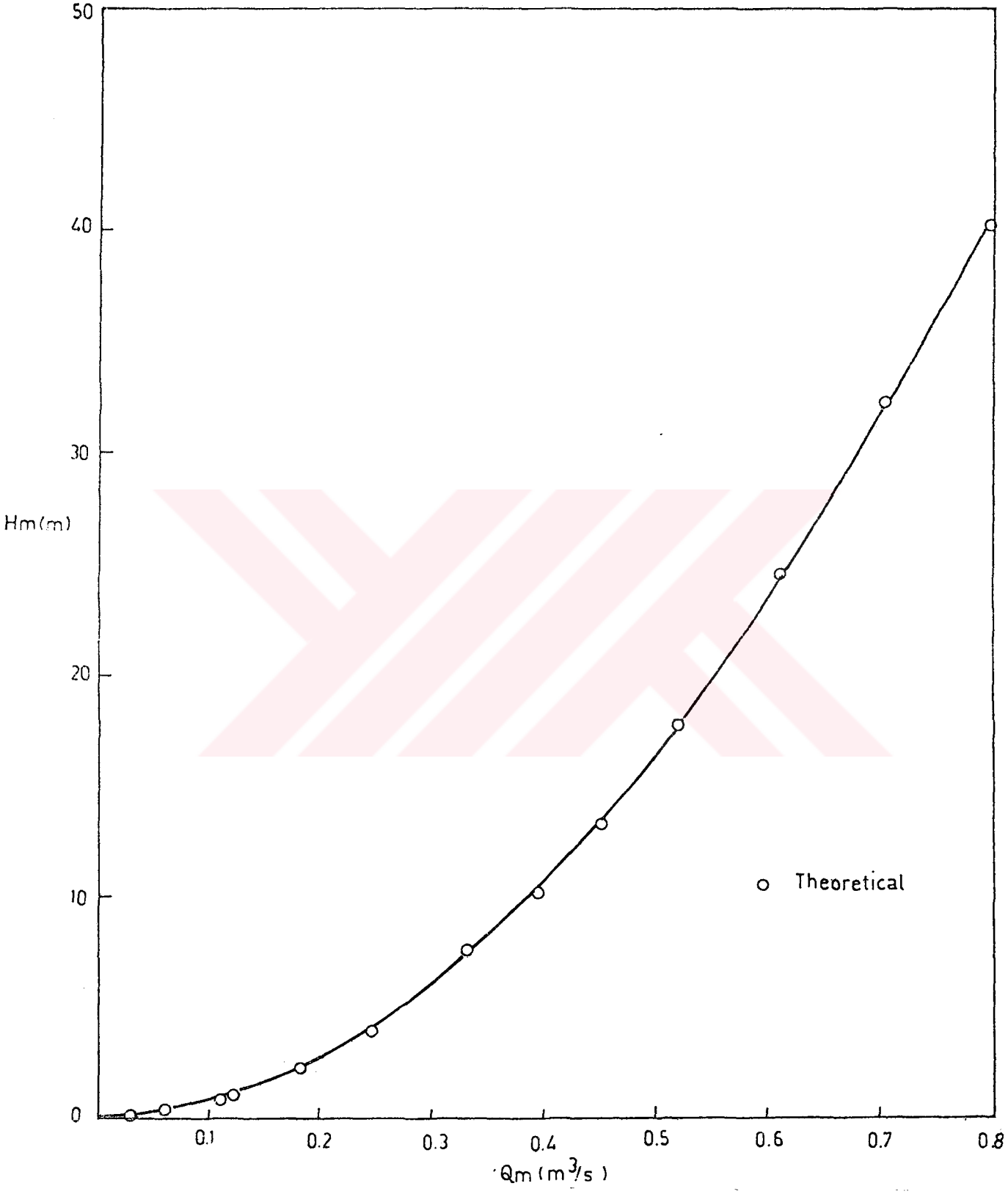

Figure 4.13. System Characteristic of the Model Tunnel

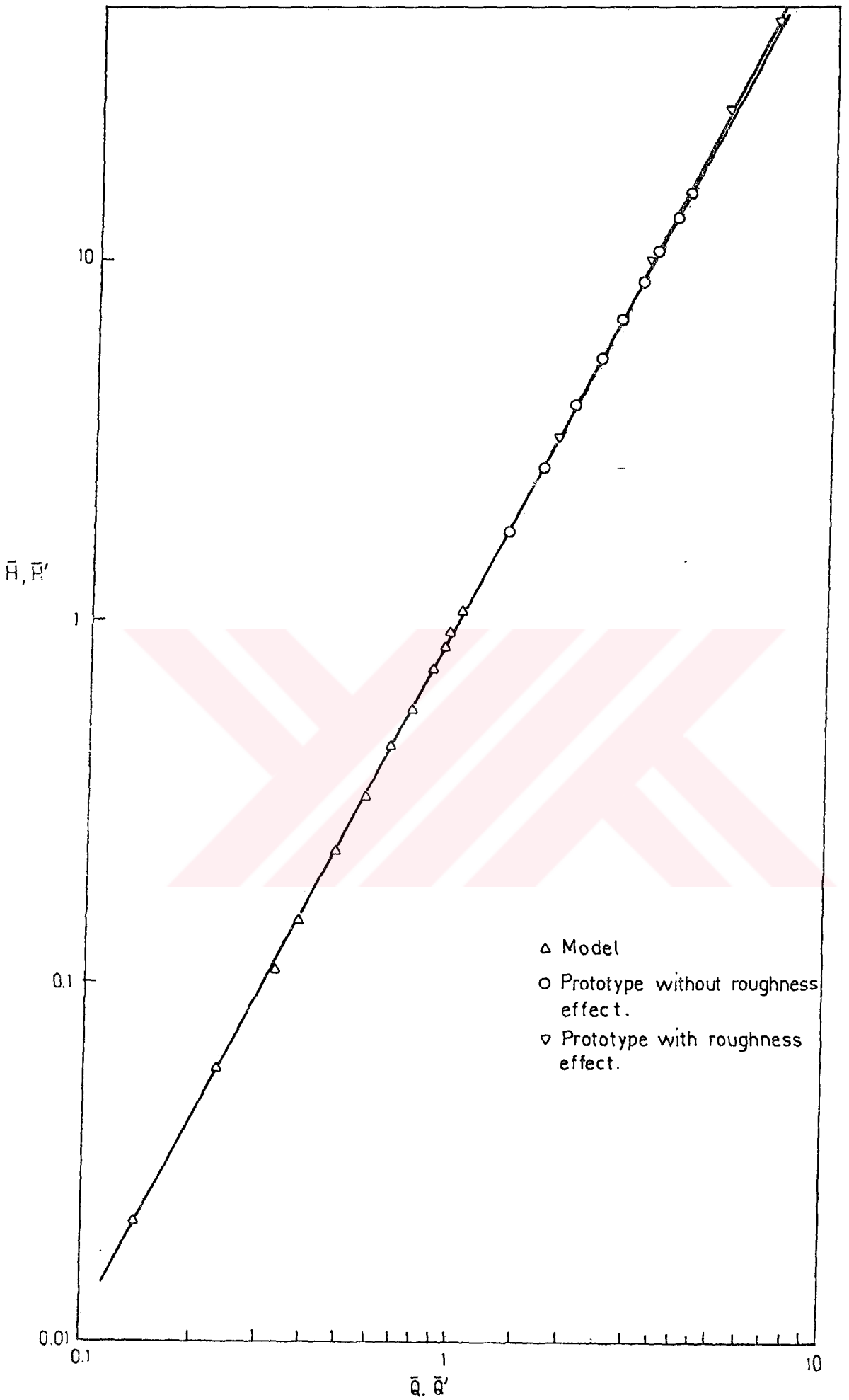

Figure 4.14. Dimensionless System Characteristics of the Designed Tunnels

CHAPTER 5

CONSTRUCTION AND INSTRUMENTATION OF THE MODEL BLOWER WIND TUNNEL

5.1 INTRODUCTION

To predict the performance of the designed prototype blower wind tunnel, such as flow quality of the test section, performance of the tunnel components etc., a model of this tunnel was required. Therefore, its 1/7 model which was designed in chapter 4 was constructed.

In this chapter, the construction and instrumentation of the model blower wind tunnel is presented.

5.2 CONSTRUCTION OF THE MODEL TUNNEL

The designed model, which has several components was constructed from pine wood, formica covered plywood and perspex. The technical drawings of the tunnel and its components are given in Drawings section of this thesis.

Each component of the tunnel was manufactured seperately. General view of the model tunnel is shown in figure 5.1. Fan section of the tunnel was produced from a bulk of wood by turning on a lathe. To prevent the eccentricity between the fan section and first part of the wide angle diffuser which was the transition region from circular to rectangular crossection, the circular part of this section was turned together with the fan section. A hand-held electric drill which was mounted on the tool holder of the lathe was used to provide the transition to rectangular crossection with rounded corners. The walls of the second and third part of the wide angle diffuser were prepared from formica covered plywood.

The frameworks throughout the tunnel were manifactured using the dowel joints as shown in Drawing 101. All of the removable frames were covered with sticky sponge strips to prevent air leakage.

The frameworks of wide angle diffuser and settling chamber were prepared seperately, after which they were assembled to produce the skeleton of these section. The prepared walls of wide angle diffuser were lined in the frameworks. After that, the corner fillets of the wide angle diffuser were placed into it. The corner fillets are shown in Drawing 104. The second and third part of the diffuser were cut so as to place a screen or other boundary layer control devices such as a honeycomb or perforated plate between them.

The construction of the contraction section started with the production of the corner contours using sheet metals. Prepared sheet contours were welded side by side to produce corner angles of the contraction. The frame of the contraction section was constructed by welding these contours to the inlet and outlet contraction frames which were produced from steel angles as shown in Drawing 106. The wetted plywood was riveted to these sheet metal angles by means of aluminum rivets. The contraction walls were manufactured from plywood. The development of the contraction walls are given in Drawings 107 and 108.

The honeycomb was placed in a frame which was removable from the settling chamber, therefore, different honeycombs may be used by just changing the frame. The settling chamber arrangement with honeycomb frame are shown in Drawing 112.

The roof and one of the side walls of the test section which are shown in figure 5.2 were formed from 3 mm thick perspex, while floor of the test section was constructed out of duplex formica covered plywood. This part was designed in such a way to enable the placement of a model in the test section by removing it. The other side wall is also movable and it was produced from two layer perspex to provide the sealing of the test section wall.

The nacelle, shown in Drawing 114, was manifactured from pine wood by using copy arrangement of the lathe so that the desired profile was given preciselly. The straightener vanes which connect the nacelle to the fan section were also produced from pine wood in the airofoil shape as shown in Drawing 115

The constructed tunnel was mounted an a large table. The drive system and the fan unit was mounted on another table to prevent the vibration tranmission to the the tunnel.

The used drive system and fan was available in the laboratory. Drive unit consists of a 0.55 kW, 1410 rpm electric motor and a multi-stepped V-belt pulley arrangement which was designed to provide five different shaft speeds namely: 825, 1125, 1500, 2000 and 2500 rpm. The drive shaft was supported by the ball bearings. The bearing supports of the drive shafts are mounted on a chasis.

5.3 THE MEASURING INSTRUMENTS

5.3.1 The Test Section Yaw Meter Traversing Mechanism

A yawmeter traversing mechanism as shown in Drawing 116 was designed and constructed to determine the spatial variations in the flow direction in the test section. Two linear and one angular motion could be attained by the mechanism. In the spanwise direction the mechanim is carried by an endless helical gear traversing mechanism, while in pitchwise direction only the probe is in motion by the square rod as seen in Drawing 116.

Three-tube yawmeter probe which had been modified from the Conrad yawmeter [45] was designed with a probe angle, θ =35°. Hypodermic needles with a 1 mm outside diameter were used as the yawmeter probe. To prevent the deflection of the needles while honing, the needles were placed in the 35° angled copper tubes of 1 mm inside diameter. Then it was honed in the special honing stone and finished with sandpaper. One hypodermic needle was placed to the

middle of the 2-angled tubes and soldered side by side as shown in Drawing 116 part 8. The produced yawmeter probe was bent to give the proposed dimensions in reference [45].

The rotation of the probe was achieved by a micrometer which was in contact with the rotating arm of the yawmeter. A spring was used to keep the mechanism in desired position, avoiding backlash. The length of the rotating arm is 20 mm. Therefore, the movement of 0.036 mm of the micrometer produces an anglar rotation of 0.1°. Figure 5.3 shows the yawmeter mounted on the test section.

5.3.2 The Free-Stream Velocity And Static Pressure Traverse Mechanism

The variation of the total head over the crossection of the test section was measured with the designed traverse mechanism as shown in Drawing 117. It consists of a plate with a channel to traverse tube carrier by an endless screw. To prevent swaying about the tube carrier a top plate onto the mechanism was mounted. A steel angle with a channel on one side was mounted on the tunnel wall to translate the traverse mechanism into desired position.

The pitot tubes that were used with this traversing mechanism have an internal diameter of 0.85 mm and an external diameter of 2.35 mm. To obtain the insensitivity to yaw angle about ± 23° [4], the tube mouth was holed

An another traversing mechanism was designed and constructed to traverse the total head and static head in the settling chamber. This mechanism consists of a 1.5 m transmission rod on which a key channel was machined along the half of this length and a pitot comb with one static tube as shown in Drawing 118.

5.3.3 The Boundary Layer Traverse Mechanism

The velocity traverses across the boundary layer were made with pulley type traverse mechanism shown in figure 5.4. This mechanism was

designed and constructed by Albayrak in reference [5]. The mechanism carries the flat ended pitot tube on a block that slides up and down on a vertical bar by means of metal ribbon connected to another block. This block moves along a horizontal bar with the micrometer.

The traversing apparatus that was used possessed an amount of backlash of the mechanism, it was very important to take the values of total head in one direction.

By using the double sided sellotape, the traverse mechanism were fixed to the test section floor. A flexible steel cable was used to operate the traversing mechanism from outside of the test section. The micrometer could be read to an accuracy of 0.005 mm.

5.3.5 The Manometers

Two null type micromanometers and one inclined multitube manometer that has 11 measuring tubes were used during the experiments. The static pressures along the tunnel were measured using the multitube manometer. The measurement error in the multitube manometer due to the head difference between the manometer reservoir and tubes was about 0.2 % . One of the null type micromanometers was used to measure the reference velocity and to detect the yaw angle by null reading method, while the other micromanometer was used to measure the total and static heads. The measurement error in the null type micromanometers was about 0.3 %. To increase the sensitivity of the manometers, multitube type was inclined to an angle of 15°, while the others were inclined to 6° with the horizontal.

Alcohol was used as the manometer fluid. The density of the alcohol was measured and found to be 807 kg/m^3.

Figure 5.1. General View of the Model Tunnel

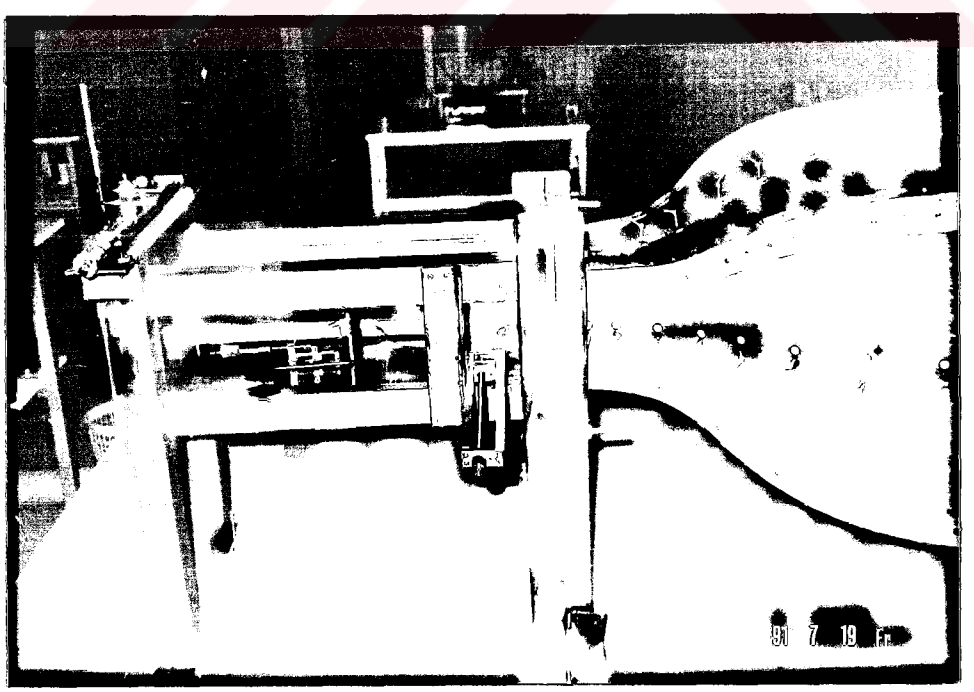

Figure 5.2. Test Section of the Model Tunnel

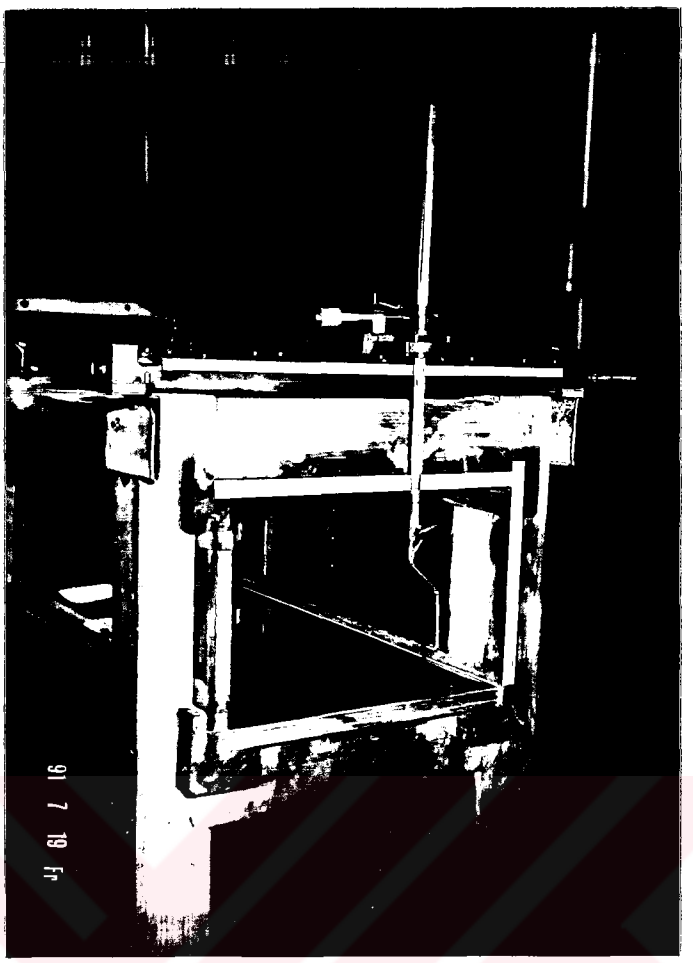

Figure 5.3. Yawmeter Traversing Mechanism Mounted on the Test Section

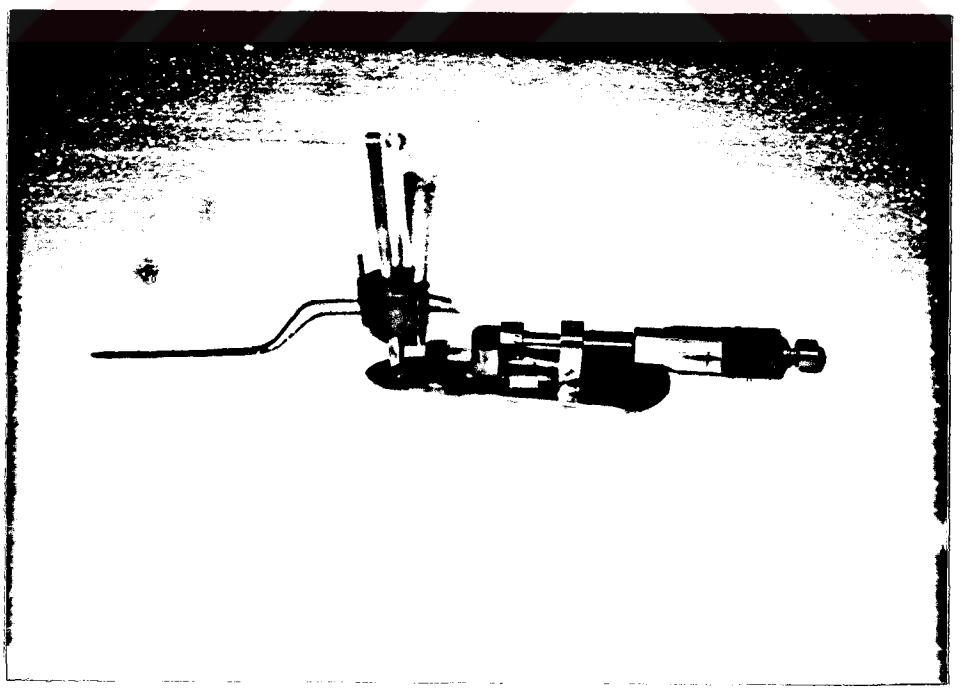

Figure 5.4. Pulley Type Boundary Layer Mechanism

CHAPTER 6

EXPERIMENTAL STUDY AND THE DISCUSSION OF THE EXPERIMENTAL RESULTS

6. 1 INTRODUCTION

The test results of the model tunnel are presented in this chapter. The tests regarding to the flow quality in the test section were performed at different stations along the test section. After this, pressure variations at the contraction and at settling chamber were determined. The system characteristic of the model tunnel was determined, and this was compared with the theoretical design characteristics of the model and prototype tunnels mentioned in chapter 4.

6. 2 EXPERIMENTAL METHODS

6. 2. 1 Reference Tunnel Speed

To measure the reference free stream dynamic head at the test section, a pitot tube was placed to the test section side wall with a static pressure tapping at the same crossection. They were located at a station 5 cm from the test section inlet. Since the test section was very small, a hypodermic needle which had an outside diameter of 0.7 mm was used as the pitot tube to avoid excess wake behind it.

In the determination of all dimensionless free stream velocity and pressure coefficients, the readings taken from the reference pitot tube and static hole was used.

To convert the manometer readings to STP (Standard Temperature and Pressure) conditions a correction chart which was

given in reference [5] was used. The chart shown in figure 6.1 gives the correction factor as a function of ambient temperature and atmospheric pressure. This correction also takes into account of the effect of the temperature variations on the density of the manometer fluid.

The motor speed of the fan was affected from the main line voltage fluctuations during the experiments. Therefore, small variations of the unit Reynolds number could not be prevented.

6. 2. 2 Determination of Mean Velocity at the Test Section

The mean fluid velocity at a crossection of the test section was required to determine the hydraulic resistance of the tunnel and its system characteristic.

To calculate the mean velocity in a rectangular crossection, the graphical integration method or the log-linear method which was described in reference [46] may be used. Since the graphical integration method requires very large number of measurements with less accuracy then log-linear method, the log-linear method was used to determine the mean velocity. Some of the results were checked with graphical integration method and the maximum deviation between them was found to be 1 % . The calculation of mean velocity V , by log-linear method is described in Appendix 5.

6. 2. 3 The Yaw Angle Measurement

The yaw angle traverses were performed using the mechanism which is shown in figure 5.3.

The yaw angle was measured by using the null point detection method. In this method the yaw meter was rotated around itself until the tip of the probe coincides with the direction of the flow. This was detected by the zero pressure difference in the micromanometer which was connected to the angled pitot tubes. Hence, the direction of the flow is a function of the displacement of the micrometer which

was attached to yawmeter mechanism. The yawmeter was calibrated according to the micrometer distance. The calibration curve is given in figure 6.2 and the yaw angle can be expressed as,

$$\alpha = 19.56 - 2.81755\ S \qquad (6.1)$$

where α is the flow angle and S is the distance travelled by the micrometer

6. 2. 4 The Boundary Layer Total Head Traverses

The flat ended pitot tube used in traversing the boundary layer by using the pulley type boundary layer traversing mechanism which was explained in section 5.3.3. The velocity distribution in the boundary layer was determined by measuring the total pressure at different points normal to the surface and by measuring the static pressure. The static pressure was measured by a static pressure tube which was located at a spanwise distance of 3 cm away from the pitot tube.

Due to the high velocity gradient close to the wall, especially in laminar boundary layer, the effective center of the pitot tube is diferrent than the geometric center of the pitot tube as was explained in reference [5]. Therefore, the pitot readings were corrected by shifting the geometric center of the pitot tube by an amount of 0.07 mm.

The boundary layer traversing mechanism was calibrated by using the surface contact indicator which was described in reference [5].

6. 3 THE CALIBRATION OF THE MODEL TUNNEL

The velocity variation across the crossection of the test section was determined by the test section traversing mechanism which was described in section 5.3.2. The velocity readings were non-dimensionalized by using the reference velocity.

The test section crossections were traversed at three different streamwise locations to determine the velocity variations. The velocity readings were obtained for three different reference tunnel speeds. Figures 6.3, 6.4 and 6.5 show the variation of free stream velocity at the streamwise locations of 5 cm, 35 cm and 57 cm downstream from the inlet of the test section for the reference velocities of 8.912 m/s, 6.58 m/s and 4.9 m/s respectivelly.

In figures 6.3, 6.4 and 6.5 the measuring points of the free stream velocity were located along the dimensionless spanwise direction, M_o, at seven dimensionless pitchwise locations of N_o. The pitchwise and spanwise lengths were non-dimensionalized according to the test section height of 143 mm. The center of the cartesian coordinates of the test section crossection is at the left bottom corner of the inlet crossection when looking towards the downstream direction.

It was observed from the above figures that the variation of the free stream velocity over the crossections of the test section were found to be within ± 0.4 % of the mean velocity of the corresponding section. This value is in the recommended range of reference [4].

From figures 6.3, 6.4 and 6.5 the maximum increase of the free stream velocity in streamwise direction is observed as 1.8 % for all reference speeds. This amount of increase is due to the absence of the divergence of the test section walls or the absence of corner fillets.

In figures 6.6, 6.7, 6.8 and 6.9 the velocity maps of the test section crossection at the exit were plotted. The velocity readings across the crossection were non-dimensionalized with the maximum velocity of the crossection. It is observed from these maps that the useful area of the test section crossection, for testing purposes, is about 80 % of the crossectional area of the test section exit. Because of the existence of the secondary flow on the corners, the velocity at the corners were less than the central part. At the central portion of the figures, the velocity variation was ± 0.4 % of the mean value.

The yaw angles were traversed at the exit of the test section

crossection. Figure 6.10 shows the variation of the yaw angle with respect to the dimensionless spanwise direction, M_0, at seven dimensionless pitchwise stations, N_0.

Since the actual direction of the neutral axis of the yawmeter probe could not be known, the yaw angles were measured with respect to an arbitrary reference direction. The flow angularity at the centre of the test section was arbitrarily assumed to be zero and at all other stations flow angularity was measured with respect to the axis passing through the centre of the test section. As is shown in figure 6.10, the variation of the yaw angles at the crossection of the test section exit are between ± 1° including the wall effects. However, at the central part of the crossection this value decreases to ± 0.5°. The maximum variation of the yaw angle was observed on the top-right quadrant of the test section. This variation may be caused from the inhomogenity of the honeycomb at this part.

Figure 6.11 shows the variation of yaw angle along the spanwise direction at the centerline of the test section exit for the reference velocities of 8.81 m/s, 6.475 m/s, 4.84 m/s and 3.6 m/s. According to this figure the variation of the yaw angle for the above mentioned range of velocities is not greater than ± 0.5°.

The yaw angles were also measured from the centerline of the spanwise direction, along the pitchwise axis of the test section exit. Figure 6.12 gives the test results for the same reference velocities of figure 6.11. The maximum variation of the yaw angles in spanwise direction is ± 0.5° while in pitchwise direction is about ± 0.3°.

6. 4 THE BOUNDARY LAYER VELOCITY PROFILES AND THEIR DEVELOPMENT

The boundary layer velocity profiles were measured using the pulley type boundary layer traverse mechanism shown in figure 5.4.

The measurements were taken along the centerline of the floor of the test section at four different streamwise stations from the inlet

of the test section, namely; x = 2 cm, x =17 cm, x = 29 cm, x = 53 cm. The boundary layer velocity profiles at these stations for the unit Reynolds numbers which are $5.96x10^5$, $4.355x10^5$ and $3.25x10^5$ are shown in figure 6.13. From this figure it is seen that the boundary layer thickness at the inlet and exit of the test section are 3 mm and 5.5 mm respectivelly. The measurements are taken at favorable pressure gradient. In order to have a zero pressure gradient in the streamwise direction, the walls of the test section should be diverged by an amount equal to the difference of the boundary layer displacement thickness at inlet and exit of the test section.

The integral quantities of the boundary layer which are the displacement and momentum thicknesses were evaluated using the definitions [42]:

$$\delta^* = \int_0^\infty \left(1 - \frac{u}{U}\right) dy \qquad (6.2)$$

$$\theta = \int_0^\infty \frac{u}{U}\left(1 - \frac{u}{U}\right) dy \qquad (6.3)$$

where δ^* and θ are the displacement and momentum thicknesses respectivelly.

The integration of the equations 6.2 and 6.3 were performed using a computer program which fit a parabolic arc to each three points of the integrand. The displacement thickness and momentum thickness variation along the test section is given in figures 6.14 and 6.15 respectivelly. From this figure the net boundary layer displacement growth, $\Delta\delta^*$, at the centerline of the floor of the test section is found as 0.826 mm. This causes an increase in the exit average velocity of the test section of about 1.9 % . This is in agreement with the results of figure 6.3 which gives an increase of average velocity of 1.8 % .

Assuming the net growth of the displacement thicknesses have the same value at four walls of the test section, the divergence angle, γ, of the test section walls to provide a zero pressure gradient along the

walls were estimated from;

$$\tan \gamma = \frac{\Delta\delta^*}{L_o} \tag{6.4}$$

The divergence angle of one wall is found as 0.083° for the values of $\Delta\delta^*$= 0.826 mm and L_o = 570 mm. However, the construction of the diverged test section wall is difficult. Therefore, the divergence of the corner fillets were recommended in reference [5]. The fillet crossection of the test section inlet and divergence angle were found from;

$$A_1 = A_2 - 2cd \tag{6.5}$$

where A_1 and A_2 are the crossection areas of the test section inlet and exit respectivelly. c and d are the fillet dimensions at the inlet of the test section as shown in figure 6.16. Since the exit crossectional area of the test section is;

$$A_2 = A_o = 0.030602 \text{ m}^2$$

and inlet area of the test section is;

$$A_1 = \frac{A_o}{1.019} = 0.0300314 \text{ m}^2$$

The inlet corner fillet dimensions were found as; c = 13.8 mm and d = 20.7 mm with an angle of divergence 1.154°.

For the prototype test section the dimensions of the corner fillets were recommended as c = 97 mm, d = 145 mm with a divergence angle of 1.154°.

Figure 6.17 gives the displacement thickness and momentum thickness which are multiplied with the square root of the reference Reynolds number, $\sqrt{\frac{U_{ref}}{\nu}}$, with respect to x so as to observe the variation of the integral quantities at different unit Reynolds

numbers. The maximum variation between the displacement thickness corresponding to the respective unit Reynolds numbers are 6.6 % while the maximum variation between momentum thicknesses are 7.43 %.

6. 5 DETERMINATION OF THE TUNNEL PERFORMANCE

To determine the pressure variation at the exit of the wide angle diffuser and inlet to the contraction, the traverse mechanism that was shown in Drawing 118 was used. The measurements were taken from the center of the height of the crossection, along the spanwise direction.

Figure 6.18 shows the experimental results for the four reference velocities namely 8.89 m/s, 6.54 m/s, 4.9 m/s and 3.63 m/s. In this figure, the variation of pressure coefficient at the diffuser exit, Cp_{de}, and at contraction inlet, Cp_{ci} are given with respect to dimensionless width of the settling chamber, M_c. It is seen that Cp_{de} is about ± 5 % of its mean. However, the variation of Cp_{ci} is found as ± 0.5 % of the mean value Cp_{ci}.

The variation of the pressure coefficients along the roof and along one of the side wall of the contraction were determined by measuring the static pressure with static tappings which were placed along the centerline of the walls as shown in figure 5.2. Figures 6.19 and 6.20 give the variation of pressure coefficients, Cp_c, of roof and side wall of the contraction with respect to the dimensionless contraction length, x/L_c. The experiments were done for four reference velocities. As is seen in figures 6.19 and 6.20, as the reference velocity increases the pressure coefficients decreases.

As shown in figure 6.20, flow seperation was not observed along the roof wall of the contraction; whereas at the tested side wall of the contraction flow seperation observed.This is shown in figure 6.19.

Theoretical H-Q characteristics of the model tunnel were compared with the experimentally determined H-Q characteristics. This was accomplished by experimentally determining the head developed by

the fan, H_f, and the flow rate of the fan, Q_f. Therefore, the static pressures of the fan outlet were measured for the four mean tunnel speeds which were calculated by log-linear method given in Appendix 2.

The fan total head were found from equation;

$$H_f = \frac{P_f}{\rho g} + \frac{V_f^2}{2g} \qquad (6.6)$$

where P_f and V_f are the pressure and velocity of the fan outlet. Inserting the expression:

$$V_f = V_o \frac{A_o}{A_f}$$

into the equation 6.5, it is found that;

$$H_f = \frac{P_f}{\rho g} + (\frac{A_o}{A_f})^2 \frac{V_o^2}{2g} \qquad (6.7)$$

Therefore, H_f was calculated in terms of the mean test section velocity and static pressure of the fan outlet. Since the fan discharge was found from, $Q = V_o A_o$, the system characteristic of the model tunnel was constructed. The experimental results are listed at table 6.1. The experimental H_f and Q_f values were plotted on figure 6.21 and compared with the theoretical system characteristic of the model tunnel.

In table 6.1, H_f and Q_f values are also non-dimensionalized in terms of the H'_{Re} and Q'_{Re} values of the model tunnel at reference Reynolds number which was explained in section 4.4. At the reference Reynolds number, Re = 2.18×10^5, the values of H'_{Re} and Q'_{Re} had been calculated and are presented in table 4.5 as;

H'_{Re} = 26.884 m

Q'_{Re} = 0.64264 m^3/s

The experimental $\overline{H}_f$ and $\overline{Q}_f$ results were plotted in figure 6.22 and are compared with the dimensionless theoretical system characteristics of designed model and prototype. As is seen from figure 6.22 the theoretical head requirement of the designed model tunnel overestimates the actual head of the tunnel by about 10 % for the same flowrate.

6. 6 CONCLUSIONS

The model blower wind tunnel was calibrated and the performance of the model tunnel was investigated. Conclusions derived from the test results may be listed as follows:

1. The velocity nonuniformity at the test section was found as ± 0.4 % of the mean value.

2. In the test section, the increase of the free stream velocity in the streamwise direction was 1.8 %.

3. The effective uniform velocity area is 80 % of the test section crossectional area at exit.

4. The variation of yaw angles including the side and corner effects are ± 1°. At the central portion of the test section this value decreases to ± 0.5° in spanwise direction and ± 0.3° in pitchwise direction.

5. The difference of the boundary layer displacement thickness between the inlet and exit of the test section floor is 0.826 mm. To provide a zero pressure gradient in the streamwise direction, a 0.083° tapered test section walls or 1.154° tapered corner fillets with a dimensions of 13.8 mm by 20.7 mm are required.

6. The velocity nonuniformity at the diffuser exit was decreased

by 68.4 % at the contraction inlet with the aid of the honeycomb and screen.

7. The theoretical head requirement of the fan which drives the tunnel at the same flowrate is 10 % greater than the actual head requirement.This imply that the theoretical design calculations overestimate the fan parameters.

Table 6.1. The actual H and Q requirements of the model tunnel

V_0(m/s)	Q_f(m^3/s)	H_f(m)	$\overline{Q}'_f$	$\overline{H}'_f$
3.6	0.11	0.7894	0.17	0.0294
4.94	0.151	1.413	0.233	0.053
6.6	0.203	2.485	0.313	0.0924
9.1	0.2785	4.57	0.43	0.17

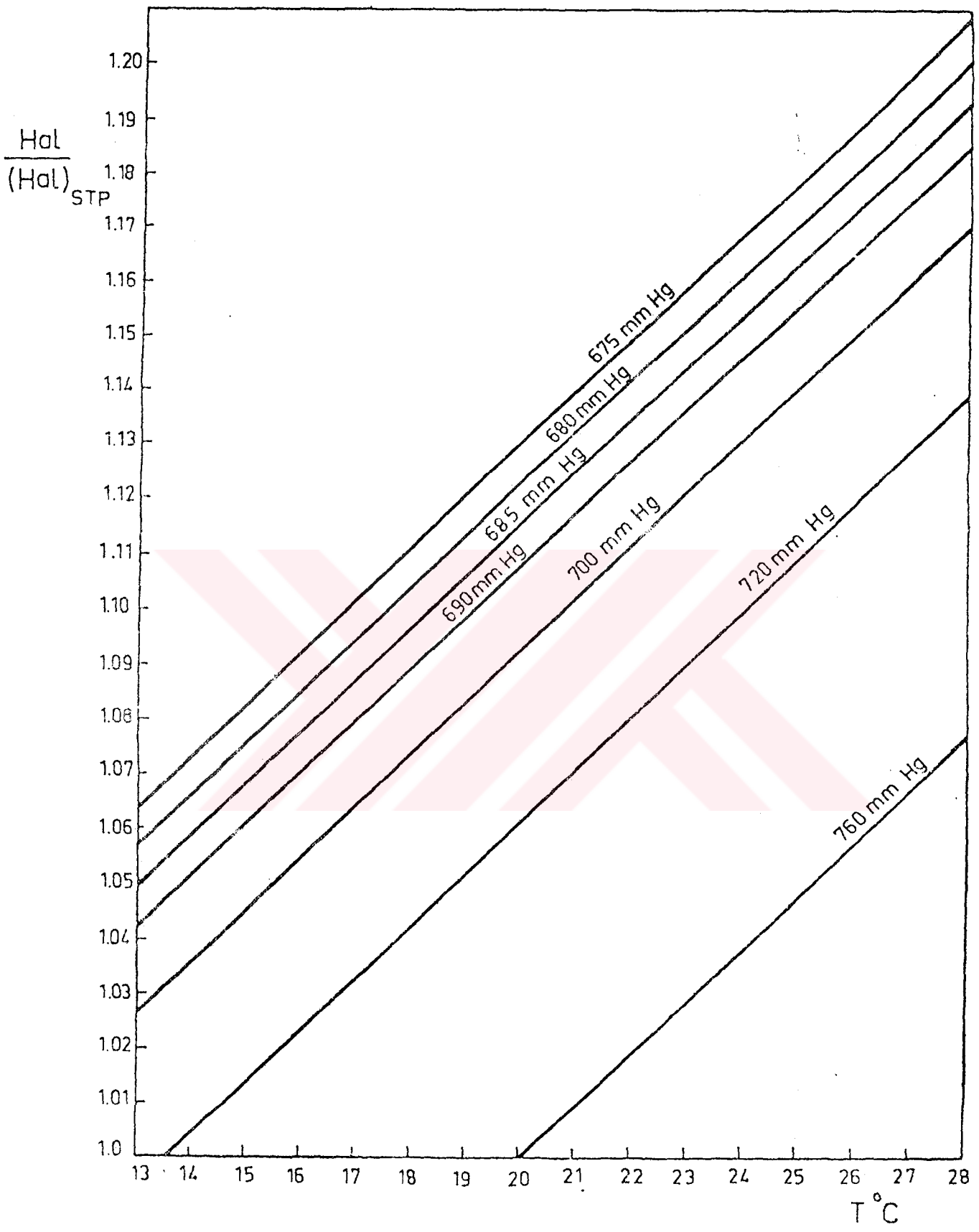

Figure 6.1. Diagram to Find the Head of Alcohol Manometer for Constant Unit Reynolds Number Tunnel Operation

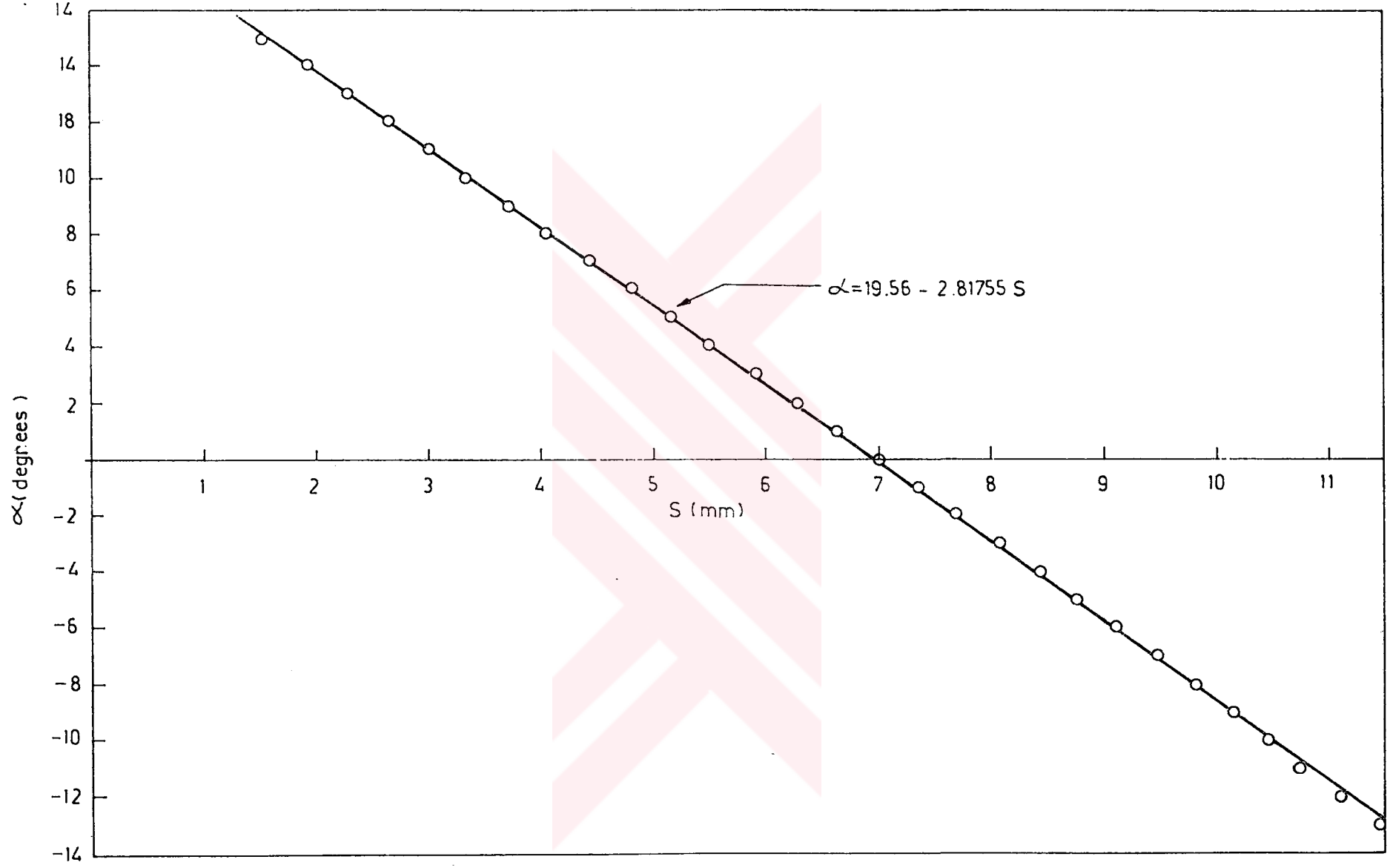

Figure 6.2. Yawmeter Calibration Curve

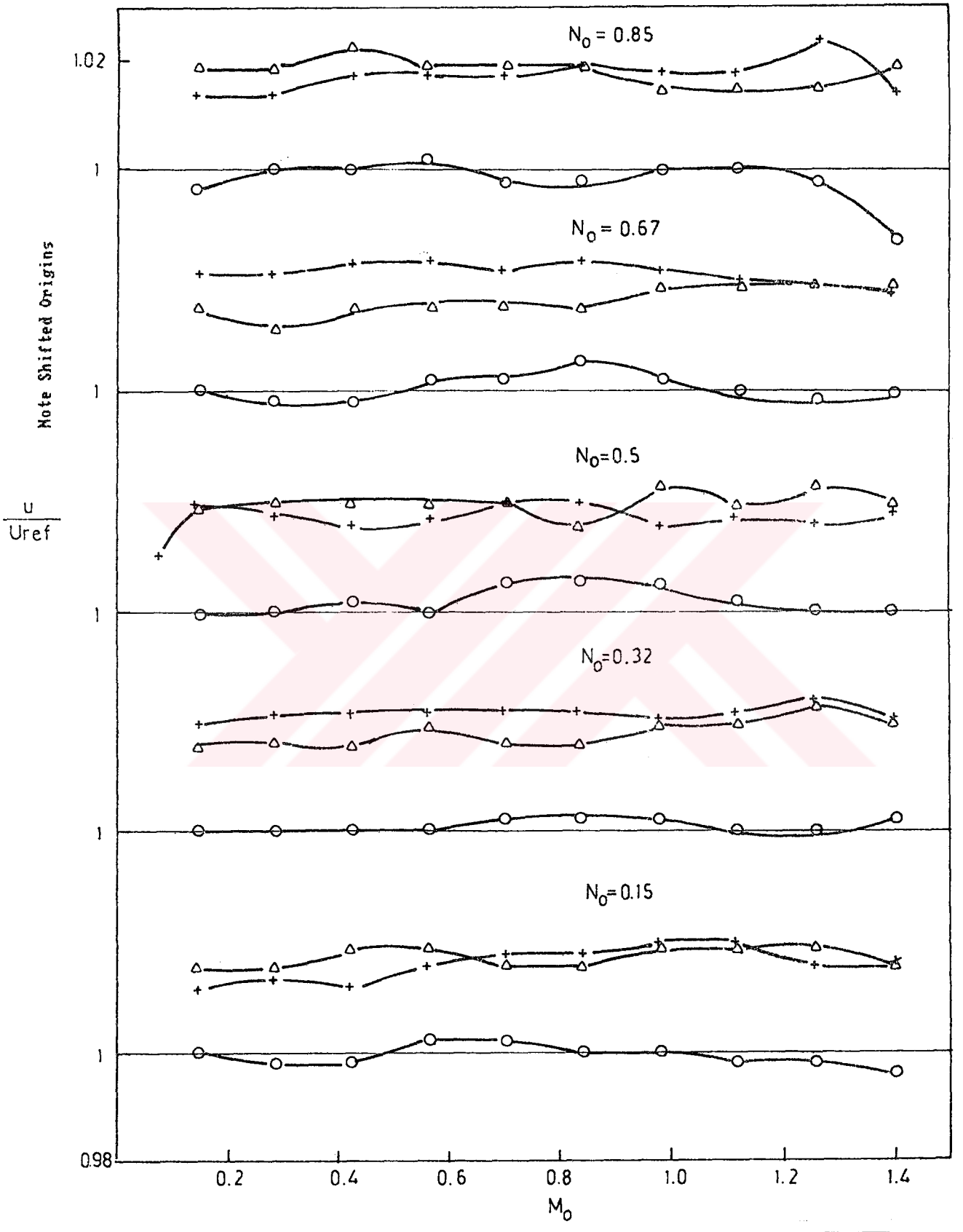

Figure 6.3. Variation of the Free-Stream Velocity over the Crossection of the Test Section for U_{ref} = 8.912 m/s

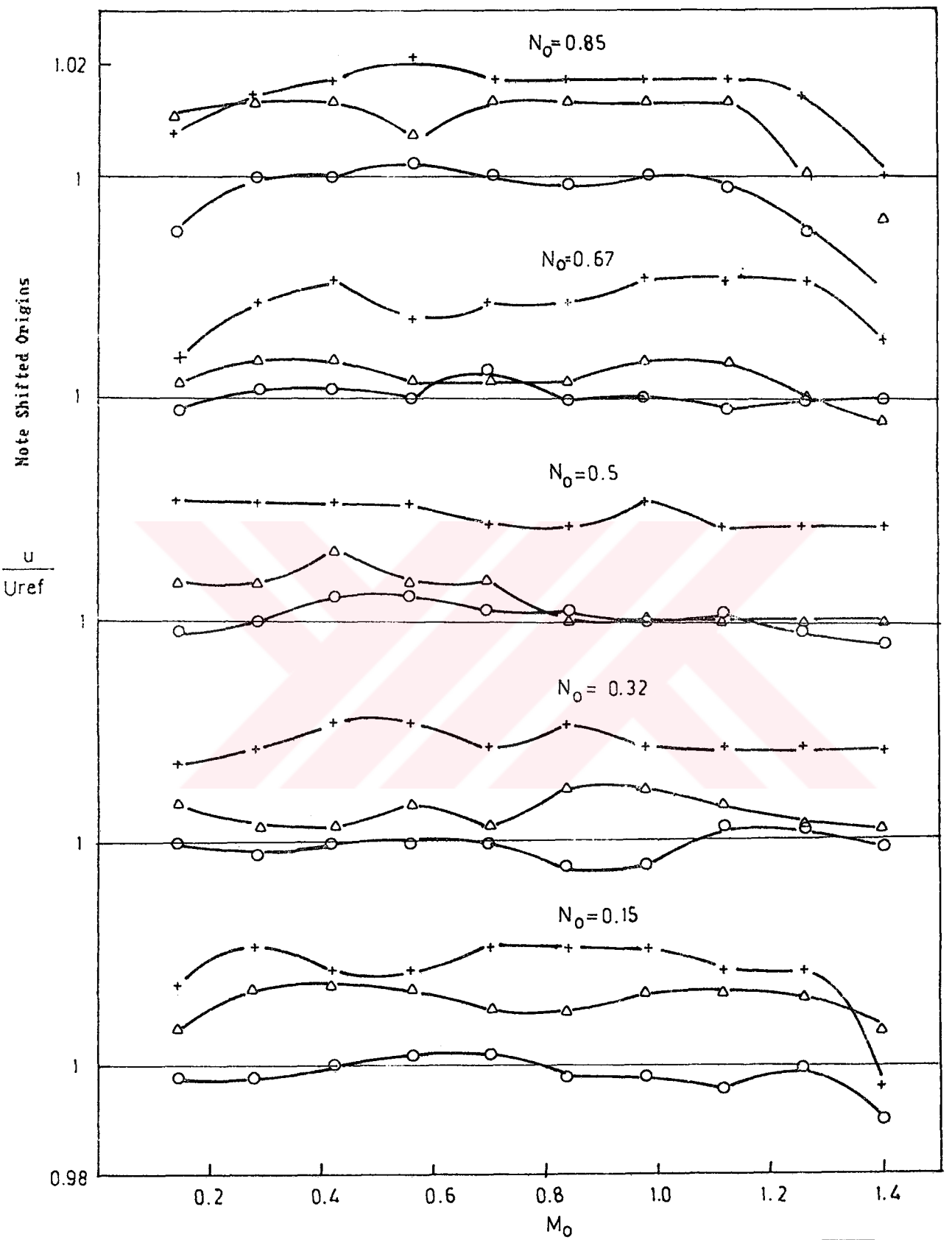

Figure 6.4. Variation of the Free-Stream Velocity over the Crossection of the Test Section for U_{ref} = 6.58 m/s

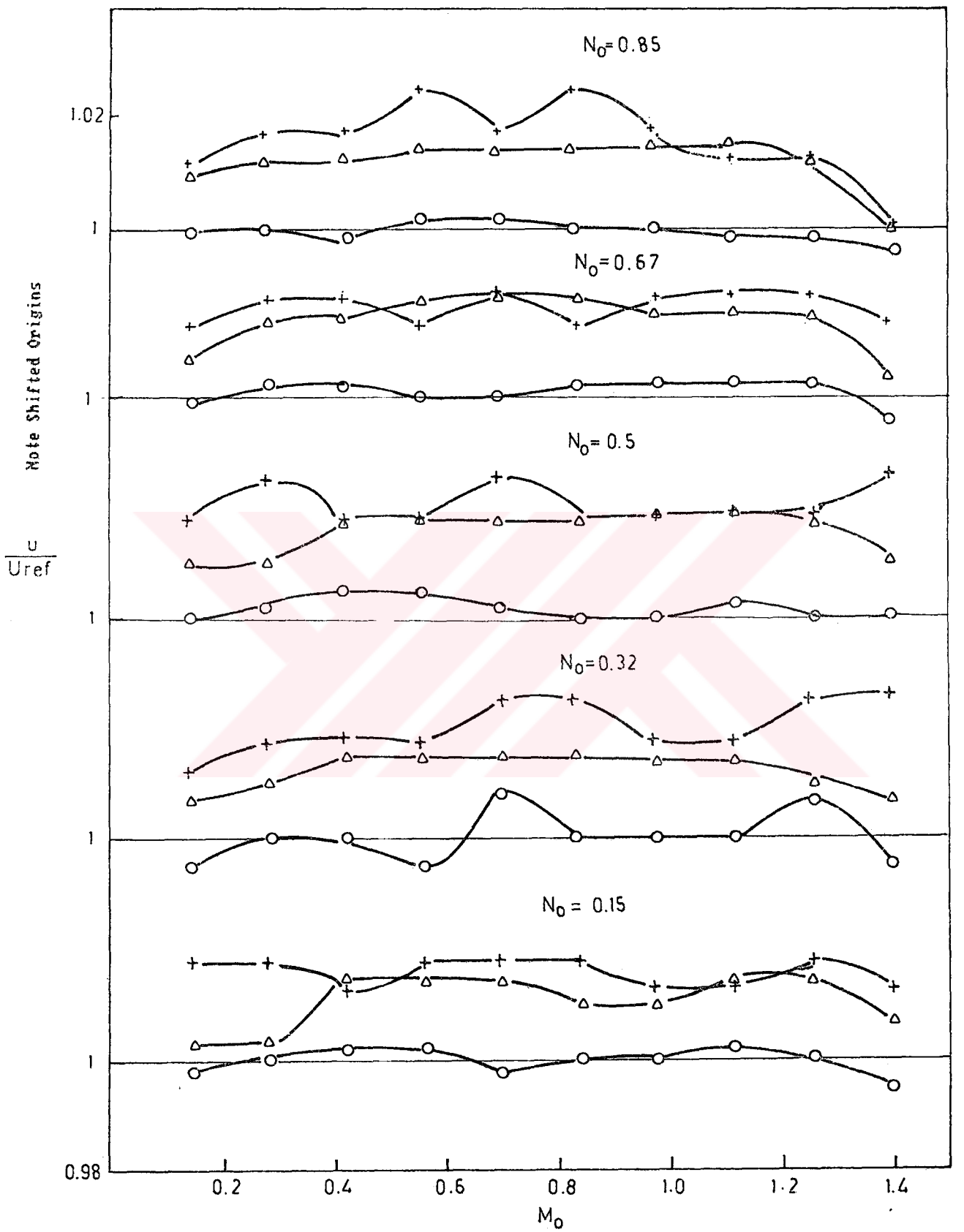

Figure 6.5. Variation of the Free-Stream Velocity over the Crossection of the Test Section for U_{ref} = 4.9 m/s

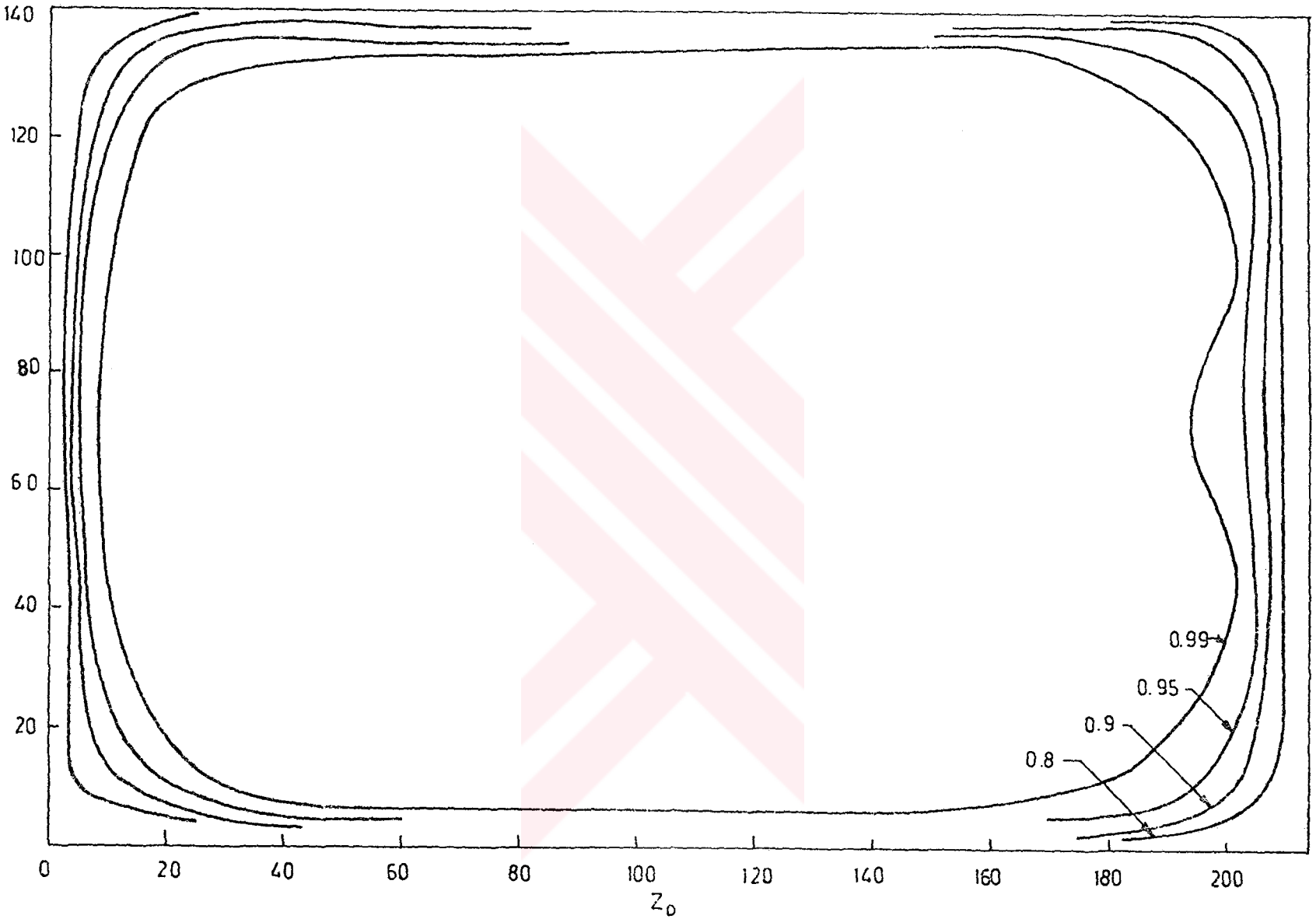

Figure 6.6. Velocity Mapp of the Crossection of the Test Section Exit at U_{max}= 9.12 m/s

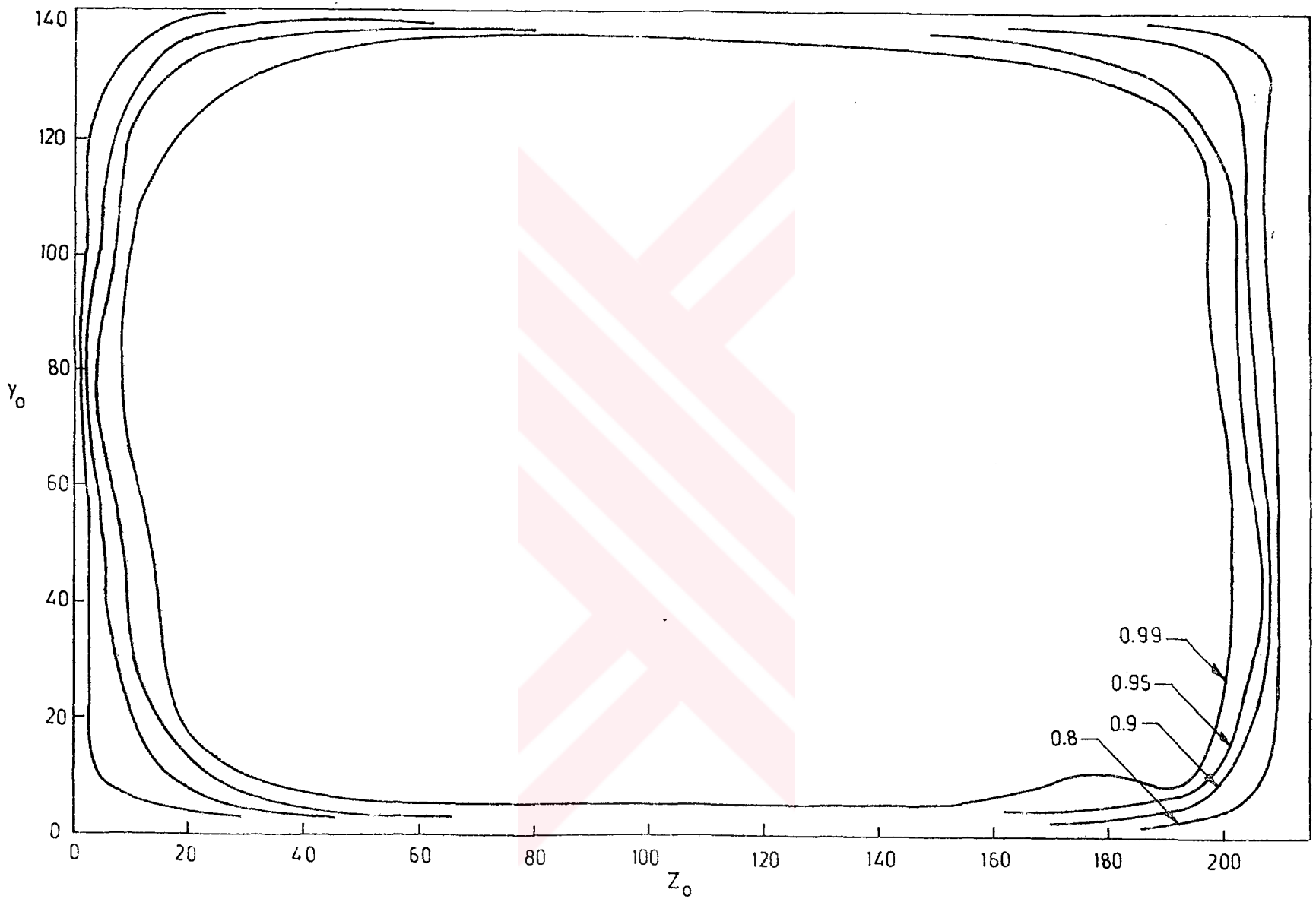

Figure 6.7. Velocity Mapp of the Crossection of the Test Section Exit at U_{max}= 6.66 m/s

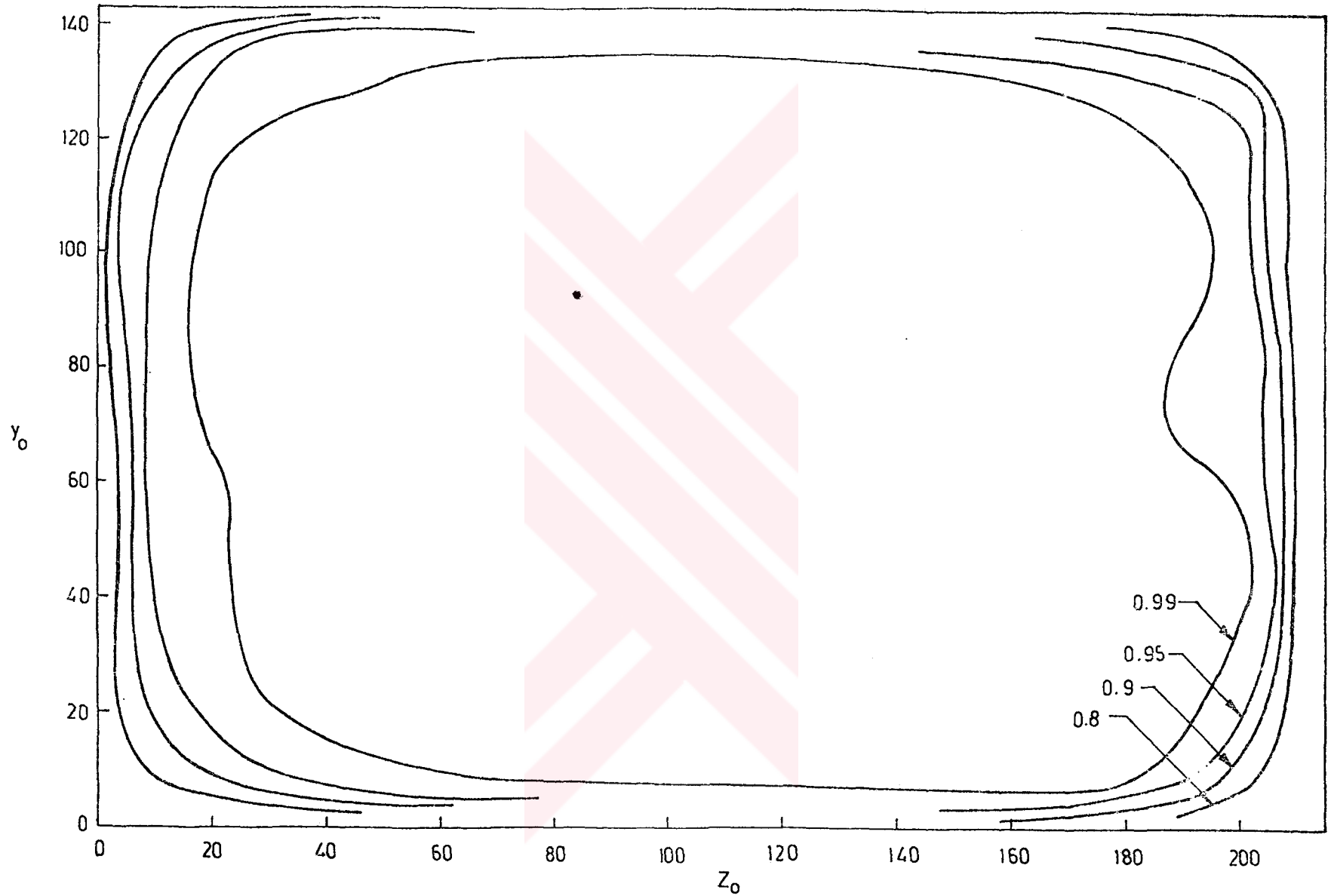

Figure 6.8. Velocity Mapp of the Crossection of the Test Section Exit at U_{max}= 4.93 m/s

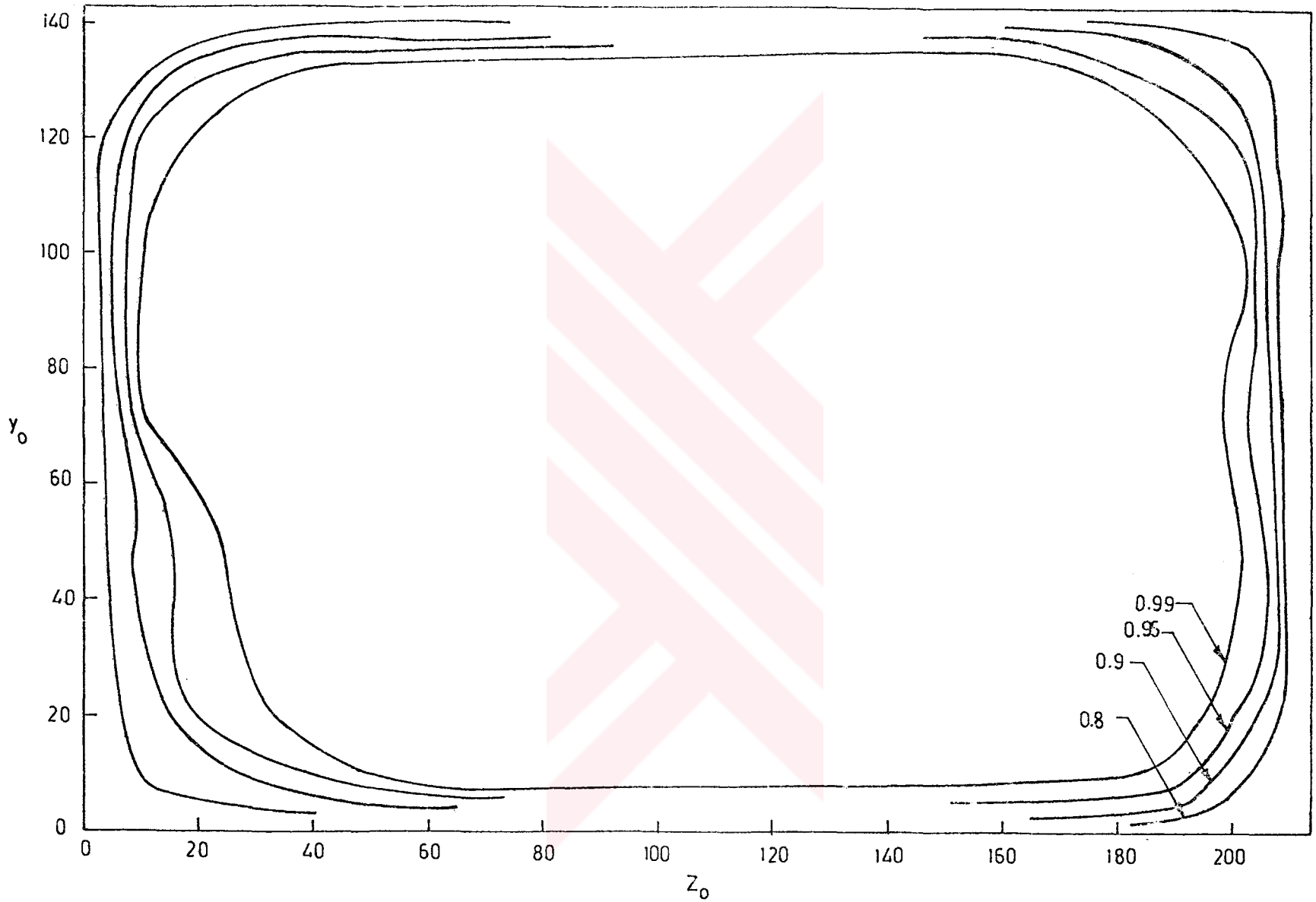

Figure 6.9. Velocity Mapp of the Crossection of the Test Section Exit at U_{max}= 3.61 m/s

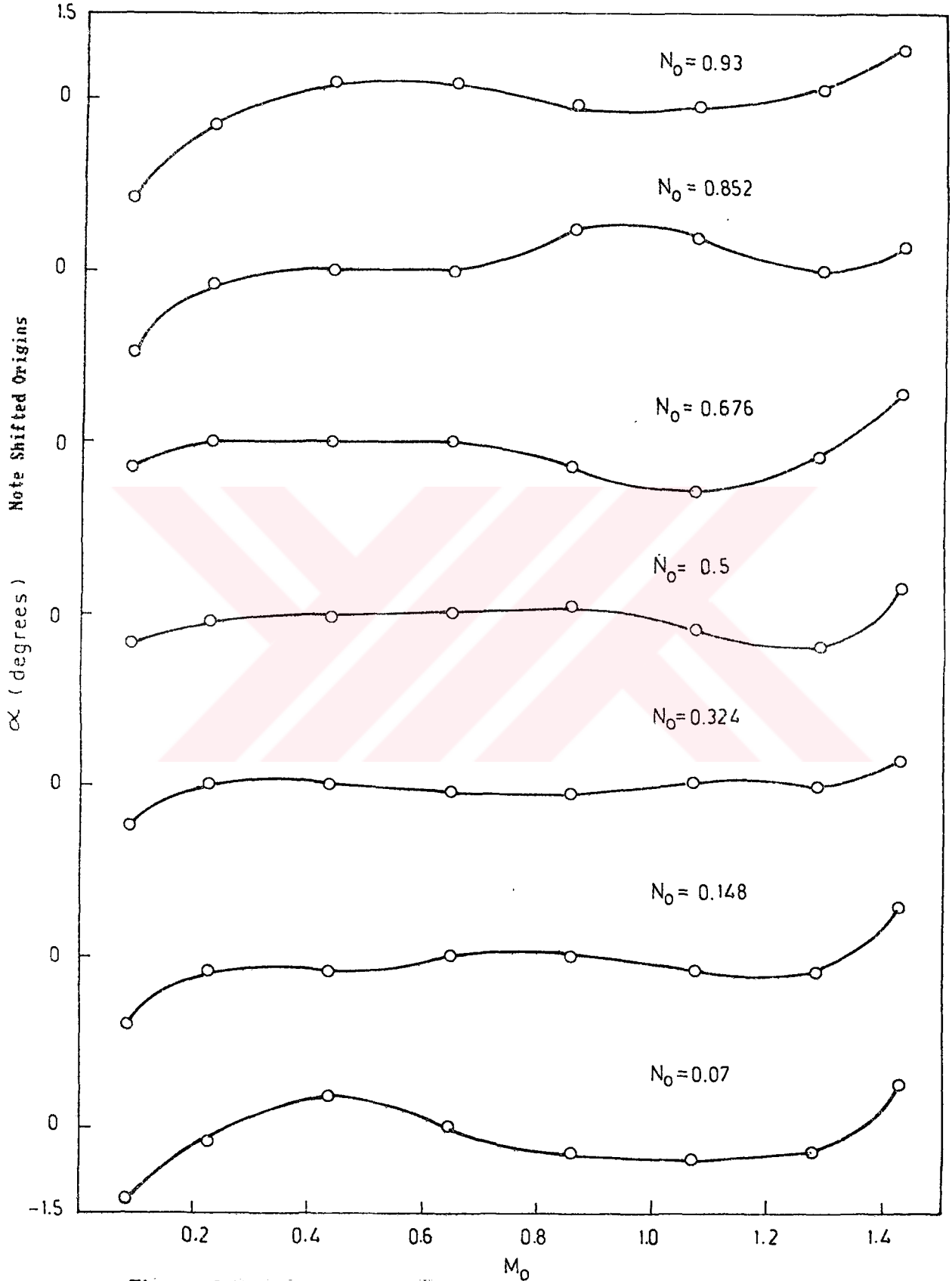

Figure 6.10. Variation of the Yaw Angle on the Crossection of the Test Section Exit at U_{ref} = 8.81 m/s

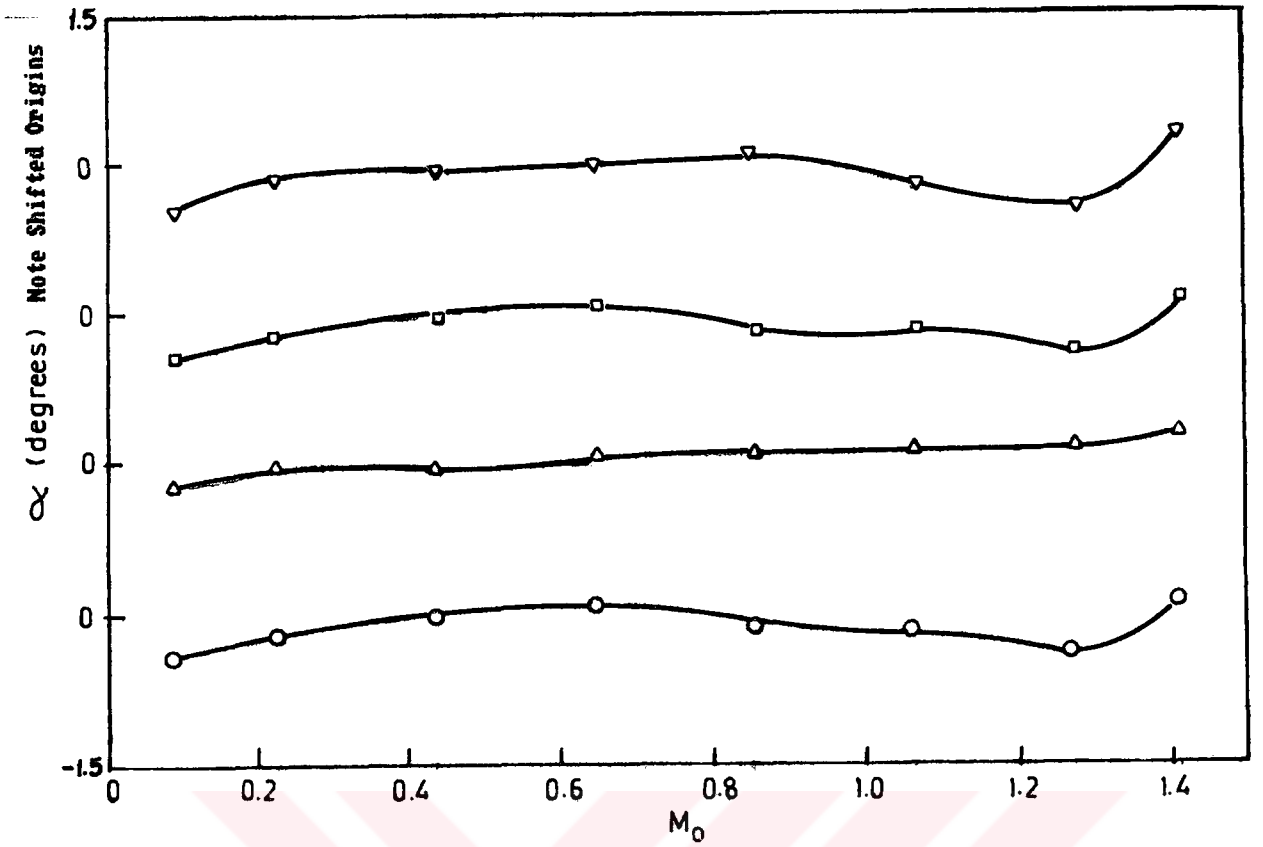

Figure 6.11. Variation of the Yaw Angle on the Spanwise Centerline of the Test Section Exit

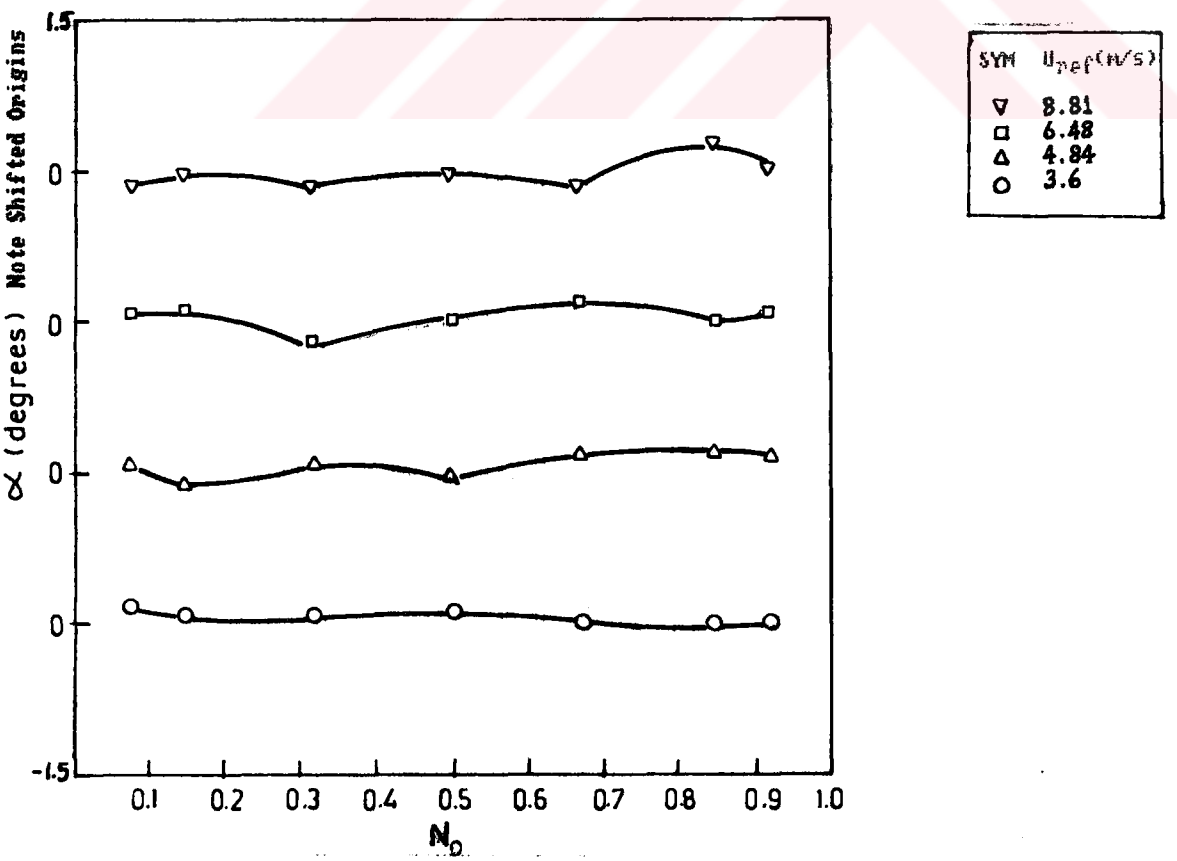

Figure 6.12. Variation of the Yaw Angle on the Pitchwise Centerline of the Test Section Exit

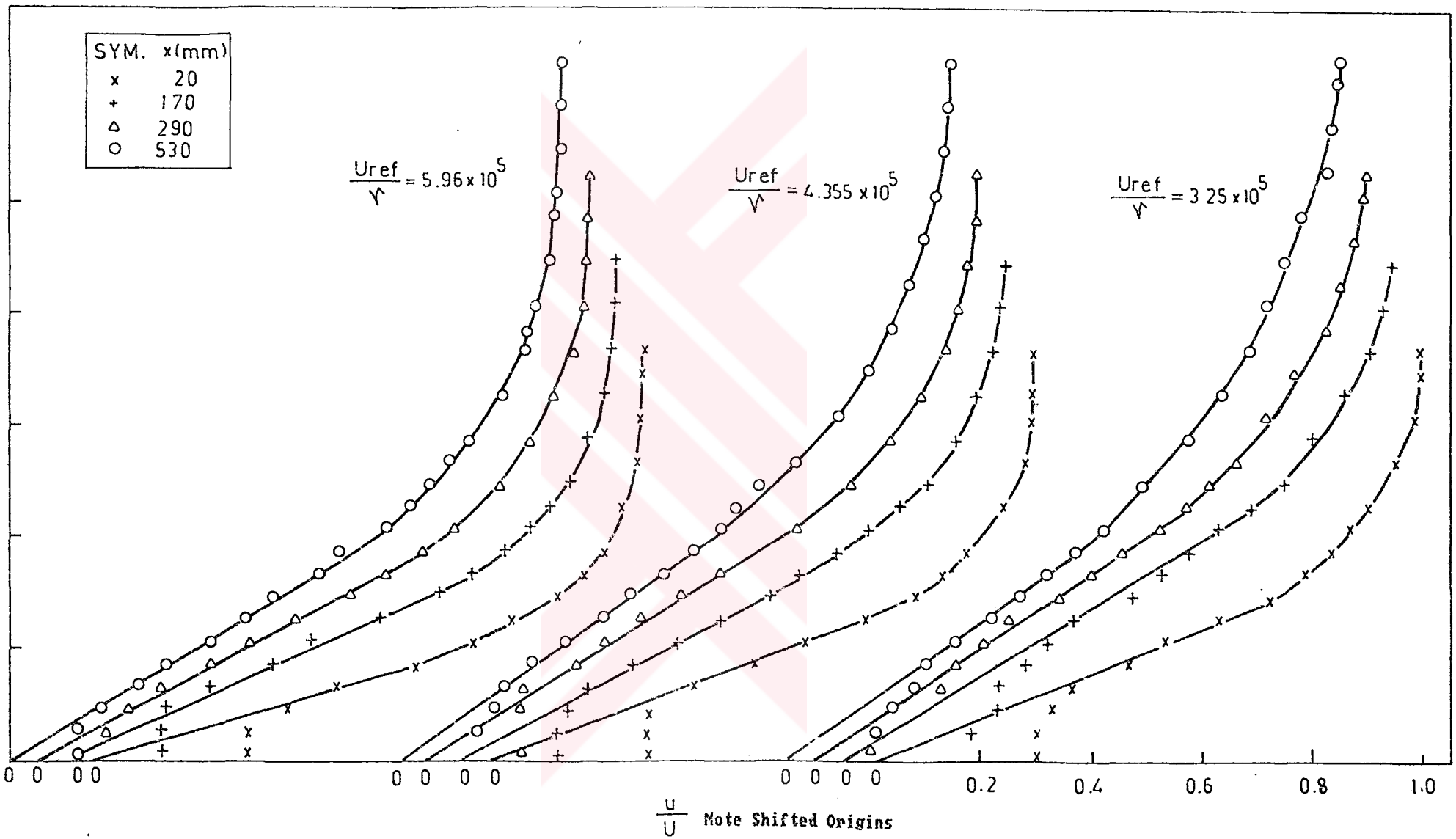

Figure 6.13. Boundary Layer Development along the Test Section

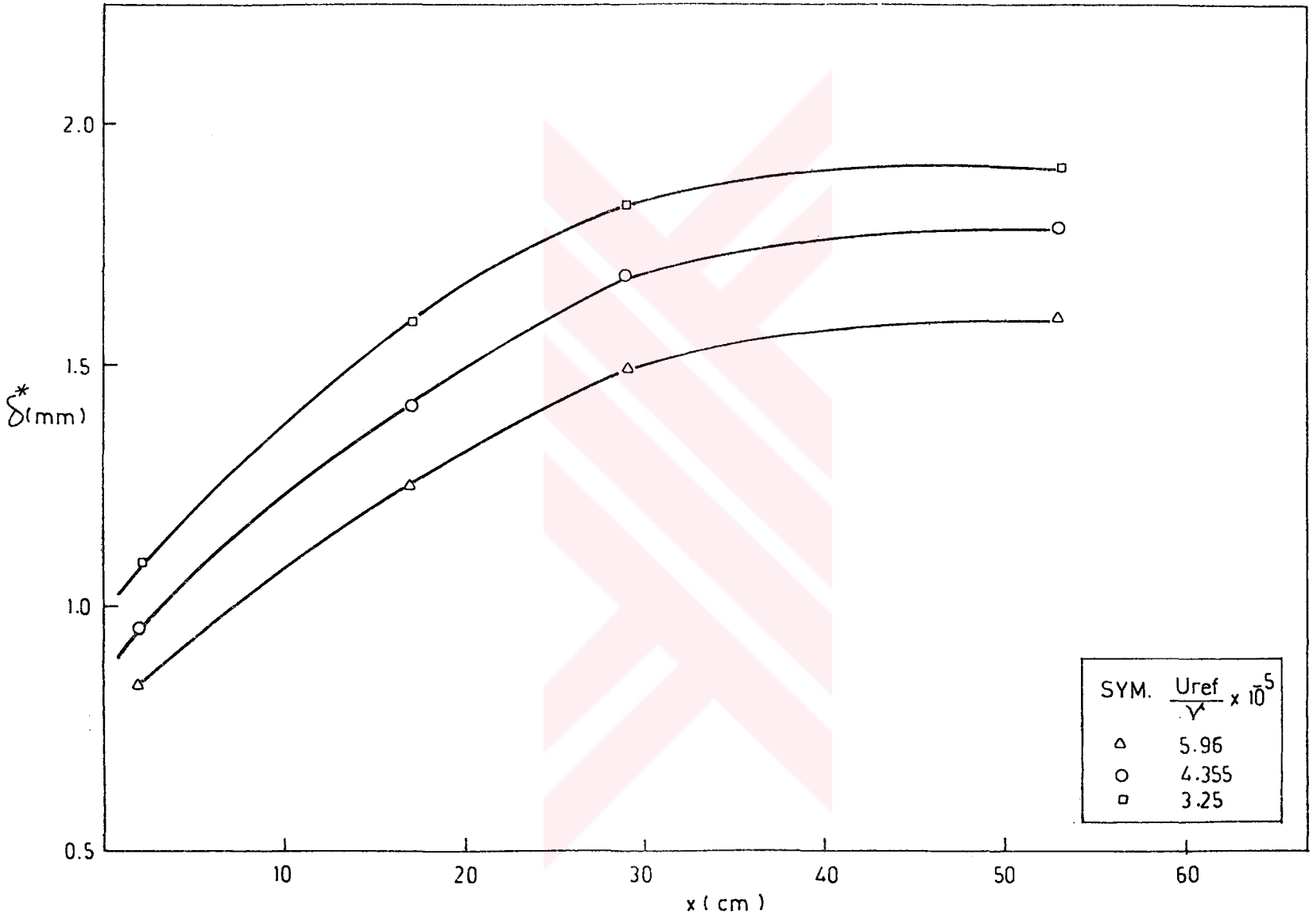

Figure 6.14. Variation of the Boundary Layer Displacement Thickness along the Test Section

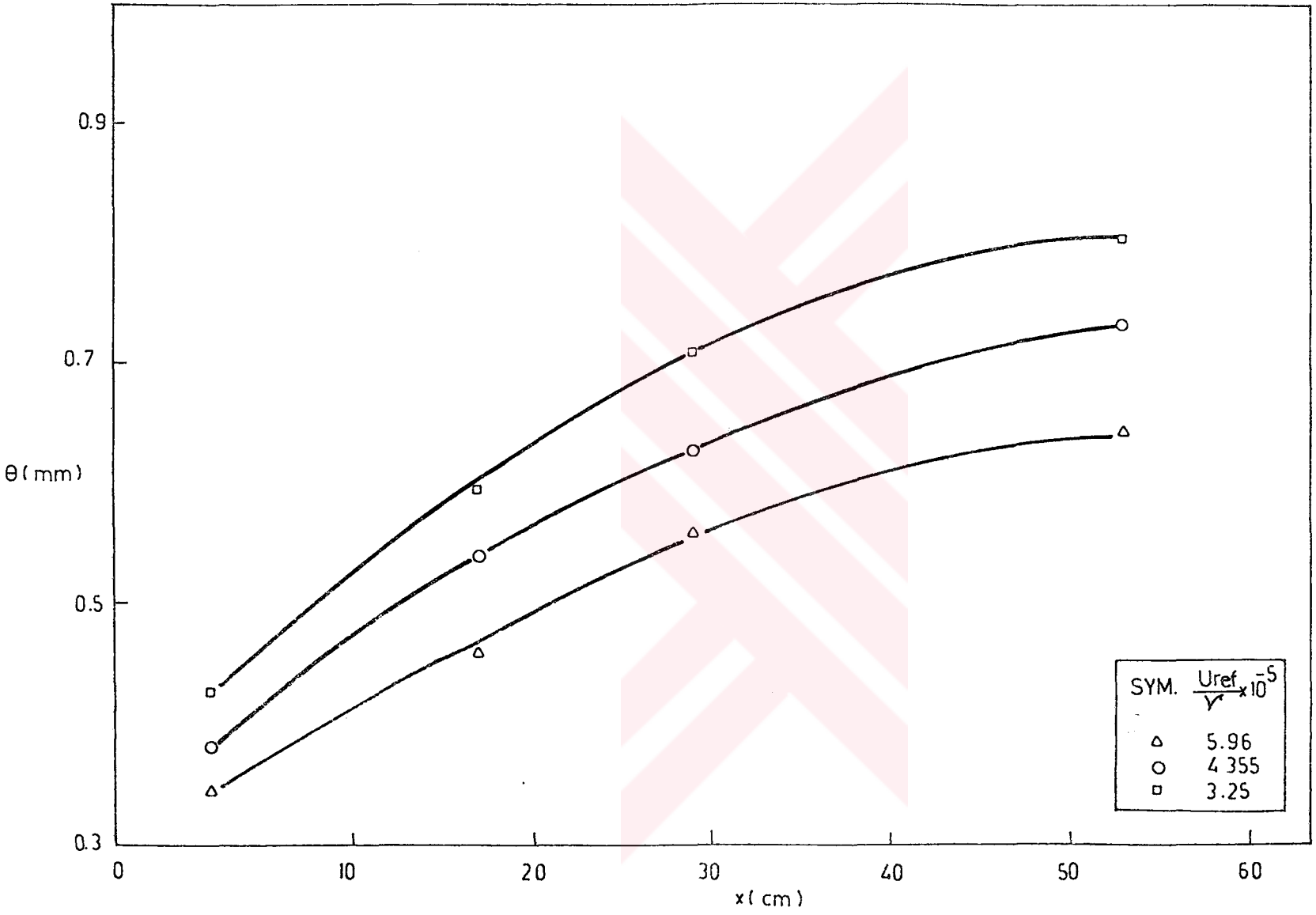

Figure 6.15. Variation of the Momentum Thickness along the Test Section

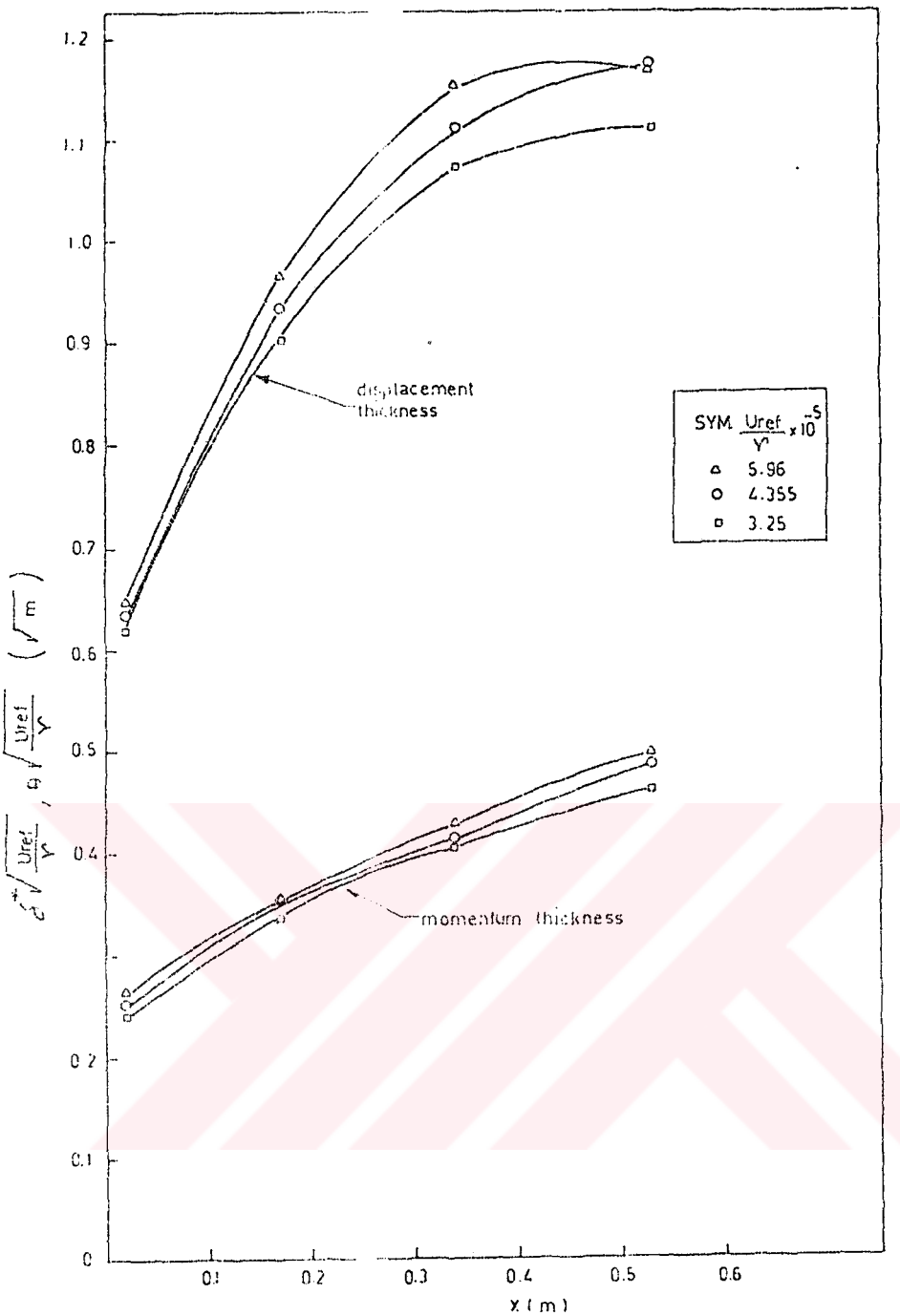

Figure 6.17. Boundary Layer Development in terms of the Unit Reynolds Number along the Test Section

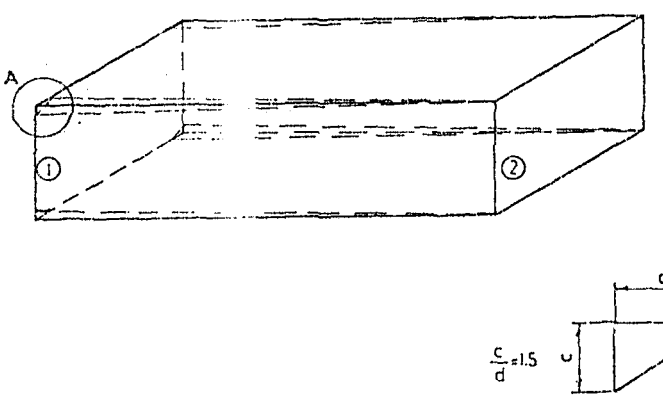

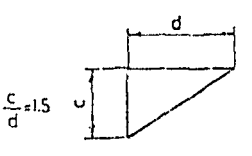

Detail A

Figure 6.16. Divergence of the Test Section Corner Fillet

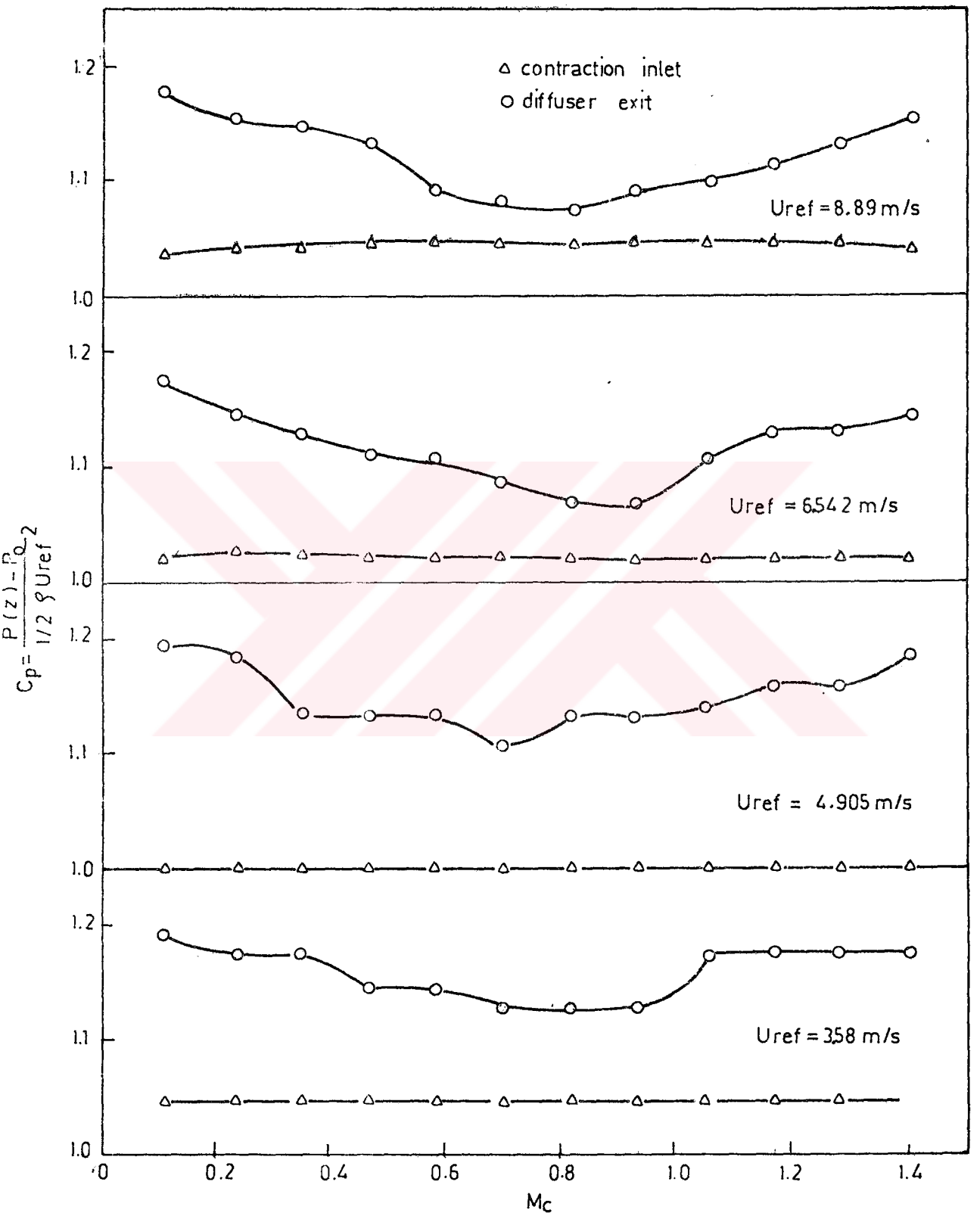

Figure 6.18. Variation of Static Pressure Coefficient along the Spanwise Direction in the Settling Chamber

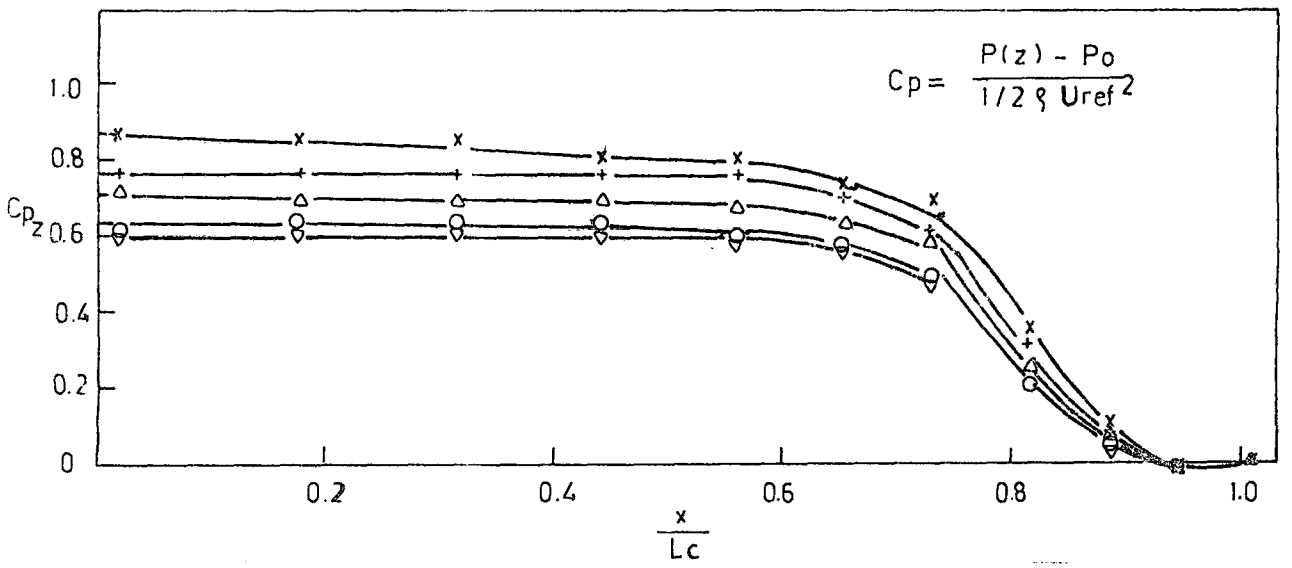

Figure 6.19. Variation of Static Pressure Coefficient along the Side Wall of the Contraction

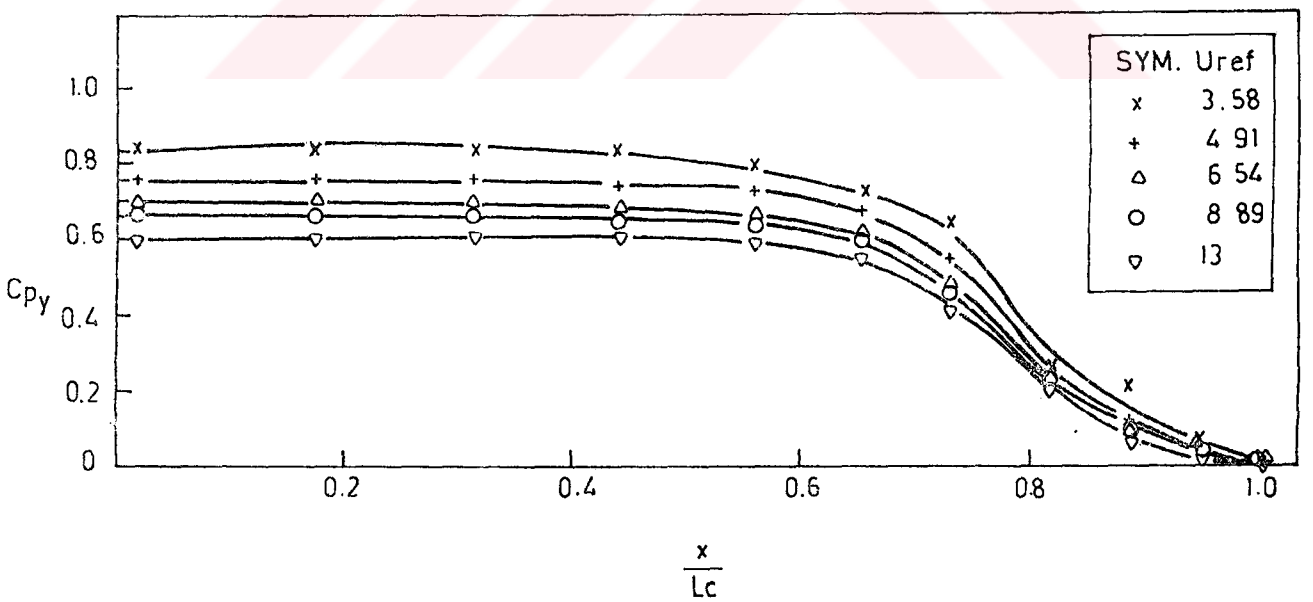

Figure 6.20. Variation of Static Pressure Coefficient along the Roof of the Contraction

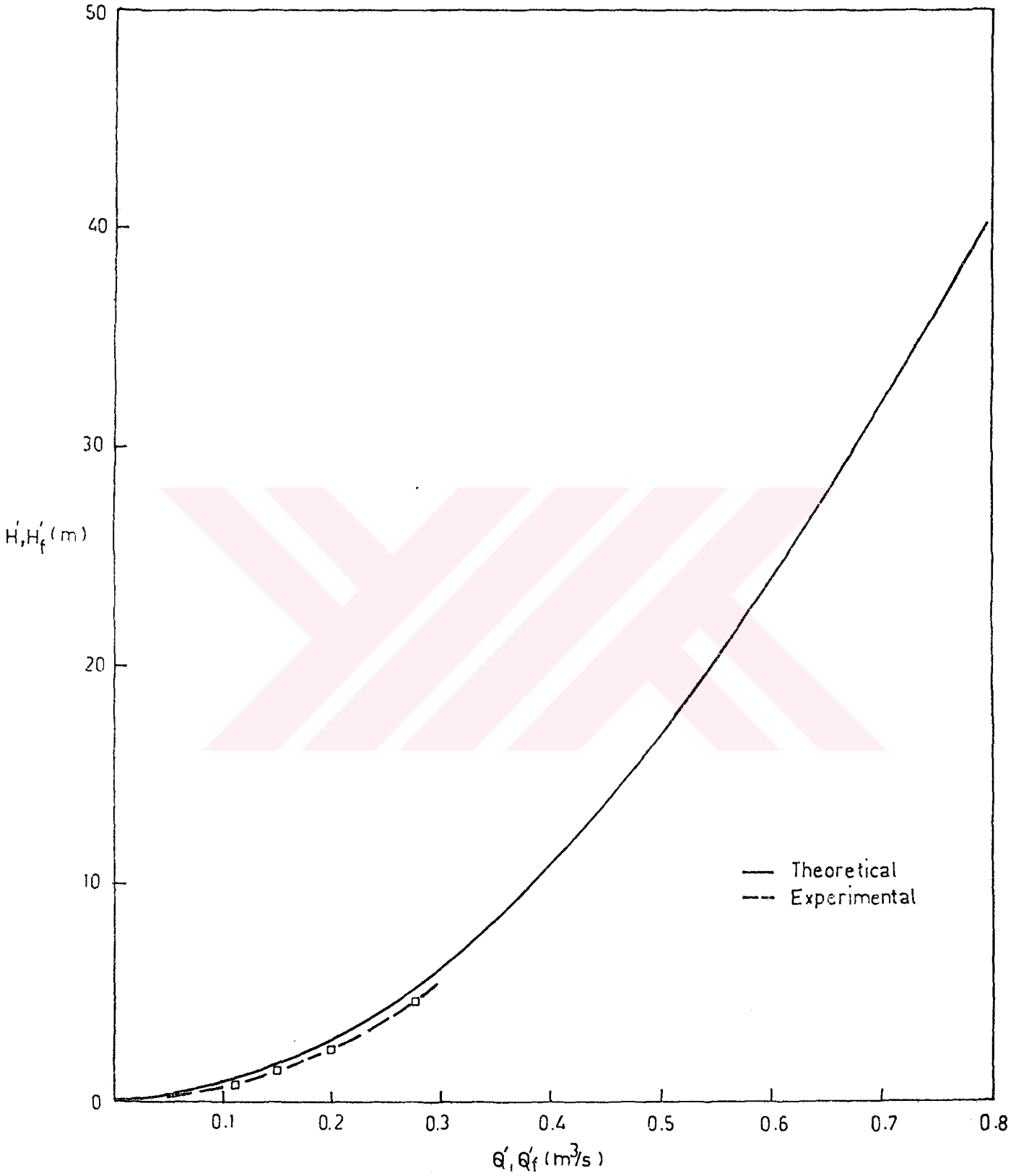

Figure 6.21. Theoretical and Experimental System Characteristics of the Model Tunnel

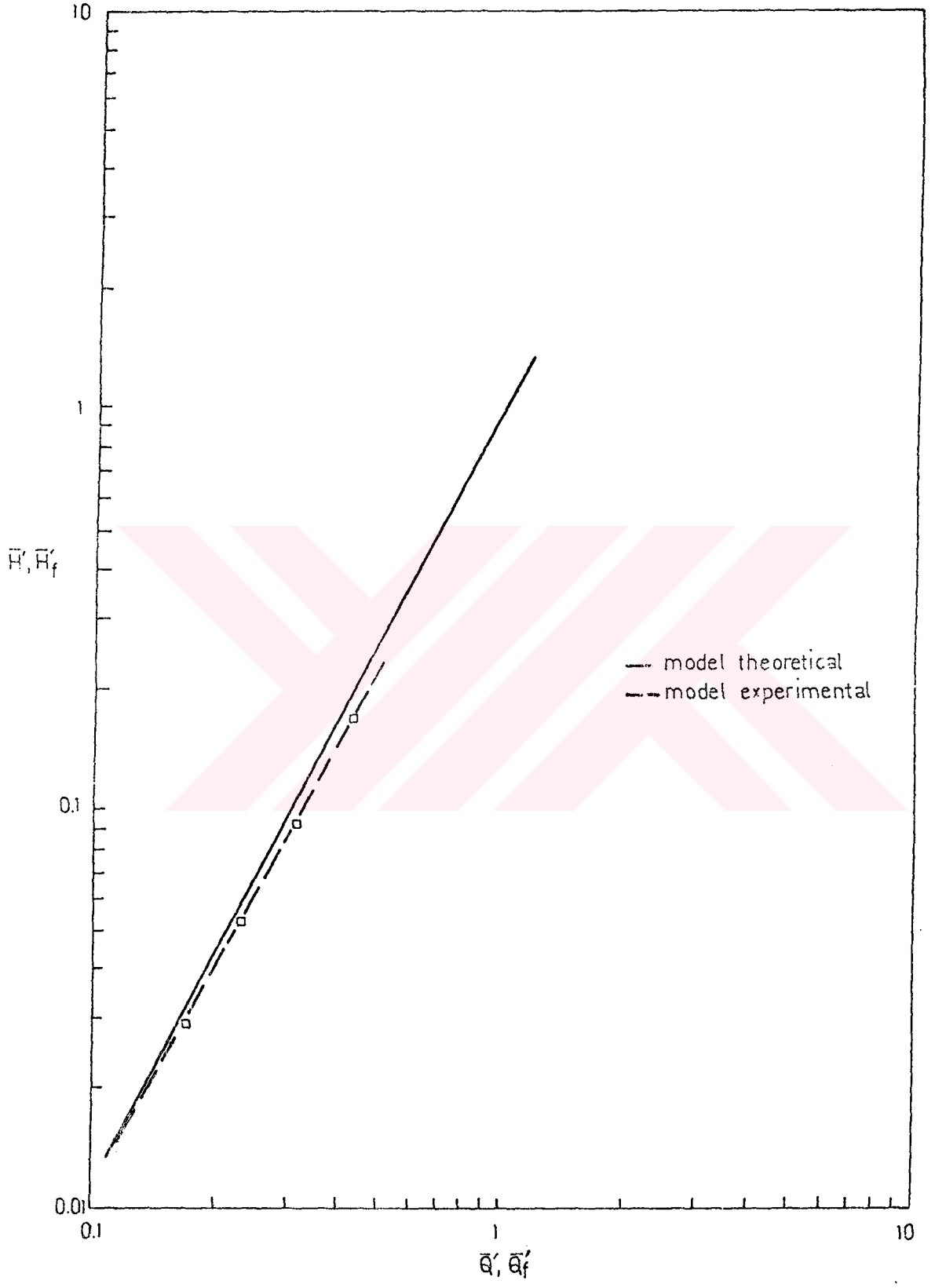

Figure 6.22. Theoretical and Experimental System Characteristics of the Model Tunnel in Dimensionless Form

CHAPTER 7

CONCLUSIONS AND RECOMMENDATIONS FOR FURTHER WORK

A prototype tunnel and its model were designed by applying a similarity analysis. The designed model tunnel was constructed and tested to predict the performance of the prototype tunnel.

The conclusions of the test results were given in section 6.6. Although the flow quality of the tunnel components were investigated, a more systematic study is required at a wider velocity range. Therefore the aim of the further work after installing stepless speed control unit should be;

1. The performance of the wide angle diffuser may be investigated with different boundary layer control methods such as screens, perforated plates, honeycombs which may be installed between the second and third diffuser sections in order to prevent flow seperation and increase flow quality at the exit of the diffuser.

2. The honeycombs with different crossections and length to diameter ratios may be tested in the settling chamber. The design charts for the pressure drop coefficients of the honeycombs may be constructed in terms of,

$$K_h = f\left(Re_\infty , \zeta, \frac{l_h}{d_h} \right)$$

as a guide for the tunnel designer. Additionally the effects of the honeycomb on the flow uniformity in the test section may be studied.

3. A test section with adaptive walls may be used instead of the present test section of the model tunnel to minimize the interference effect of the model which is to be placed in the test section.

LIST OF REFERENCES

1. Durand, W.F., 1943. "Aerodynamic Theory", Durand Reprinting Committee.

2. Pankhurst, R.C. and Holder, D.W., 1966. "Wind Tunnel Technique", Sir Isaac Pitman and Sons.

3. Pope, A. and Happer, J.J., 1966. "Low Speed Wind Tunnel and Their Instrumentation", John Willey and Sons.

4. Gorlin, S.M. and Slezinger, I.I., 1966. "Wind tunnels and their Instrumentation", Isreal Program For Scientific Translations Ltd., Jerusalem.

5. Albayrak, K., 1984. "Investigation of the Boundary Layer Transition, the Turbulent Boundary Layer Development and the Recovery Length of the Turbulent Boundary Layer Behind Three Dimensional Roughness Elements", Ph.D. Thesis, METU, Turkey.

6. Mehta, R.D., 1977. "The Aerodynamic Design of Blower Tunnels with Wide Angle Diffusers", Prog. Aerospace Sci., pp. 59-120.

7. Mehta, R.D., and Bradshaw, P., 1979. "Design Rules for Small Low-Speed Wind Tunnels", Aeronautical Journal, pp. 433-449.

8. Greenway, M.E., and Wood, C.J., 1979. "The Oxford University 4mx2m Industrial Aerodynamics Wind Tunnel", Journal Of Aerodynamics, pp. 43-70.

9. Gentry, G.L., 1981. "Description of 0.186 Scale Model of High Speed Duct of National Transonic Facility", NASA, TM-81949.

10. Thwaites, B., 1946. "Design of Contractions of Wind Tunnels", R. and M. 2278.

11. Tulapurkara, E.G., 1980. "Studies on Thwaites' Method for Wind Tunnel Contraction", Aeronautical Journal, pp. 167-169.

12. Cohen, M.J. and Ritchie, N.J.B., 1962. "Low Speed Three Dimensional Contraction Design", Journal of Royal Aeronautical Society, pp. 294-297.

13. Tsien, H.S., 1943."On the Design of a Contraction Cone for a Wind Tunnel", Journal of Aeronautical Sciences, Vol.10

14. Lam, K. and Pomfret, M.J., 1985. "Design and Performance of a Low Speed Wind Tunnel", Int. Journal of Mechanical Eng. Educ., pp. 161-172.

15. Barger, L.R., and Bowen, J.T., 1972. "A Generalized Theory for the Design of Contraction Cones and other Low Speed Ducts", NASA, D-6962.

16. Chemielewski, G.E., 1974. "Boundary Layer Considerations in the Design of Aerodynamic Contractions", Journal of Aircraft, pp. 435-438.

17. Mikhail, M.N., 1979. "Optimum Design of Wind Tunnel Contractions", AIAA Journal, pp. 471-477.

18. Morel, T., 1975. "Comprehensive Design of Axisymmetric Wind Tunnel Contractions", Journal Of Fluids Eng., pp. 225-233.

19. Batil, S.M. and Hoffman, J.J., 1986. "Aerodynamic Design of Three Dimensional Subsonic Wind Tunnel Inlets", AIAA Journal, pp. 268-269.

20. Tulapurkara, E.G. and Bhalla, V.Y.K., 1988. "Experimental Investigation of Morel's Method for Wind Tunnel Contractions", Journal of Fluids Eng., pp.45-47.

21. Alston, L.L., 1968. "High Voltage Technology", Oxford University.

22. Gibson, M.M., 1959. "The Design and Performance of a Streamline Diffuser with Rapid Expension", A.R.C., pp. 21, 126.

23. Libby,P.A., and Reiss, H.R., 1951. "The Design of Two Dimensional Contraction Sections", Quarterly of Applied Mathematics, Vol.IXB, pp.95-98.

24. Yegen, I., 1982. "The Effects of Spherical Roughness Elements on Transition and Boundary Layer Development", Ph. D. Thesis, METU, Turkey.

25. Collar, A.R., 1939. "The Effect of a Gauze on the Velocity Distribution in a Uniform Duct.", R.& M., No.1867.

26. Weighardt, K.E.G., 1953. "On the Resistance of Screens" Aeronautical Quarterly, Vol.4, p.186.

27. Bradshaw, P., 1965. "The Effect of Wind Tunnel Screens on Nominally Two Dimensional Boundary Layers", Journal of Fluid Mechanics, Vol.22, Part 4, pp. 679-687.

28. Schubauer, G.B., 1950. "Aerodynamic Characteristics of Damping Screens", NACA, TN-2001.

29. Loehrke, R.I. and Nagib, H.M., 1976. "Control of Free Stream Turbulence by Means of Honeycombs a Balance between Suppression and Generation", Journal Of Fluids Eng., pp. 342-353.

30. Lumley, J.L. and Mcmahon, J.F., 1967. "Reducing Water Tunnel Turbulence by Means of a Honeycomb", Journal of Basic Eng., pp. 764-770.

31. Smith, C.R., 1975. "A Note on Diffuser Generated Flow Unsteadiness", Journal of Fluids Eng., pp. 377-379.

32. Cockrel, D.J. and Markland, E., 1974. "Diffuser Behaviour a Review of Past Experimental Work-Relevant Today", Aircraft Eng., pp. 16-20.

33. Hussain, A.K.M.F. and Ramjee, V., 1976. "Effects of the Axisymmetric Contraction Shape on Incompressible Turbulent Flow", Journal of Fluids Eng., pp. 58-69.

34. Ramjee, V., and Hussain, A.K.M.F., 1976. "Influence of Axisymmetric Ratio on Free Stream Turbulence", Journal of Fluids Eng., pp. 506-515.

35. Tulapurkara, E.G. and Ramjee, V., 1980. "Effect of Contraction on Screen Generated Turbulence", Aeronautical Journal, pp. 290-295.

36. Winter, K.G. and Boyd, C., 1981. "A Speculation on the Influence of Compressibility on the Performance of a Wind Tunnel Contraction Cone", Aeronautical Journal, pp. 387-389.

37. Roberson, J.A. and Crowe, C.T., 1985. "Engineering Fluid Mechanics", Houghton Mifflin Company, Boston, pp. 274-302.

38. Douglas, J.F. and et al., 1985. "Fluid Mechanics", Pitman Pub. Ltd., Masachusetts.

39. Langhaar, H.L., 1951. "Dimensional Analysis and Theory of Models", John Willey and Sons Inc.

40. Pankhurst, R.C., 1964. "Dimensional Analysis and Scale Factors", The Institude of Physics and Physical Society.

41. Eck, B., 1962. "Fans", Springer-Verlag, Berlin.

42. Schlichting, H., 1979. "Boundary Layer Theory", 7. Edition, McGraw-Hill Series in Mech. Eng., McGraw-Hill Book Company, NewYork, U.S.A.

43. Wallis, R.A., 1961. "Axial Flow Fans, Design and Practice", NewYork, Academic Press.

44. Uskaner, Y.A., 1990. "Determination of Design Parameters for Optimum Operation of a Cross Flow Fan" Ms. Thesis, METU Gaziantep, Turkey.

45. Bryer, D.W. and Pankhurst, R.C., 1971. "Pressure-Probe Methods for Determining Wind Speed and Flow Direction", N.P.L., Her Majesty's Stationery Office, London.

46. Over, E. and Pankhurst, R.C., 1965. "Measurement of Air Flow", 4.Edition, Pergamon Press.

47. B.S. 1042: Part 2A, 1973. "Methods for the Measurement of Fluid Flow in Pipes. Part 2, Pitot Tubes", British Standards Institution, London.

APPENDICIES

APPENDIX 1

CALCULATION OF THE FAN DIAMETER

To decide on a suitable fan diameter for the given values of total head, H, discharge, Q, and rotational speed of the fan, N, the following procedure that was given in reference [41] may be followed:

1. For the given H, Q and N calculate the speed coefficient, σ, of the fan from:

$$\sigma = n_s \frac{(Q)^{1/2}}{(2gH)^{3/4}} 2(\pi)^{1/2} \qquad (A1.1)$$

where n_s is the rotational speed in revolution per second.

2. To determine the diameter coefficient, δ_f, figure A1.1 was used, which was given in reference [41]. The required diameter was calculated from:

$$D_f = \delta_f \frac{2\ (Q)^{1/2}}{(2gH)^{1/4}\ (\pi)^{1/2}} \qquad (A1.2)$$

3. Then, the pressure coefficient, ψ, and the flow coefficient, ϕ, could be determined from the experessions

$$\psi = \frac{1}{\delta_f^2\ \sigma^2} \qquad (A1.3)$$

and

$$\phi = \frac{1}{\sigma\ \delta_f^3} \qquad (A1.4)$$

respectivelly or from figure A1.2.

4. The formula for the hub ratio, HR, is given as:

$$HR = (0.8\ \psi)^{1/2} \qquad (A1.5)$$

For the estimated values of K_T, V_0 and N the required values for equation A1.1 were calculated as:

$$H = K_T \frac{V_0^2}{2g} = 72.16 \text{ m}$$

$$Q = V_0 A_0 = 49.5 \text{ m}^3/\text{s}$$

$$n_s = \frac{N}{60} = 12.5 \text{ rps}$$

then, σ is calculated as:

$$\sigma = 1.35$$

The value of the diameter coefficient, δ_f, was obtained from figure A1.1 as 1.6. Using the equation A1.2, the diameter of the fan is determined as:

$$D_f = 2.07 \text{ m}$$

Equations A1.3 and A1.4 give the values of pressure coefficient ψ as 0.214 and ϕ as 0.181. The same values were also read from figure A1.2.

Then, a suitable hub ratio for the fan is estimated using equation A1.5 as 0.414.

Therefore, for the prototype tunnel which is to be designed, a fan diameter of 2.1 m with a hub ratio of 0.4 is proposed.

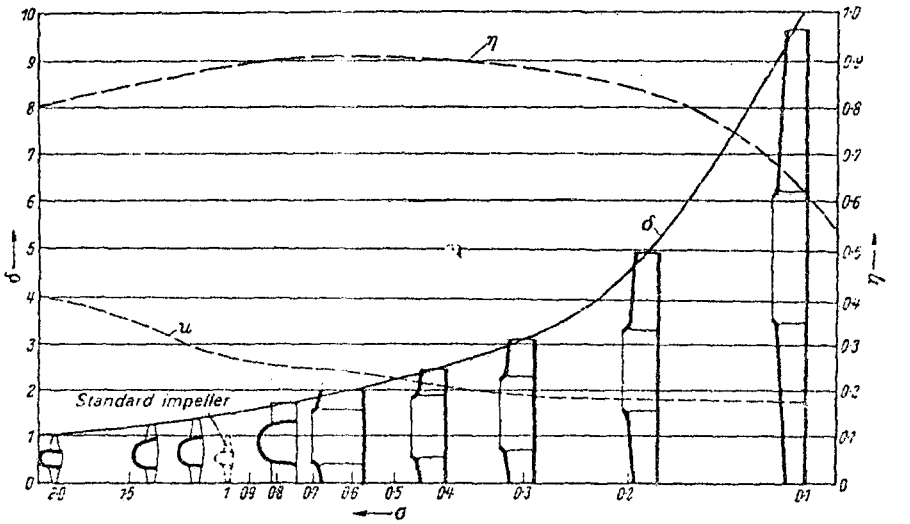

Figure A1.1. Variation of Diameter Coefficients with Speed Coefficients for Various Impellers

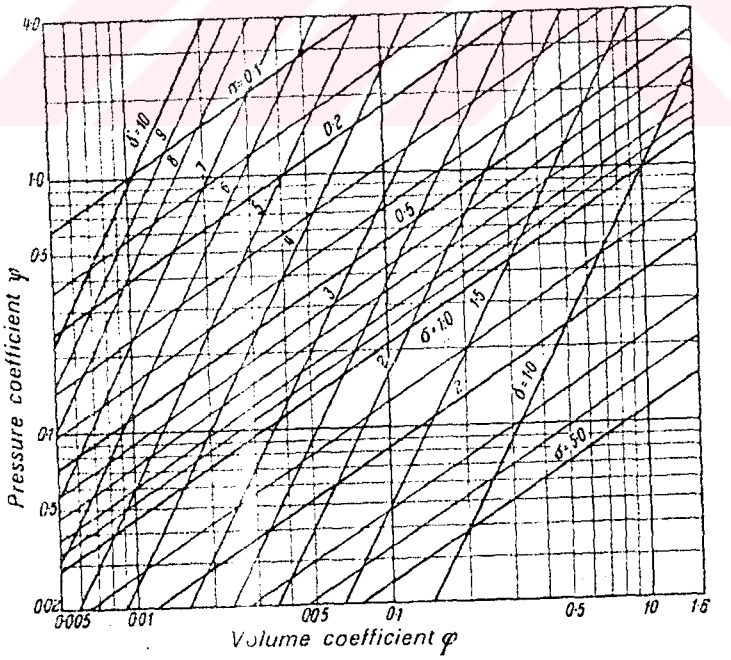

Figure A1.2. Evaluation of Dimensionless Coefficients of a Fan

APPENDIX 2

DETERMINATION OF MEAN VELOCITY IN A RECTANGULAR CROSSECTION

The mean velocity of a rectangular crossection may be found by graphical integration method [45] which requires the equation

$$V_0 = V_{max} \sum_{j=1}^{n} \sum_{i=1}^{n} \frac{V_{ij}}{V_{max}} \Delta M_i \, \Delta N_j \qquad (2A.1)$$

where M_i and N_j are the dimensionless coordinates of the crossection and V_{max} and V_{ij} are the maximum velocity ant the measured velocity of the crossection respectivelly. However, this method requires very large number of velocity measurements. Therefore, for simplicity and relativelly few velocity measurements the log-linear method which was recommended for rectangular crossection by Myles et al. in reference [46] was used.

This method is developed firstly for circular crossection. The crossection is divided into a number of annular zones with equal areas and one central zone which has the same area with that of annular zones. The velocity measurement stations were specified in references [46] and [47].

For rectangular crossection, the local velocities are measured at 26 points in the crossection along four traverse lines I, II, III, IV as shown in Figure 2A.1. The coordinates of the measuring points are given in terms of the crossection dimensions. Seven measurements are taken along the each one of the traverse lines I and IV, and six along each one of the traverse lines II and III at the points marked in the quarter duct ABCD. The formula for the mean velocity V_n in quarter duct ABCD is [46].

$$V_{n1} = \frac{1}{24}\,(2(V_1 + V_2) + 5V_3 + 3(V_4 + V_5 + V_6) + 6V_7) \qquad (2A.2)$$

where velocities V_1 to V_7 symbolizes the velocities at points 1 to 7. The mean velocity, V_o, for the crossection is found from,

$$V_o = \frac{V_{n1} + V_{n2} + V_{n3} + V_{n4}}{4} \qquad (2A.3)$$

The mean velocities were calculated according to equation 2A.2 and 2A.3 for the crossection of the test section exit. The determined mean velocities are;

$V_{o1} = 9.1$ m/s
$V_{o2} = 6.6$ m/s
$V_{o3} = 4.94$ m/s
$V_{o4} = 3.6$ m/s

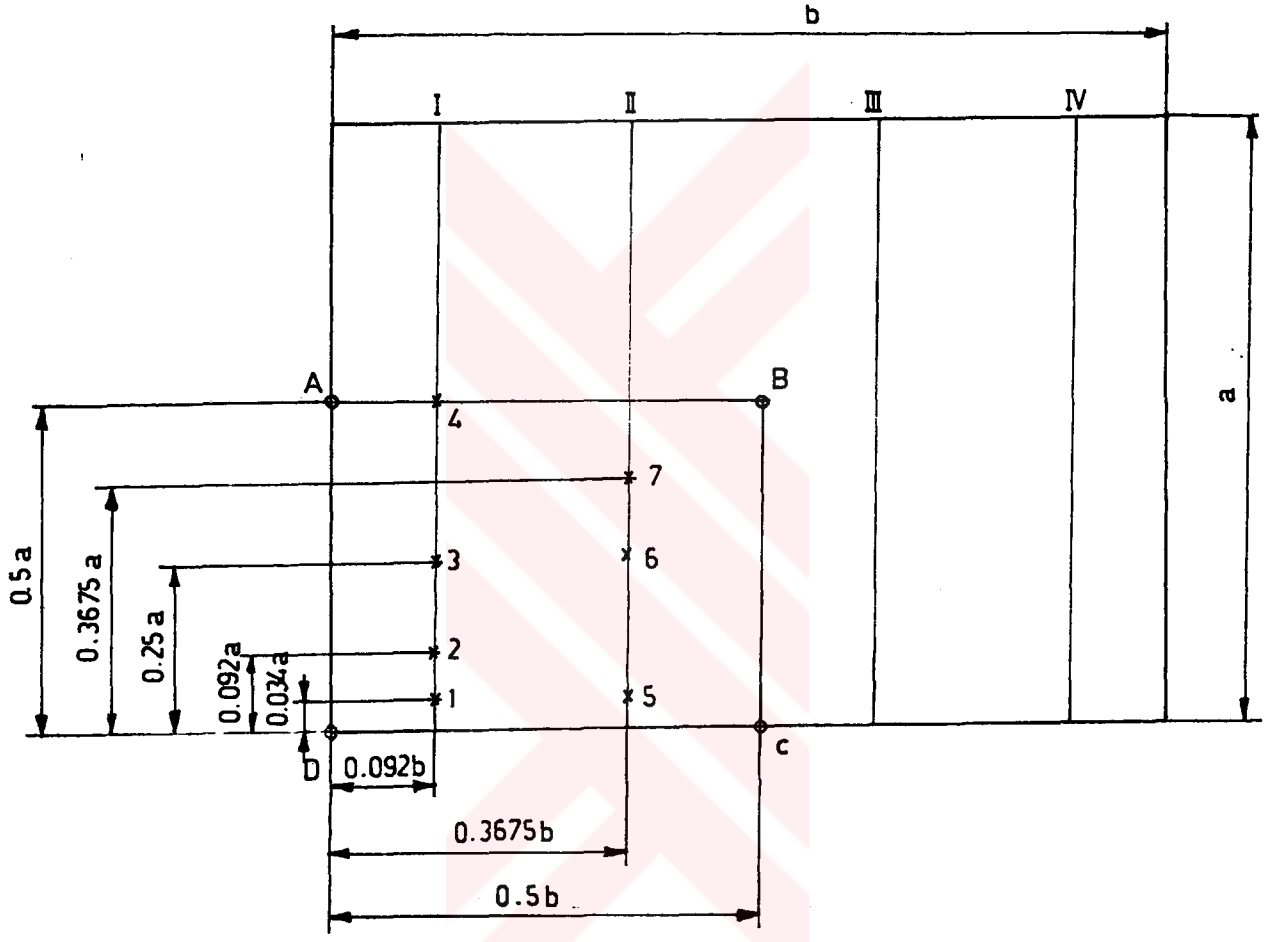

Figure A2.1 Points of Measurements in a Rectangular Duct to Determine Mean Velocity.

APPENDIX 3

DESIGN OF A STREAMLINED BODY FOR NACELLE AND STRAIGHTENER VANES

To design a streamlined body, potential flow analysis was used given in reference [38]. In this analysis a rectilinear flow is combined with a source flow to obtain a rankine body. The combined flow may be expressed as:

$$\phi = U_\infty r\cos\theta + \frac{q}{2\pi} \ln r \qquad (A3.1)$$

and

$$\Psi = U_\infty r\mathrm{Sin}\theta + \frac{q}{2\pi}\theta \qquad (A3.2)$$

where ϕ and Ψ are the velocity potential and stream function respectivelly. U_∞ is the free stream velocity and q is the streangth of the source. r and θ represents the coordinates of the Ψ and ϕ.

Taking the derivative of the stream function, ψ, with respect to the angle, θ, and equating it to zero, the coordinates of the stagnation point can be determined as:

$$a_s = \frac{q}{2\pi U} \quad , \quad \theta_s = \pi \qquad (A3.3)$$

The expression for the stream function passing through the stagnation point by using this coordinate is:

$$\Psi_s = \frac{1}{2} q \qquad (A3.4)$$

Equation A3.4 gives the value of the streamline of the solid boundary. To find the contour of the solid body, equation A3.4 may be combined with equation A.3.2 which gives:

$$\frac{1}{2}\psi = U_\infty r_s \sin\theta + \frac{q\theta}{2\pi} \qquad \text{(A3.5)}$$

The radial distance r_s to any point on the streamline ψ may be found as:

$$r_s = \frac{q(\pi-\theta)}{2\pi U_\infty \sin\theta} \qquad \text{(A3.6)}$$

Equation A3.6 describes the contour of the rankine body. As:

$$x \to \infty \quad ; \quad r_s \to \infty \quad \text{and} \quad \theta \to 0$$

therefore, the maximum thickness of the streamlined body b may be found as:

$$b_s = 2y_{max} = \frac{q}{U_\infty} \qquad \text{(A3.7)}$$

where,

$$y_{max} = r_s \sin\theta = \left.\frac{q(\pi-\theta)}{2\pi U_\infty}\right|_{\theta=0}$$

The contour of the solid body was determined for a free stream velocity of $U_\infty = 10$ m/s and maximum thickness of the body, $b_s = 1.2$ m. The contours are plotted for nacelle with a fineness ratio, f_n, of 2.5 and for straightener vanes with a fineness ratio of 5. The dimensionless streamlined body contour is given in figure A3.1. Since the maximum width of the streamlined body asymtotically increases, the trailing edge of the streamlined body can not be obtained from equation A3.6. Therefore, the body was truncated at a distance of $0.4f_n$ from the leading edge and the trailing edge of the streamlined body was plotted in a suitable way.

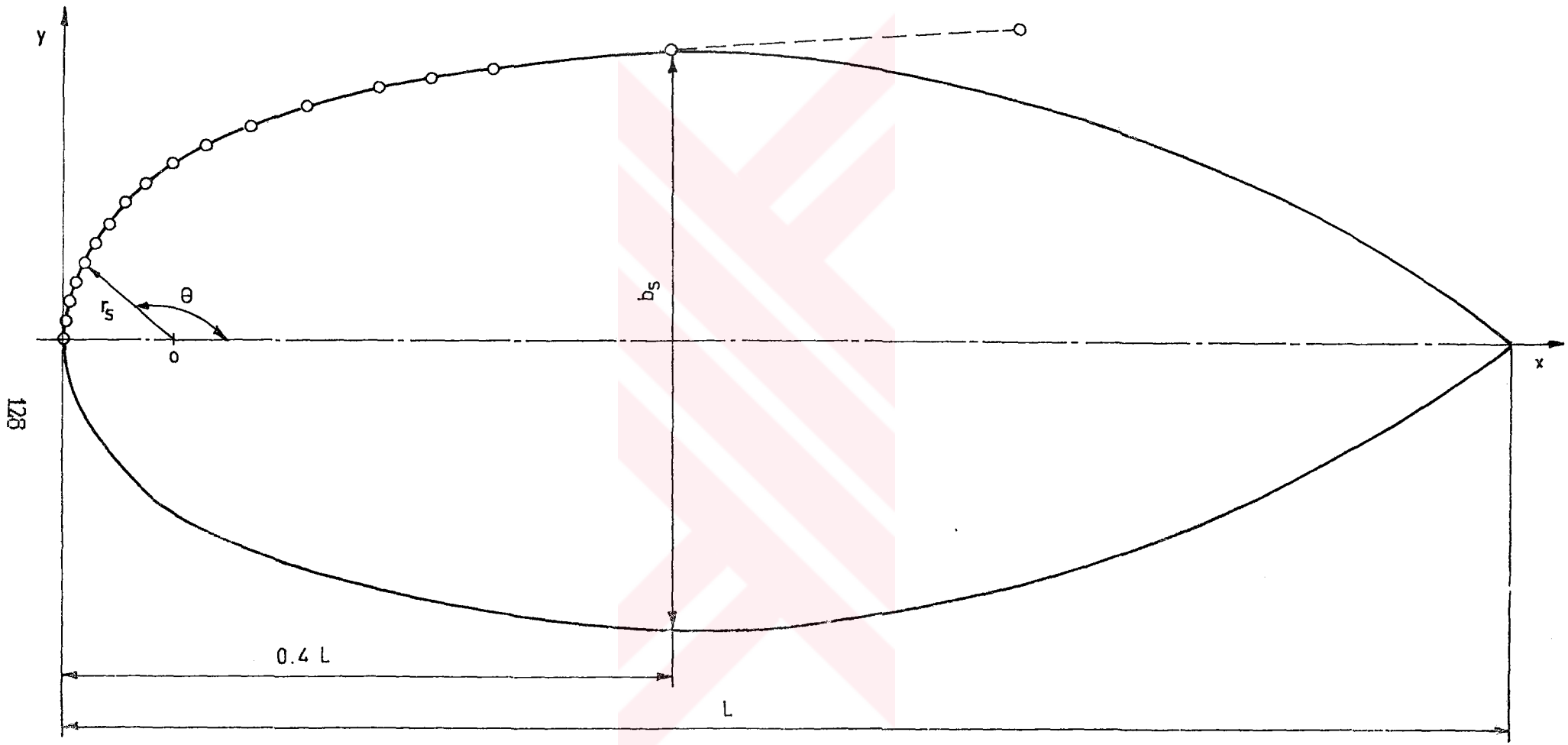

Figure A3.1. Streamlined Body Contour

APPENDIX 4

```
CC     PROGRAM FOR DETERMINATION OF HYDRAULIC LOSS COEFFICIENTS AND
CC     SYSTEM CHARACTERISTICS OF A BLOWER WIND TUNNEL
CC
CC     AO,BO,LO : HEGHT, WIDTH, AND LENGTH OF THE TEST SECTION RESP.
CC     LR : LENGTH RATIO OF CONTRACTION
CC     CR : CONTRACTION RATIO
CC     DS, LS : SCREEN DIAMETER AND MESH LENGTH
CC     LAS : LENGTH AFTER SCREEN
CC     LBH : LENGTH BEFORE SCREEN
CC     DH, LH, TH : HONEYCOMB DIAMETER, LENGTH AND THICKNESS
CC     KO : DIFUSER LOSS COEFFICIENT
CC     DF, LF : DIAMETER AND LENGTH OF THE FAN SECTION
CC     KINVIS : KINEMATIC VISCOUSITY OF AIR
CC     LO : DIFUSER LENGTH
CC     DO : HYDRAULIC DIAMETER OF THE TEST SECTION
CC     AAO : AREA OF THE TEST SECTION
CC     AC, BC, DC, AAC : HEIGHT, WIDTH, HYDRAULIC DIAMETER AND AREA
CC     OF THE TEST SECTION
CC     LC : CONTRACTION LENGTH
CC     BETA : OPEN AREA RATIO OF SCREEN
CC     NA, NB :HONEYCOMB CELL NUMBER ALONG HEIGHT AND WIDTH OF
CC     THE SETTLING CHAMBER
CC     N : NUMBER OF HONEYCOMB CELL AT SETTLING CHAMBER AREA
CC     AAH : FLOW AREA OF HONEYCOMB
CC     AH : OPEN AREA RATIO OF HONEYCOMB
CC     LT : TOTAL TUNNEL LENGTH
CC     AAF : AREA OF THE FAN SECTION
CC
CC
       REAL AO,BO,LO,LR,CR,DS,LS,LAS,LAH,LBH,DH,LH,TH,
      *KO,LF,DF,KINVIS,PI,DO,AAO,AC,BC,DC,AAC,LC,BETA,
      *AAH,AH,VO(50),Q(50),REO(50),F(50),KO(50),VC(50),KC(50)
      *,KES(50),KS(50),VH(50),REH(50),KH(50),KT(50),KT1(50),K(50)
      *,H(50),NA,NB,N,RE,LO,LT
       INTEGER I
       READ(5,*)AO,BO,LO,LR,CR,DS,LS,LAS,LAH,LBH,DH,LH,TH,
      *KO,LF,DF,KINVIS,PI,LO
       WRITE(6,1)AO,BO,LO,LR,CR,DS,LS,LAS,LAH,LBH,DH,LH,TH,
      *KO,LF,DF,KINVIS,PI,LO
       WRITE(7,1)AO,BO,LO,LR,CR,DS,LS,LAS,LAH,LBH,DH,LH,TH,
      *KO,LF,DF,KINVIS,PI,LO
     1 FORMAT(5X,'AO=',F10.5,/,5X,'BO=',F10.5,/,5X,'LO=',F10.5,/,
      *5X,'LR=',F10.5,/,5X,'CR=',F10.5,/,5X,'DS=',F10.5,/,5X,'LS=',F10.
      *5,/,5X,'LAS=',F10.5,/,5X,'LAH=',F10.5,/,5X,'LBH=',F10.5,/,5X,
      *'DH=',F10.5,/,5X,'LH=',F10.5,/,5X,'TH=',F10.8,/,5X,
      *'KO=',F10.5,/,5X,'LF=',F10.5,/,5X,
      *'DF=',F10.5,/,5X,'KINVIS=',F14.8,/,5X,
      *'PI=',F10.5,/,5X,'LO=',F10.5,/,/)
       DO=2.*AO*BO/(AO+BO)
       AAO=AO*BO
       AC=3.*AO
       BC=3.*BO
       DC=3.*DO
       AAC=AC*BC
       LC=LR*DC
```

```
      BETA=(1-DS/LS)**2
      NB=DC/DH
      NA=AC/DH
      N=NA*NB
      AAH=(PI/4.)*N*(DH-2*TH)**2
      AH=AAH/AAC
      LT=LF+LD+LBH+LH+LAH+LAS+LC+LD
      AAF=PI*DF**2/4.
      WRITE(6,3)DO,DC,AAO,AAC,AAH,AAF,AH,LC,BETA,LT
      WRITE(7,3)DO,DC,AAO,AAC,AAH,AAF,AH,LC,BETA,LT
    3 FORMAT(5X,'DO=',F10.5,/,5X,'DC=',F10.5,/,5X,'AAO=',F10.5,/,
     *5X,'AAC=',F10.5,/,5X,'AAH=',F10.5,/,5X,'AAF=',F10.5,/,
     *5X,'AH=',F10.5,/,5X,'LC=',F10.5,/,5X,'BETA=',F10.5,/,5X,
     *'LT=',F15.8,/,/)
      DO 10 I=1,49
      VO(I)=I*1.
      Q(I)=AAO*VO(I)
      REO(I)=VO(I)*DO/XINVIS
      RE=REO(I)
      F(I)=0.303/(((LOG10(RE))-0.9)**2)
      KO(I)=F(I)*LO/DO
      VC(I)=VO(I)/CR
      KC(I)=(4./9.)*F(I)*LR*(CR**4.5-1)/(CR**2.5*(CR-1))
      RES(I)=VC(I)*DS/(BETA*XINVIS)
      KS(I)=(6.5*(1-BETA)/(BETA**2))*(RES(I))**(-1./3.)
      VH(I)=VC(I)/AH
      RLH(I)=VH(I)*(DH-2*TH)/XINVIS
      IF(RLH(I).GT.4000) GO TO 222
      KH(I)=4.424-0.3586E-02*RLH(I)+0.1755E-05*RLH(I)**2-0.3941478E-09
     **RLH(I)**3+0.3103E-13*RLH(I)**4
      GO TO 223
  222 KH(I)=1.52
  223 XT(I)=XO(I)+(KC(I)+KS(I)+KH(I))/CR**2+KO*(AAO/AAF)**2
      KT1(I)=1.15*XT(I)+1.
      K(I)=KT1(I)/(2*AAO*AAO*9.81)
      H(I)=K(I)*Q(I)*Q(I)
      WRITE(6,2)I,VO(I),I,REO(I),I,F(I),I,KO(I),I,KC(I),I,KS(I),
     *I,XH(I),I,KT(I),I,KT1(I),I,Q(I),I,H(I),I,K(I)
      WRITE(7,2)I,VO(I),I,REO(I),I,F(I),I,XO(I),I,KC(I),I,KS(I),
     *I,XH(I),I,KT(I),I,KT1(I),I,Q(I),I,H(I),I,K(I)
    2 FORMAT(5X,'VO(',I3,')=',F10.5,/,5X,'REO(',I3,')=',F17.8,/,
     *5X,'F(',I3,')=',F10.5,/,5X,'KO(',I3,')=',F10.5,/,5X,'KC(',I3,
     *')=',F10.5,/,5X,'KS(',I3,')=',F10.5,/,5X,'KH(',I3,
     *')=',F10.5,/,5X,'KT(',I3,')=',F10.5,/,5X,'KT1(',I3,
     *')=',F10.5,/,5X,'Q(',I3,')=',F10.5,/,5X,'H(',I3,')=',F10.5,
     */,5X,'X(',I3,')=',F10.5,/,/,/,/)
   10 CONTINUE
      STOP
      END
```

A SAMPLE OUTPUT FOR PROTOTYPE

```
AO=     1.60000
BO=     1.50000
CO=     4.00000
CR=     1.23400
CP=     2.00000
DS=     0.00077
ES=     0.00350
L4O=     1.00000
L4H=     0.52500
LBH=     0.12500
DH=     0.02450
EH=     0.02500
TH=0.000500000
KO=     0.30000
LF=     1.20000
EF=     2.10000
KINVIS=     0.000001647
PI=     3.14160
CO=     5.20000

DO=     1.20000
DC=     3.00000
AMO=     1.50000
AMC=    13.00000
AMH=     3.26324
AMF=     3.46361
AH=     0.03617
EC=     4.62240
BETA=     0.00040
ET=     16.97883780


VO(   1)=     1.00000
REO(   1)=     72859.69750000
F(   1)=     0.01930
KO(   1)=     0.00433
KC(   1)=     0.11150
KS(   1)=     3.30452
KH(   1)=     3.70147
KT(   1)=     0.20920
KTI(   1)=     1.24058
W(   1)=     1.50000
H(   1)=     0.05323
K(   1)=     0.02610

VO(   3)=     3.00000
REO(   3)=     218574.12500000
F(   3)=     0.01537
KO(   3)=     0.05124
KC(   3)=     0.06802
KS(   3)=     2.33203
KH(   3)=     2.69061
KT(   3)=     0.17702
KTI(   3)=     1.19624
W(   3)=     4.50000
H(   3)=     0.04872
K(   3)=     0.02710

VO(   5)=     5.00000
REO(   5)=     364298.56250000
F(   5)=     0.01384
KO(   5)=     0.04648
KC(   5)=     0.06097
KS(   5)=     1.96758
KH(   5)=     2.11298
KT(   5)=     0.15412
KTI(   5)=     1.17724
W(   5)=     7.50000
H(   5)=     1.50000
K(   5)=     0.02687

VO(   7)=     7.00000
REO(   7)=     510016.00000000
F(   7)=     0.01311
KO(   7)=     0.04370
KC(   7)=     0.07574
KS(   7)=     1.79803
KH(   7)=     1.81918
KT(   7)=     0.14507
KTI(   7)=     1.16083
W(   7)=    10.50000
H(   7)=     2.91411
K(   7)=     0.02643
```

A SAMPLE OUTPUT FOR MODEL

```
AO=    0.14500
BO=    0.21400
CO=    0.57000
CR=    1.23400
CP=    0.00000
US=    0.00011
CS=    0.00050
CAO=   0.19500
CAH=   0.07500
CBH=   0.01800
DH=    0.00350
EH=    0.03200
TH=0.00011000
KO=    0.30000
CF=    0.17100
DF=    0.00000
KINV.S=    0.000016047
PI=    3.14160
CO=    0.74500

DO=    0.17144
EO=    0.01432
AIO=   0.03000
AIC=   0.27542
AIH=   0.10997
AIF=   0.07063
AH=    0.03477
CC=    0.85039
DET.=    0.02840
LT=      2.42438507

VO(  1)=    1.00000
KEO(  1)=    10409.210900000
F(  1)=    0.03118
KO(  1)=    0.10365
KC(  1)=    0.10014
KS(  1)=    6.43608
KH(  1)=    4.31075
KT(  1)=    2.29473
KTI(  1)=    1.33901
Q(  1)=    0.03060
H(  1)=    0.05822
K(  1)=   72.87639

VO(  7)=    7.00000
KEO(  7)=    72854.437500000
F(  7)=    0.01930
KO(  7)=    0.06416
KC(  7)=    0.11150
KS(  7)=    3.30451
KH(  7)=    3.70295
KT(  7)=    0.20902
KTI(  7)=    1.24037
Q(  7)=    0.21421
H(  7)=    3.09776
K(  7)=   97.50759

VO( 14)=   14.00000
KEO( 14)=   145728.07500000
F( 14)=    0.01067
KO( 14)=    0.05542
KC( 14)=    0.09951
KS( 14)=    2.97042
KH( 14)=    3.13391
KT( 14)=    0.10459
KTI( 14)=    1.21217
Q( 14)=    0.42049
H( 14)=   12.10935
K( 14)=   65.97279

VO( 21)=   21.00000
KEO( 21)=   218593.43700000
F( 21)=    0.01537
KO( 21)=    0.03111
KC( 21)=    0.06382
KS( 21)=    2.33253
KH( 21)=    2.59362
KT( 21)=    0.17043
KTI( 21)=    1.19070
Q( 21)=    0.04264
H( 21)=   26.38397
K( 21)=   55.09019
```

DRAWINGS

PROTOTYPE BLOWER WIND TUNNEL					
Part No	Part Name	Material	Quantity	Drawing No	Comments
1	Framework	Pine wood	-	101	*
2	Fan section	Plywood	1	102	
3	Transition section	Plywood	1	103	
4	W.A. diffuser 1	Plywood	1	104	
5	W.A. diffuser 2	Plywood	1	104	
6	Screens	Polyester gauze	2	-	
7	Honeycomb	Plastic pipes	-	-	**
8	Settling chamber	Plywood	1	105	24.5x220mm
9	Contraction frame	Steel	1	106	
10	Roof and floor walls of contraction	Plywood	2	107	
11	Side walls of contraction	Plywood	2	108	
12	Test section	Plywood	1	109	

* Stages in construction of the tunnel frameworks

** Settling chamber screen : 0.8x3.5 mm
Diffuser screen : 1.75x5.81 mm

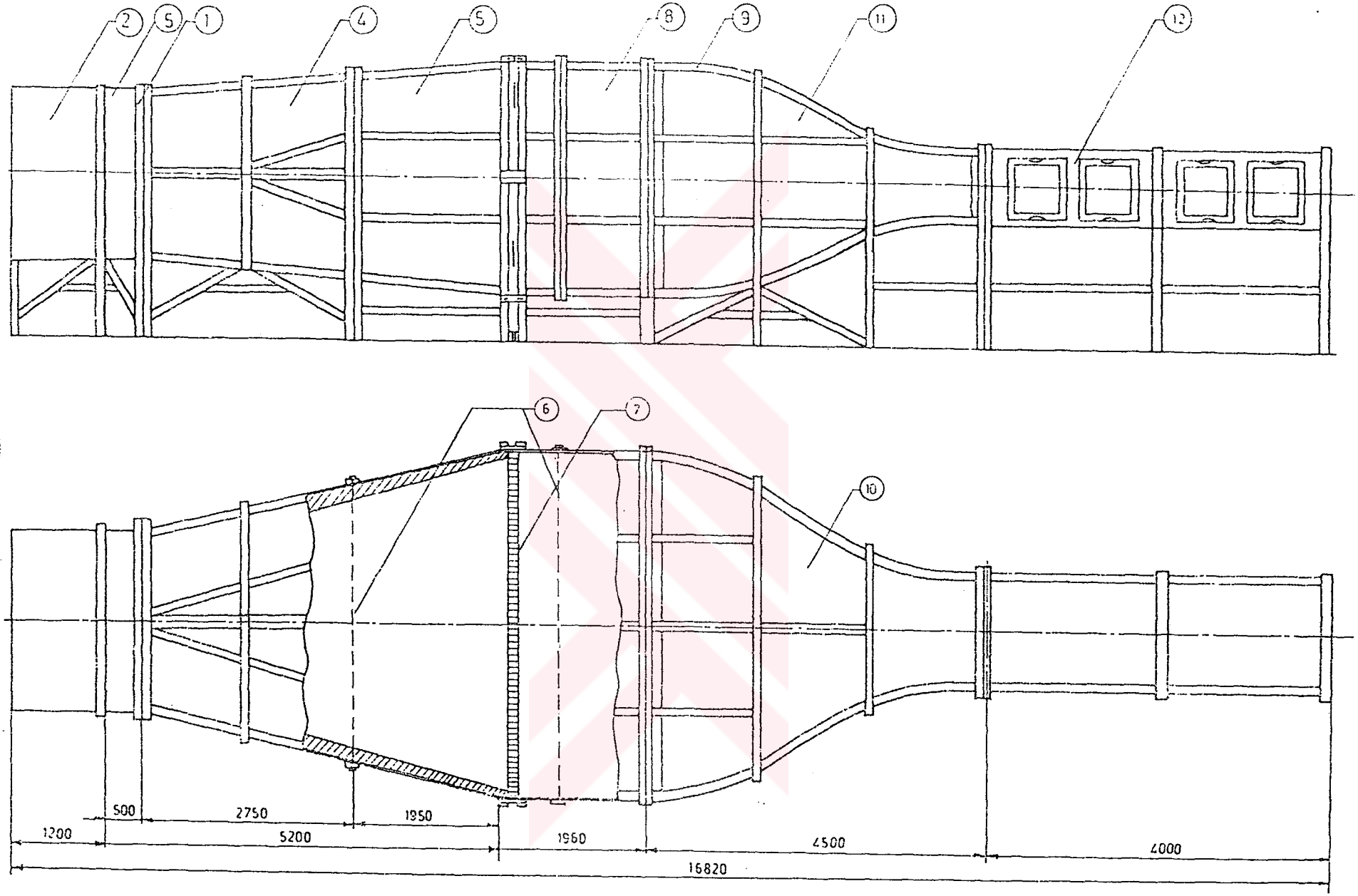

Assembly Drawing	Scale	Drawing No
Prototype blower wind tunnel	1/50	100

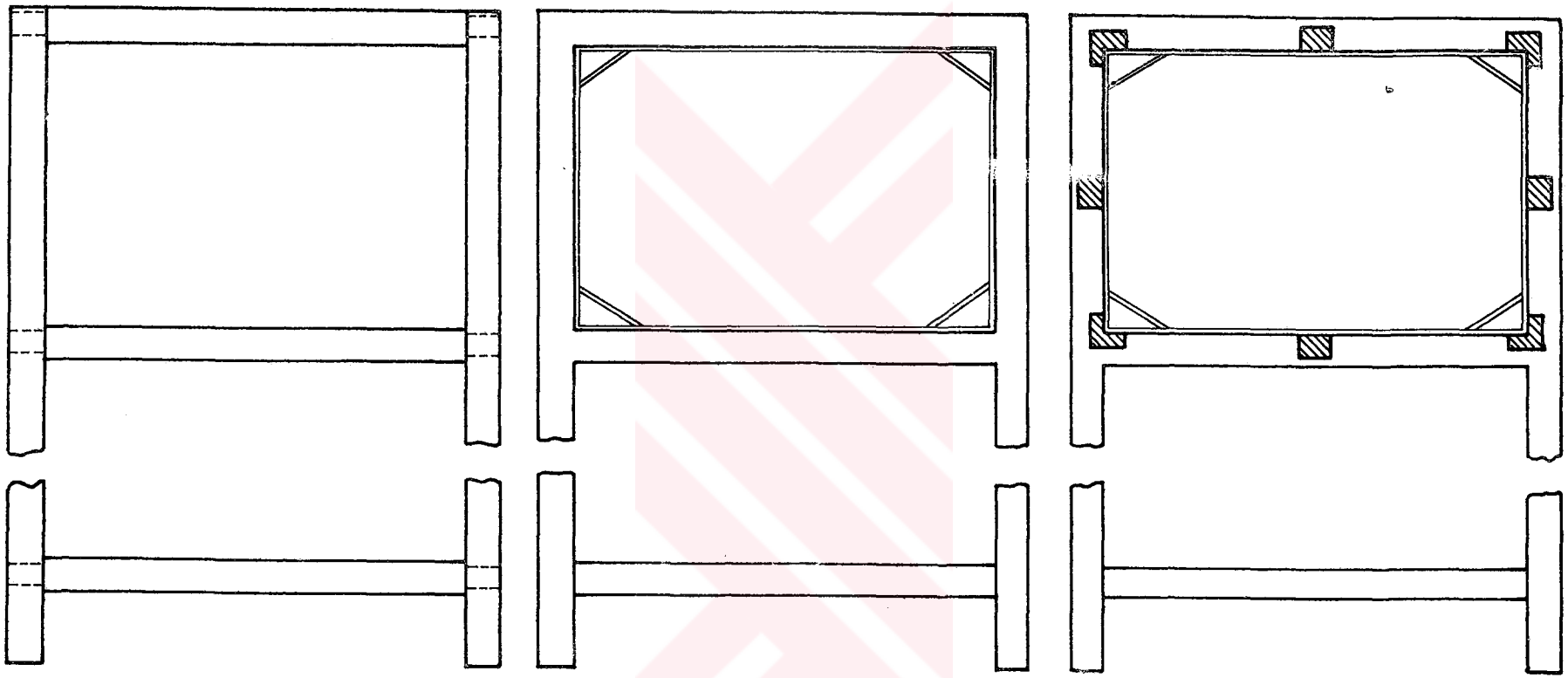

1 Pairs of end frames.

2 Plywood walls screwed into place.

3 Full-length capping strips screwed and glued.

Quantity	Scale	Part Name	Material	Drawing No
		Framework of Prototype and model	Pine Wood	101

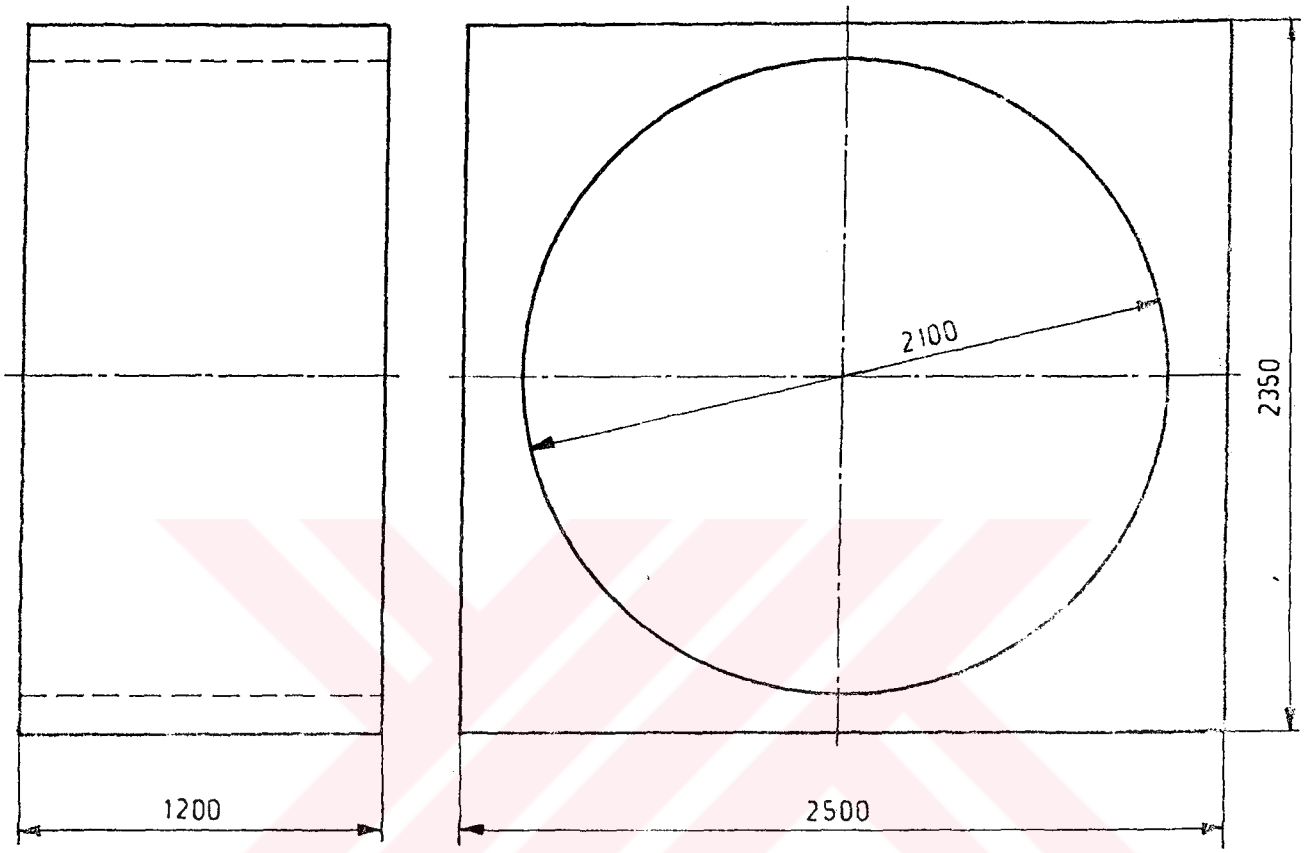

Quantity	Scale	Part Name	Material	Draw. No
1	1/25	Prototype fan section	Plywood	102
1	7/25	Model fan* section	Pine wood	

* Model dimension = $\frac{1}{7}$ Prototype dimension

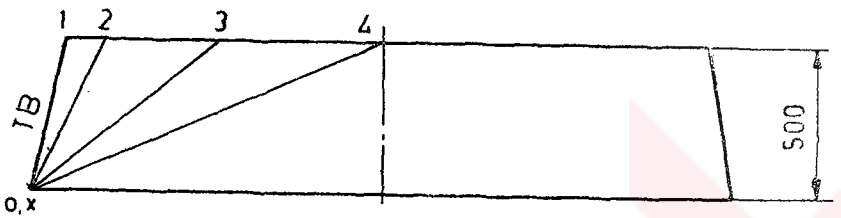

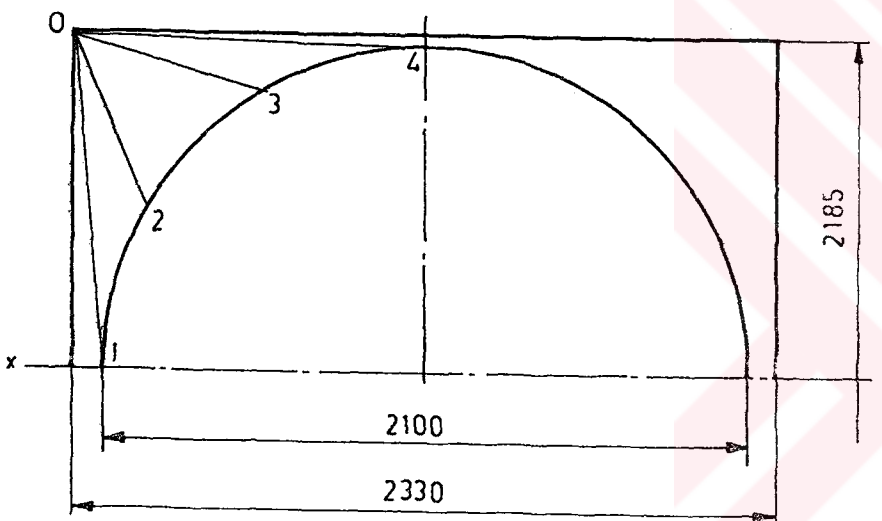

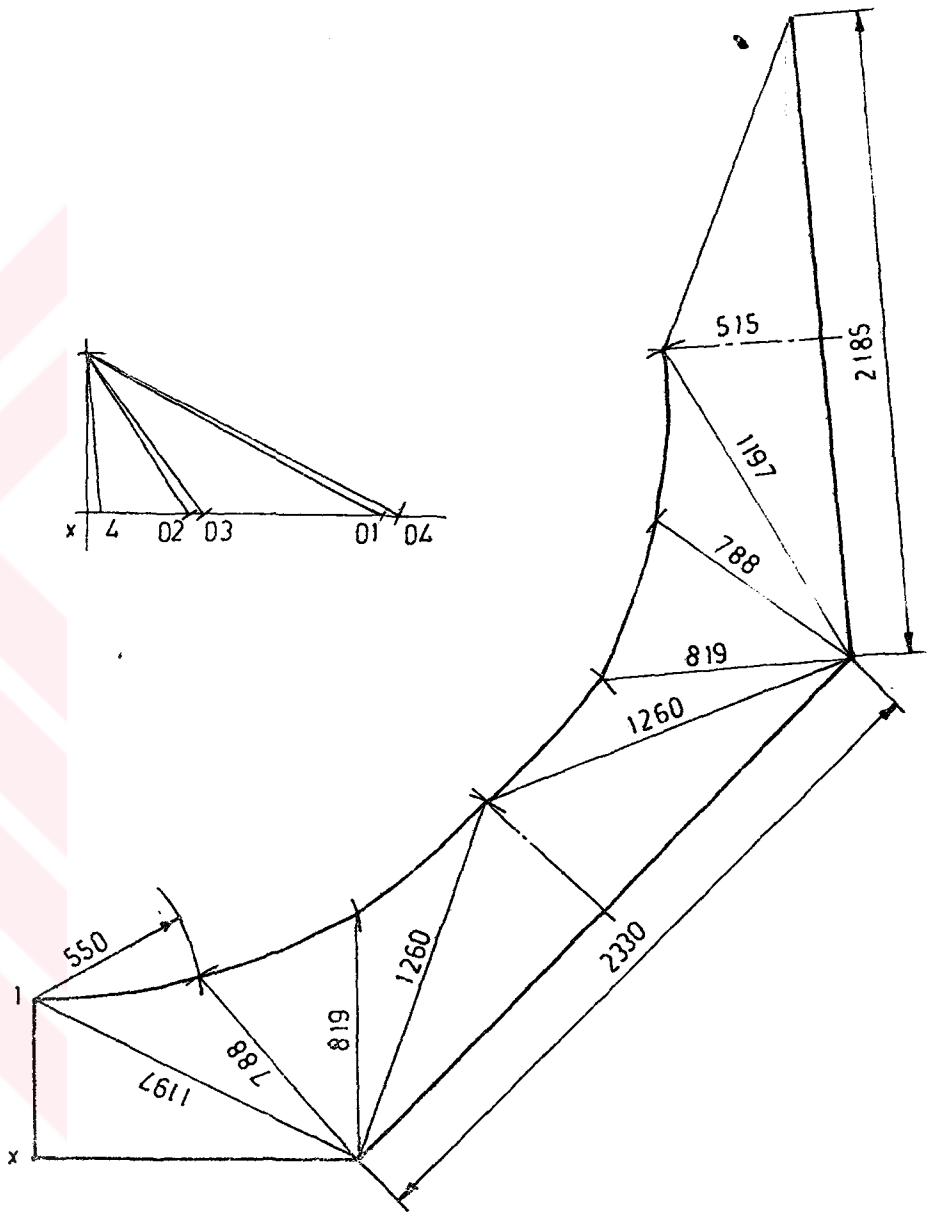

Quantity	Scale	Part Name	Matrerial	Drawing No
2	1/25	Transition Section	Plywood	103

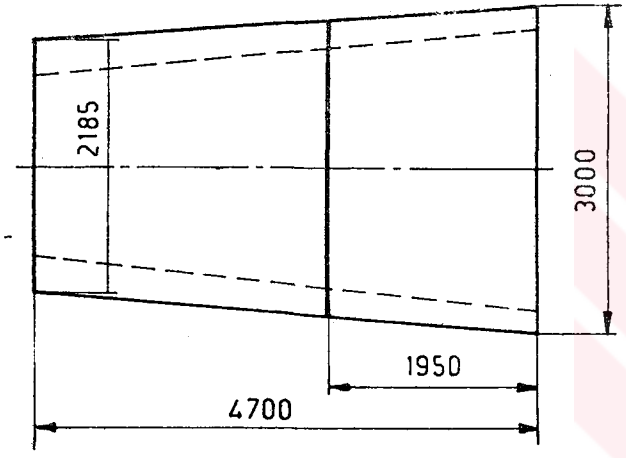

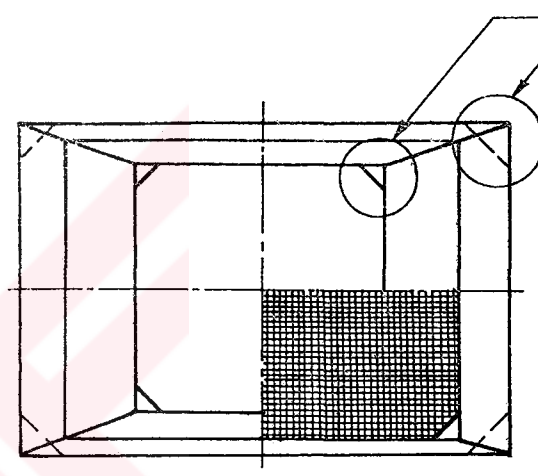

SECTION A-A

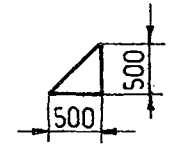

Detail A

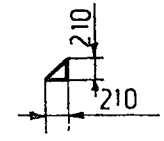

Detail B

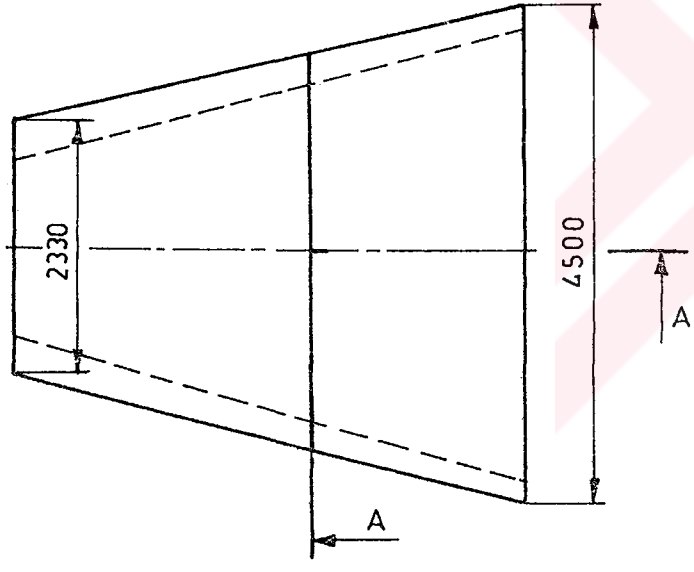

Quantity	Scale	Part Name	Material	Drawing No
1	1/70	Prototype Diffuser	Plywood	104
2	1/10	Model Diffuser *	Formica covered plywood	

* Model dimension = $\frac{1}{7}$ Prototype dimension

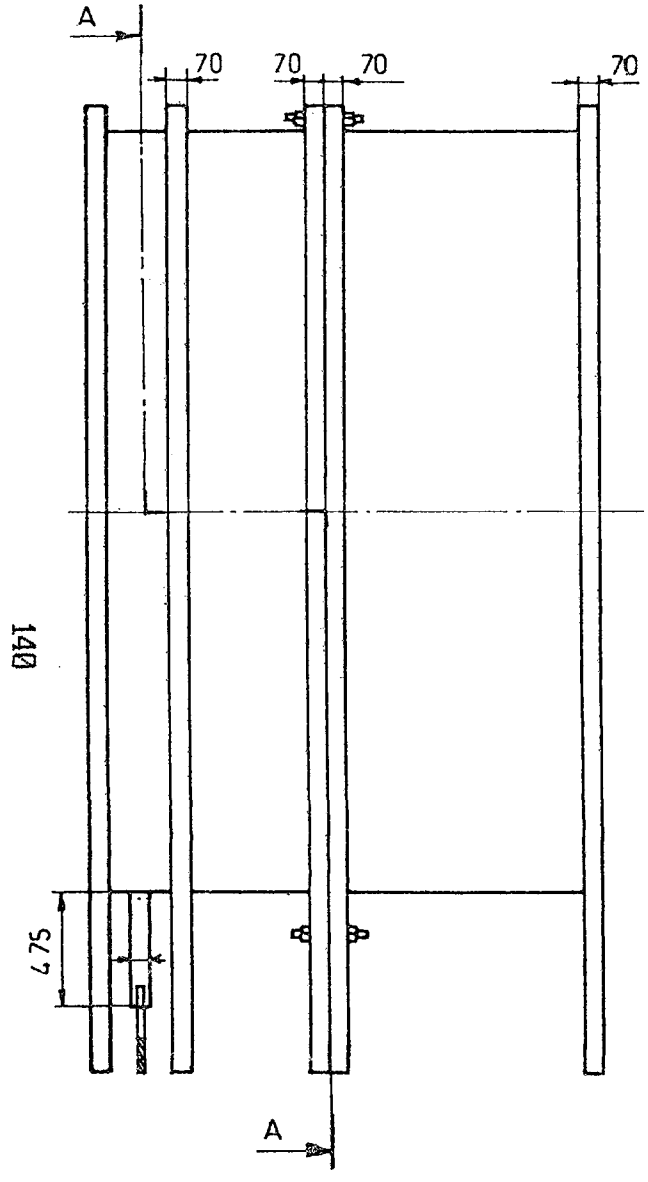

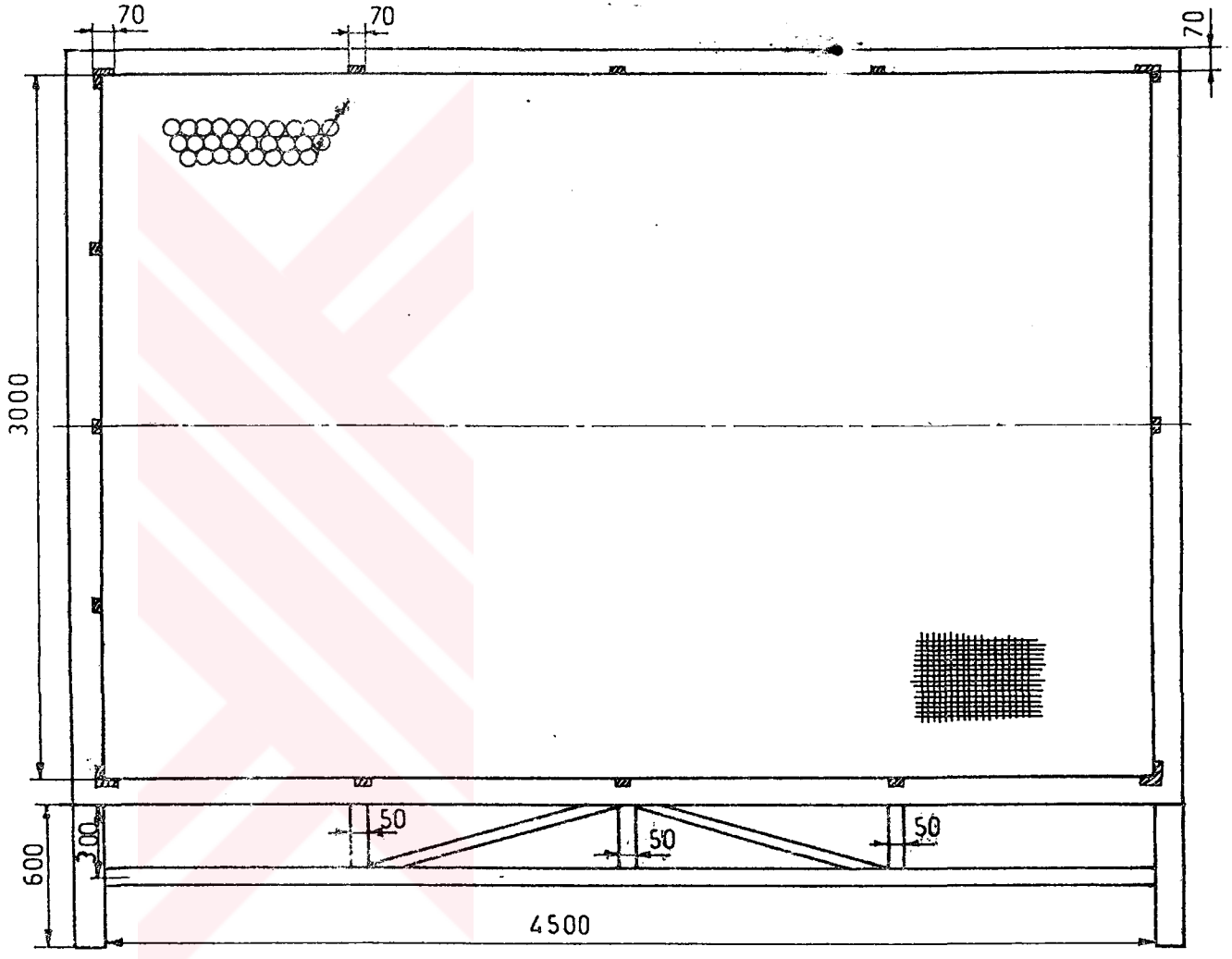

SECTION A-A

Quantity	Scale	Part Name	Material	Drawing No
1	1/30	Settling Chamber	Plywood	105

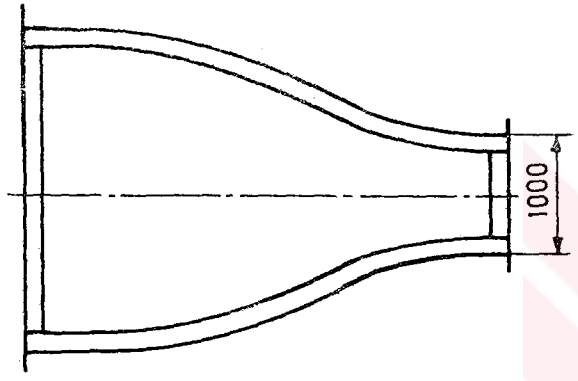

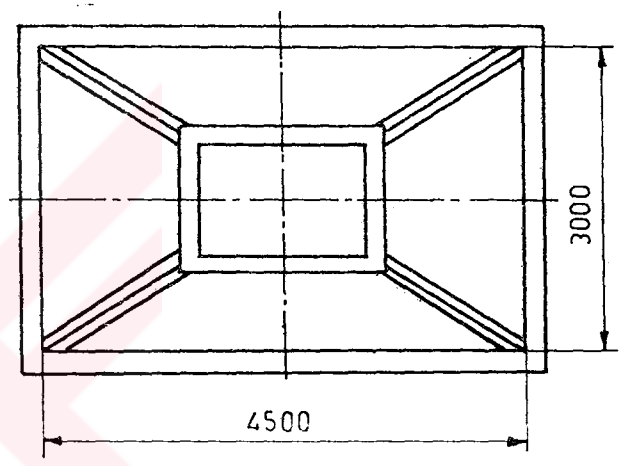

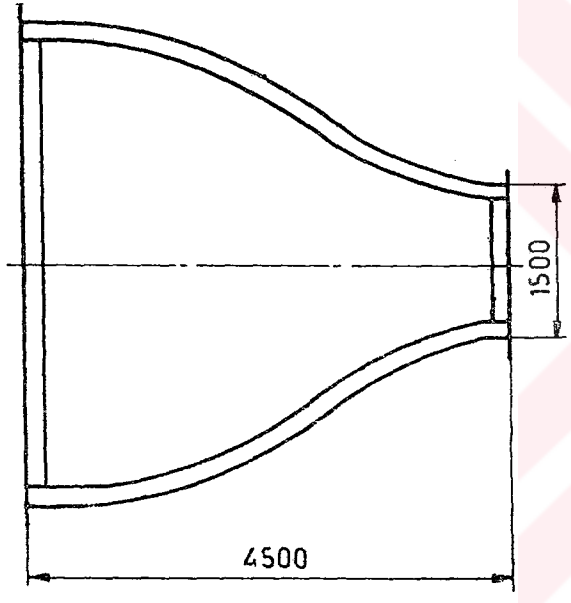

Quantity	Scale	Part Name	Material	Drawing No
1	1/70	Prototype Contraction frame	Metal Sheet	106
1	1/10	Model Contraction frame *	Metal Sheet	

* Model dimension = $\frac{1}{7}$ Prototype dimension

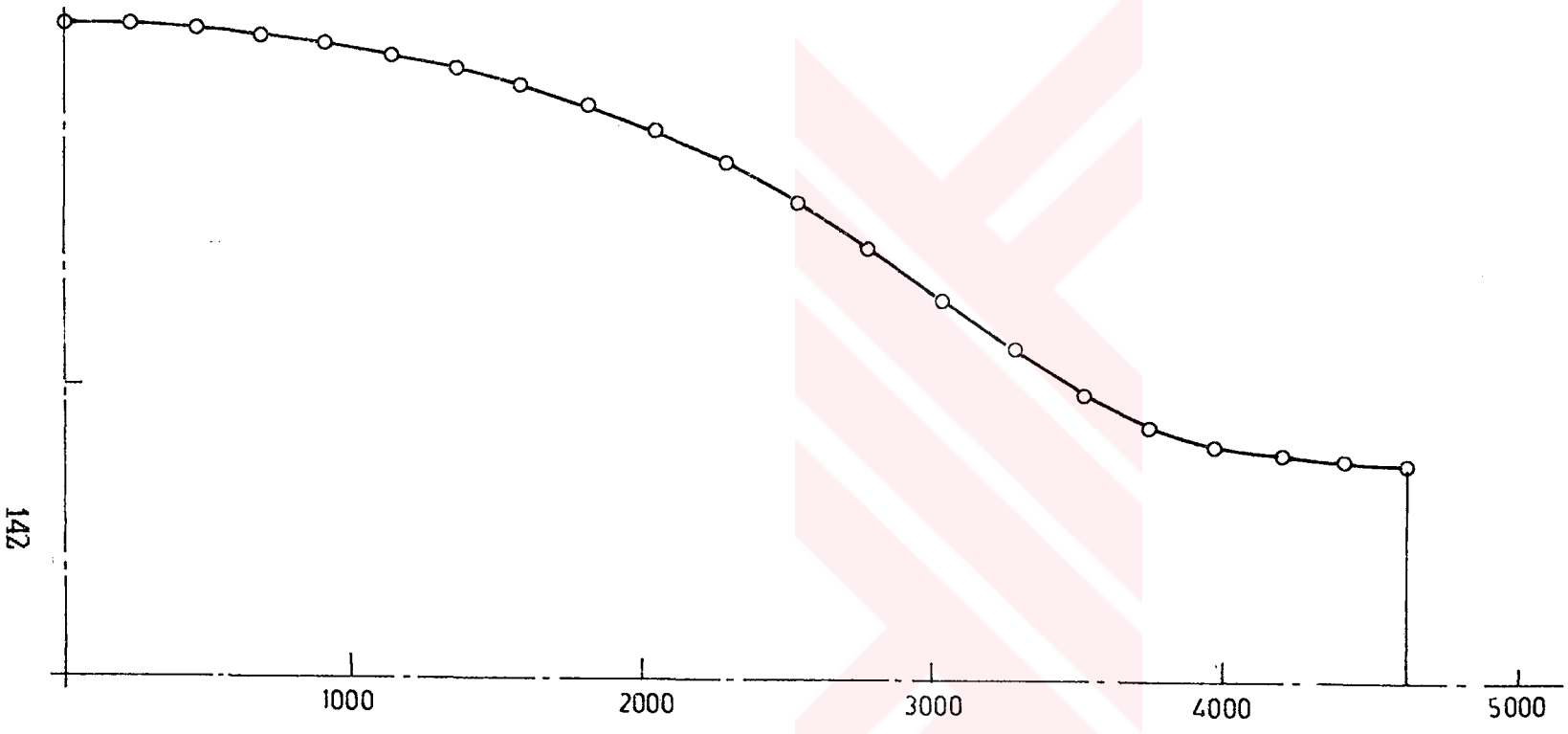

l_y	z
0	2250
225	2247
450	2233
675	2212
900	2184
1126	2147
1350	2100
1576	2044
1805	1974
2037	1883
2275	1773
2525	1643
2768	1484
3027	1312
3286	1130
3522	988
3747	875
3972	817
4208	785
4422	767
4636	751

Quantity	Scale	Part Name	Material	Drawing No.
2	1/25	Roof and Floor of Prototype Contraction	Plywood	107
2	7/25	Roof and Floor of Model Contraction *	Plywood	

* Model dimension = $\frac{1}{7}$ Prototype dimension

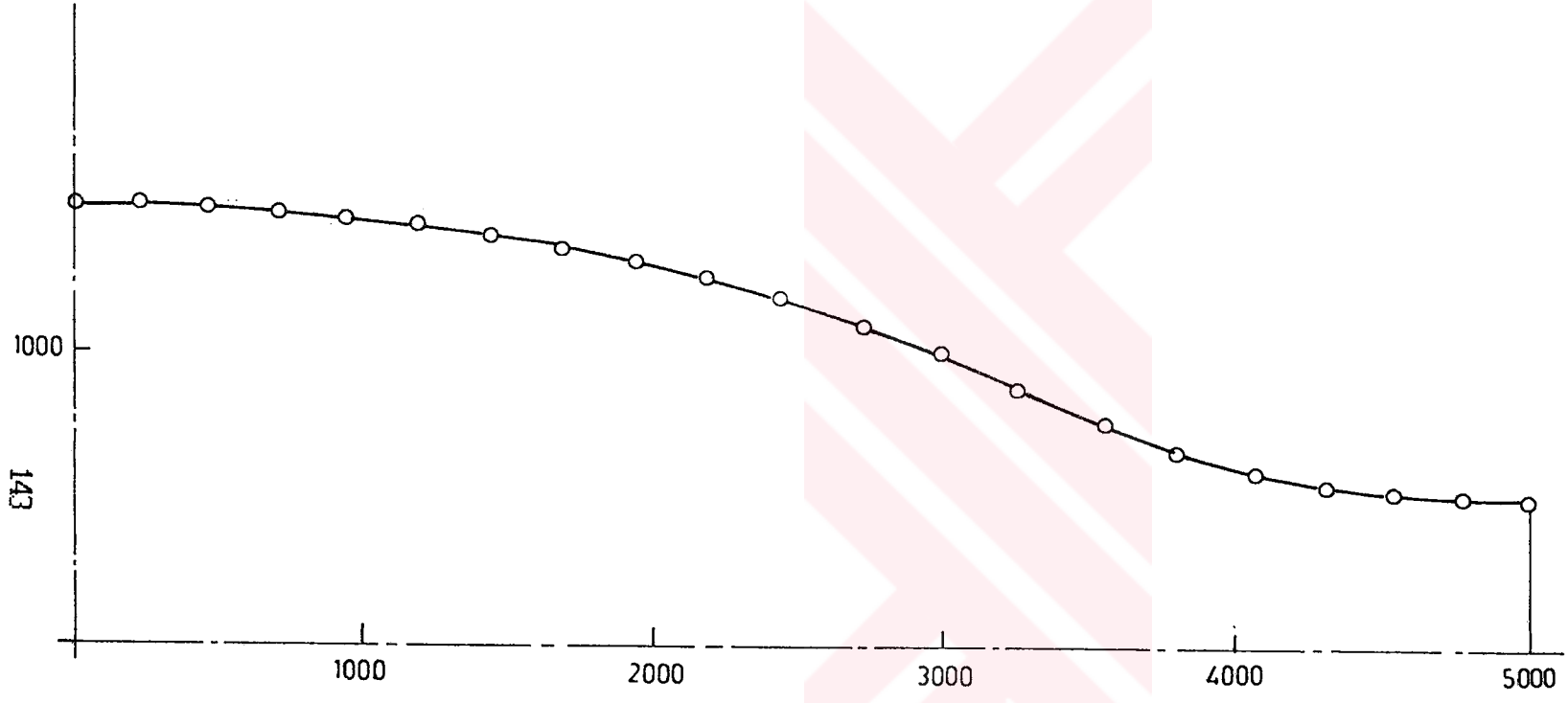

143

l_z	y
0	1500
225	1498
461	1490
709	1474
945	1454
1193	1432
1445	1400
1687	1362
1939	1315
2183	1256
2436	1182
2700	1096
2990	991
3262	873
3556	754
3826	652
4074	585
4321	545
4557	524
4781	513
5019	502

Quantity	Scale	Part Name	Material	Drawing No.
2	1/25	Side walls of Prototype Contraction	Plywood	108
2	7/25	Side walls of Model Contraction*	Plywood	

* Model dimension = $\frac{1}{7}$ Prototype dimension

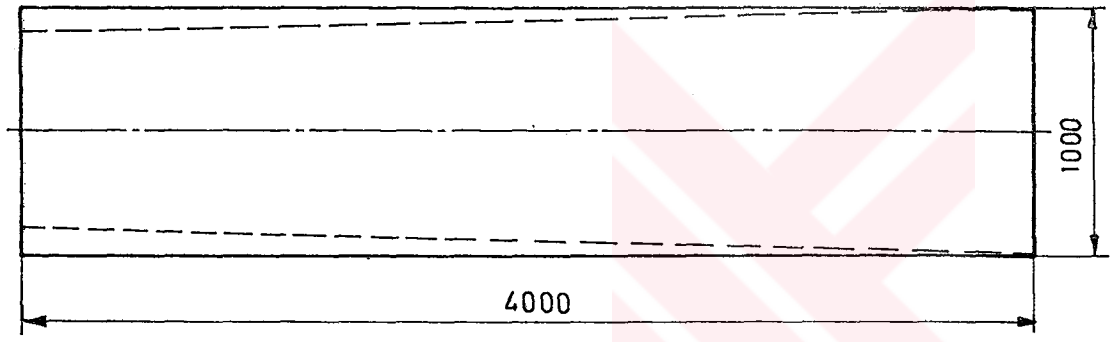

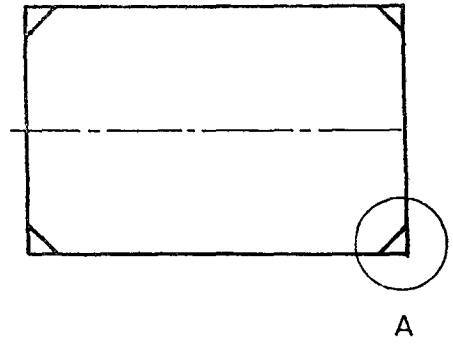

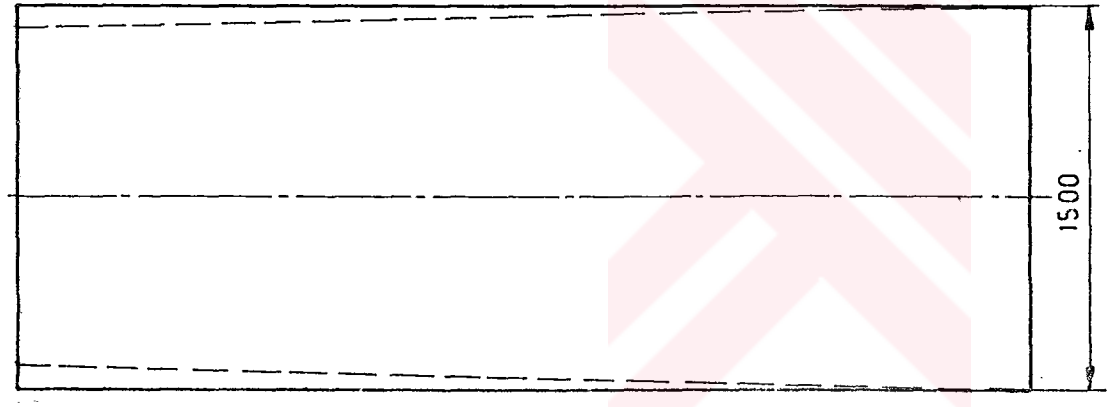

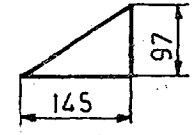

Detail A
Scale 1/10

Quantity	Scale	Part Name	Material	Drawing No
1	1/30	Test Section	Plywood	109

MODEL BLOWER WIND TUNNEL					
Part No	Part Name	Material	Quantity	Drawing No	Comments
1	Framework	Pine wood	-	101	*
2	Fan section	Pine wood	1	102	**
3	Transition section	Pine wood	1	111	
4	W.A. diffuser 1	Formica covered plywood	1	104	**
5	W.A. diffuser 2	Formica covered plywood	1	104	**
6	Screens	Polyester gauze	2	-	***
7	Honeycomb	Plastic straws	1	-	3.5x32mm
8	Settling chamber	Pine wood	1	112	
9	Contraction frame	Steel	1	106	**
10	Roof and floor walls of contraction	Plywood	2	107	**
11	Side walls of contraction	Plywood	2	108	**
12	Test section	Perspex and formica covered plywood	1	113	
13	Nacelle	Pine wood	1	114	
14	Straightener vane	Pine wood	4	115	

* Stages in construction of the tunnel frameworks.

** Same drawing with the corresponding prototype tunnel part; Model dimension = 1/7 prototype dimension.

*** Settling chamber screen: 0.11 x 0.5 mm
Diffuser screen : 0.25 x 0.83 mm

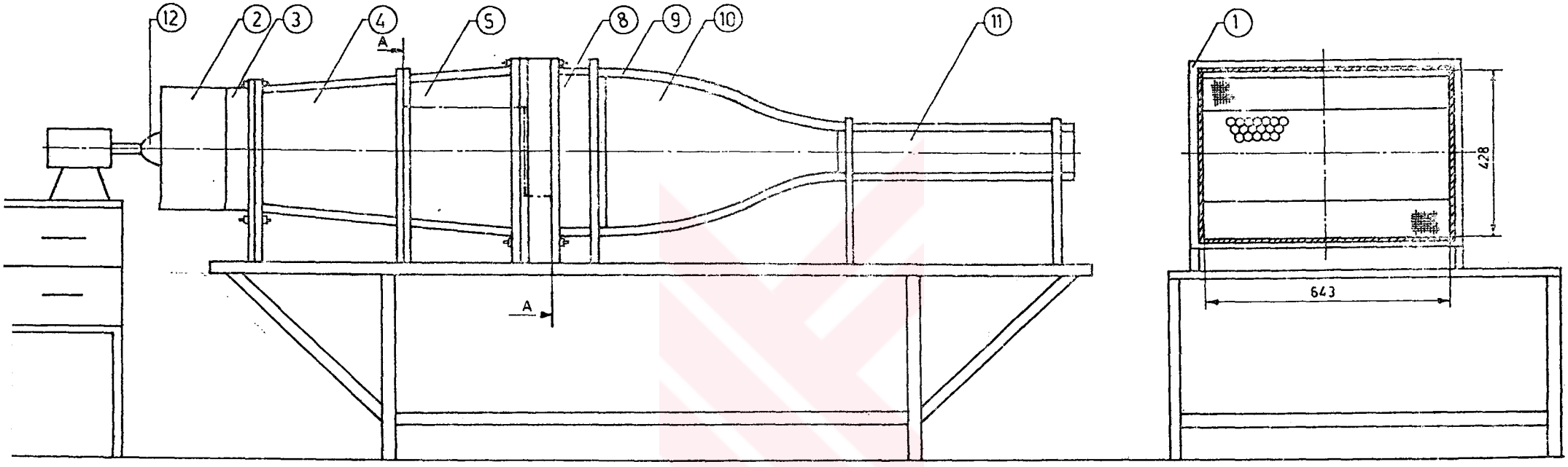

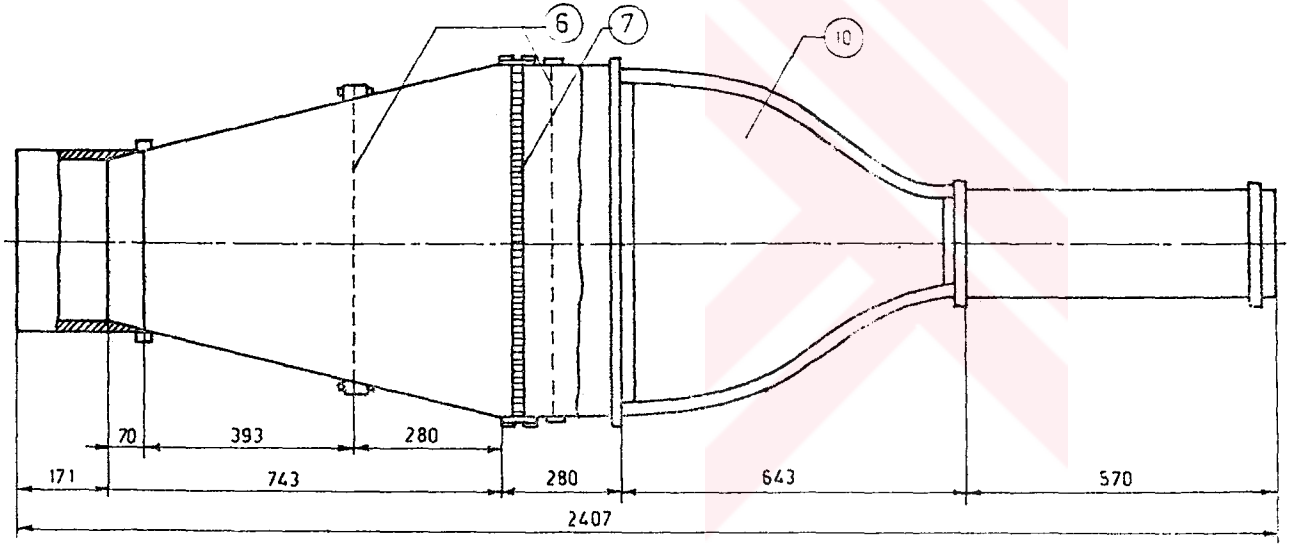

Assembly Drawing	Scale	Drawing No
Model blower wind tunnel	1/10	110

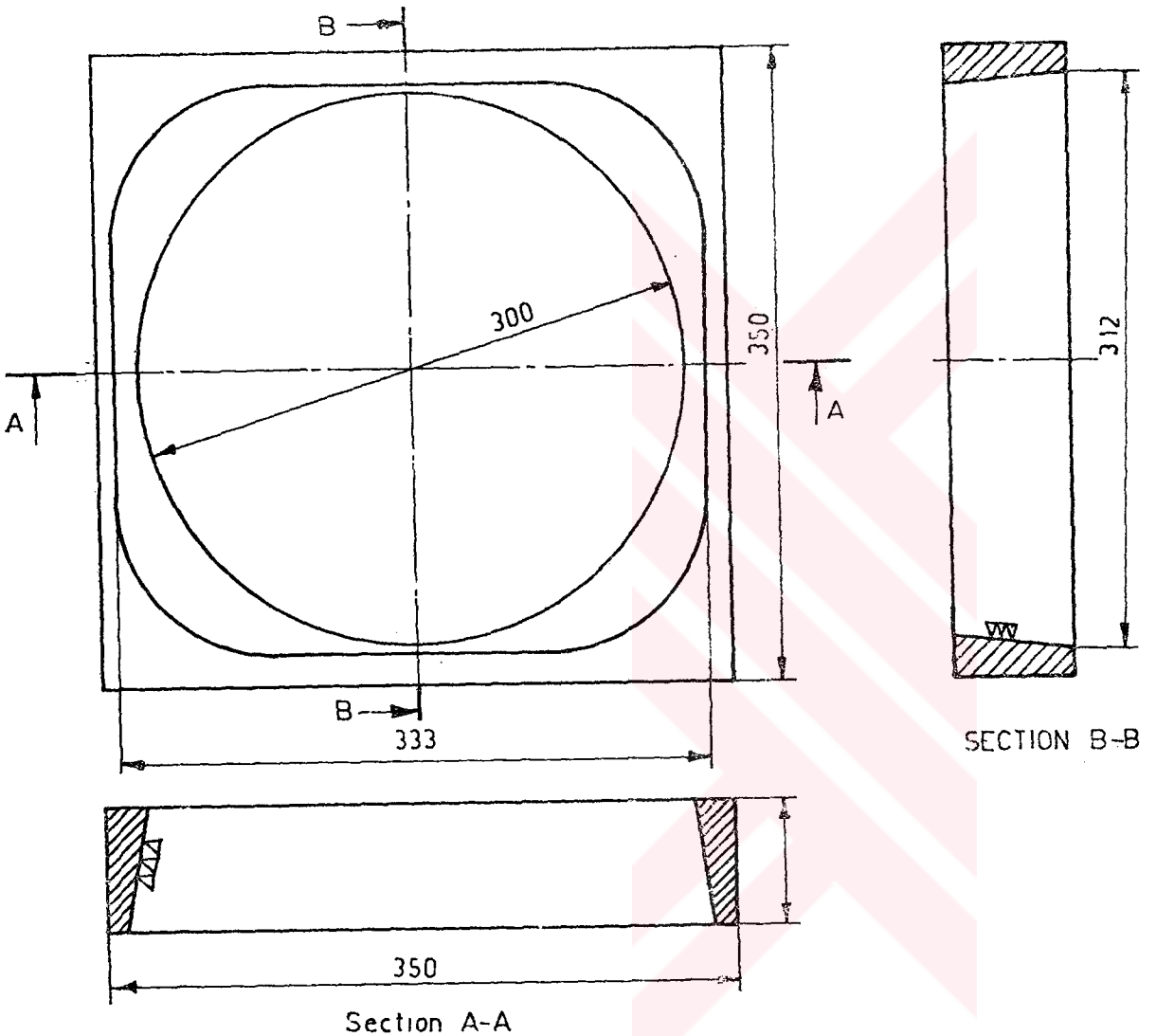

Quantity	Scale	Part Name	Material	Drawing No
1	1/4	Transition Section	Pine Wood	111

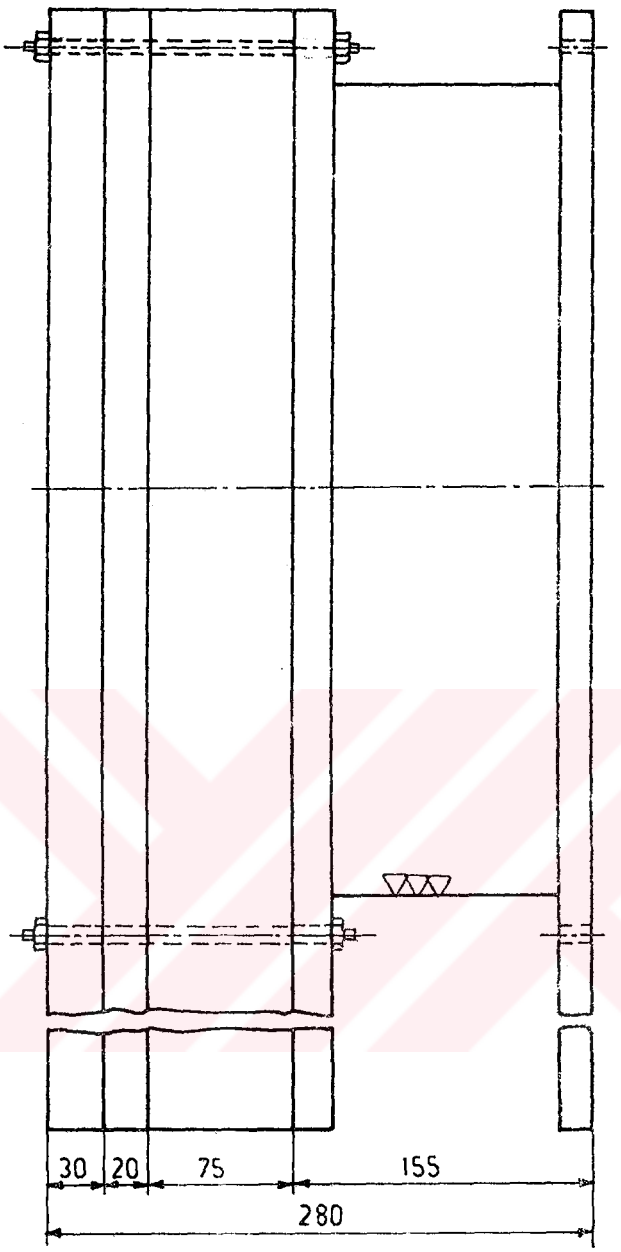

Quantity	Scale	Part Name	Material	Drawing No
1	1/4	Settling Chamber	Pinewood	112

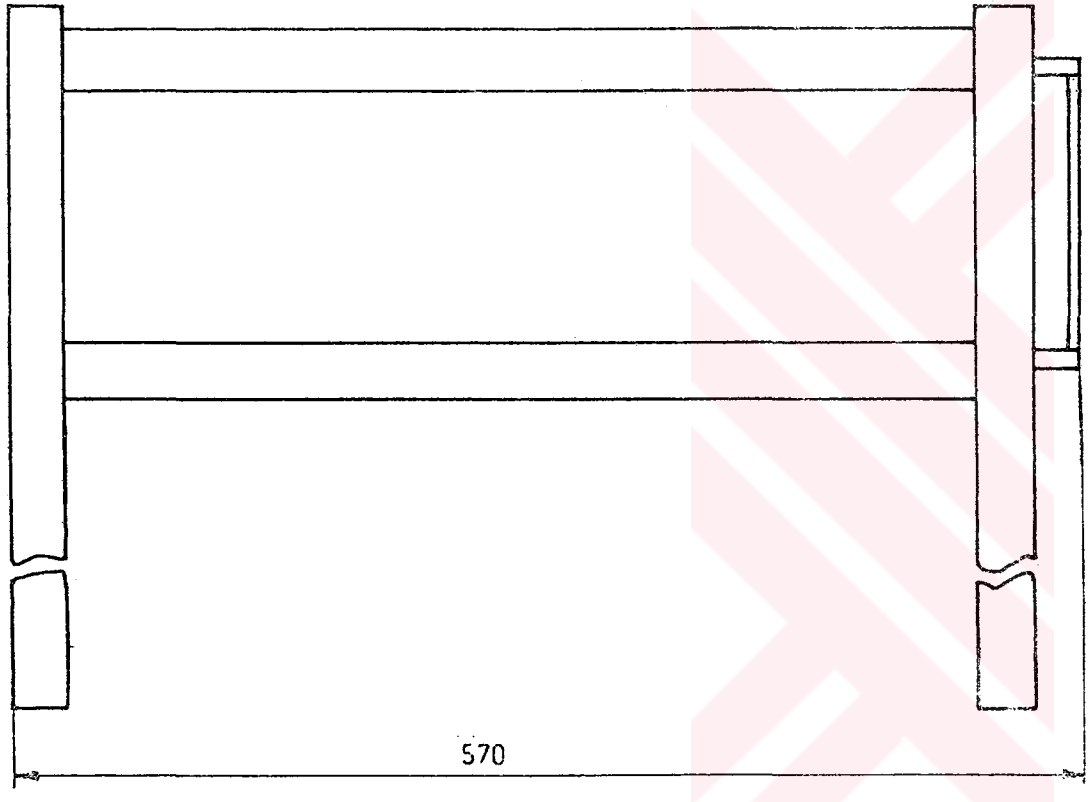

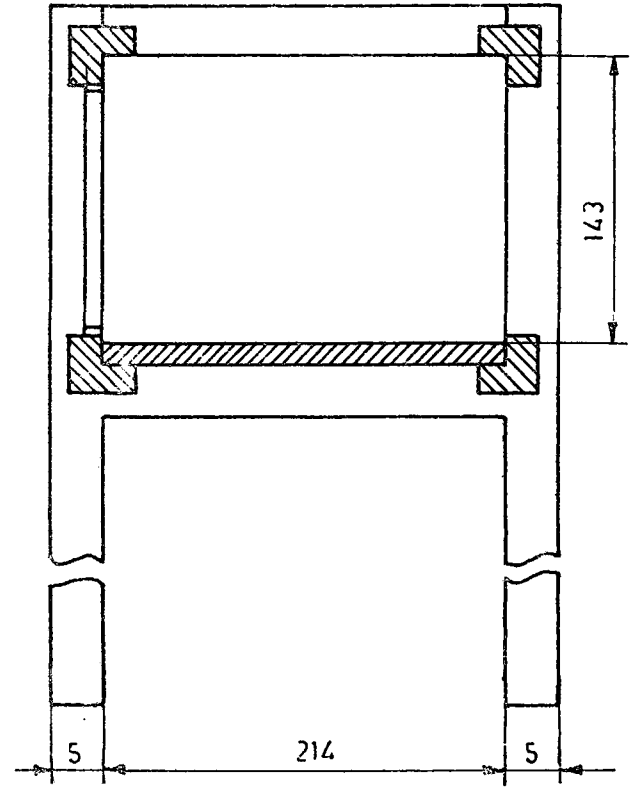

Quantity	Scale	Part Name	Material	Drawing No
1	1/4	Model Test Section	Perspex and plywood	113

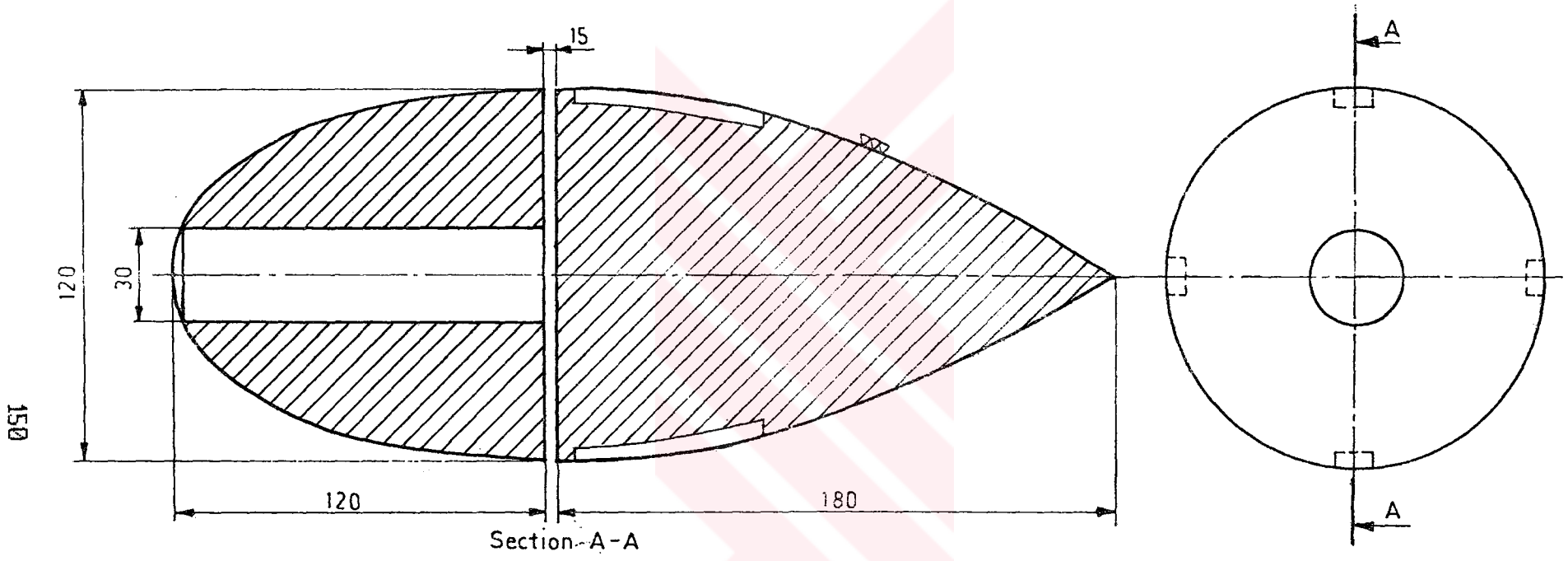

Quantity	Scale	Part Name	Material	Drawing No
1	1/2	Nacelle	Pine Wood	114

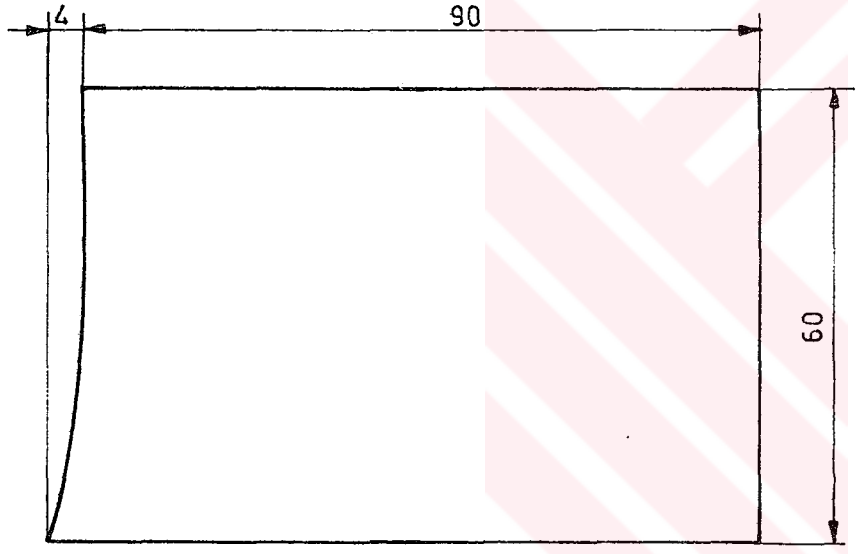

Quantity	Scale	Part Name	Material	Drawing No
4	1/1	Straightener Vane	Pine Wood	115

YAWMETER TRAVERSING MECHANISM				Drawing No 116
Part No	Part Name	Material	Quantity	Scale
1	Yawmeter plate	Brass	1	1/1
2	Connecting plate	Brass	1	1/1
3	Bearing	Brass	1	1/1
4	Rotating rod	Brass	1	1/1
5	Micrometer ring	Brass	1	1/1
6	Rotating arm	Brass	1	1/1
7	Translating rod	Steel	1	1/1
8	Yawmeter probe	Hypodermic needles	1	1/1
9	Micrometer		1	
10	Traversing gear		1	

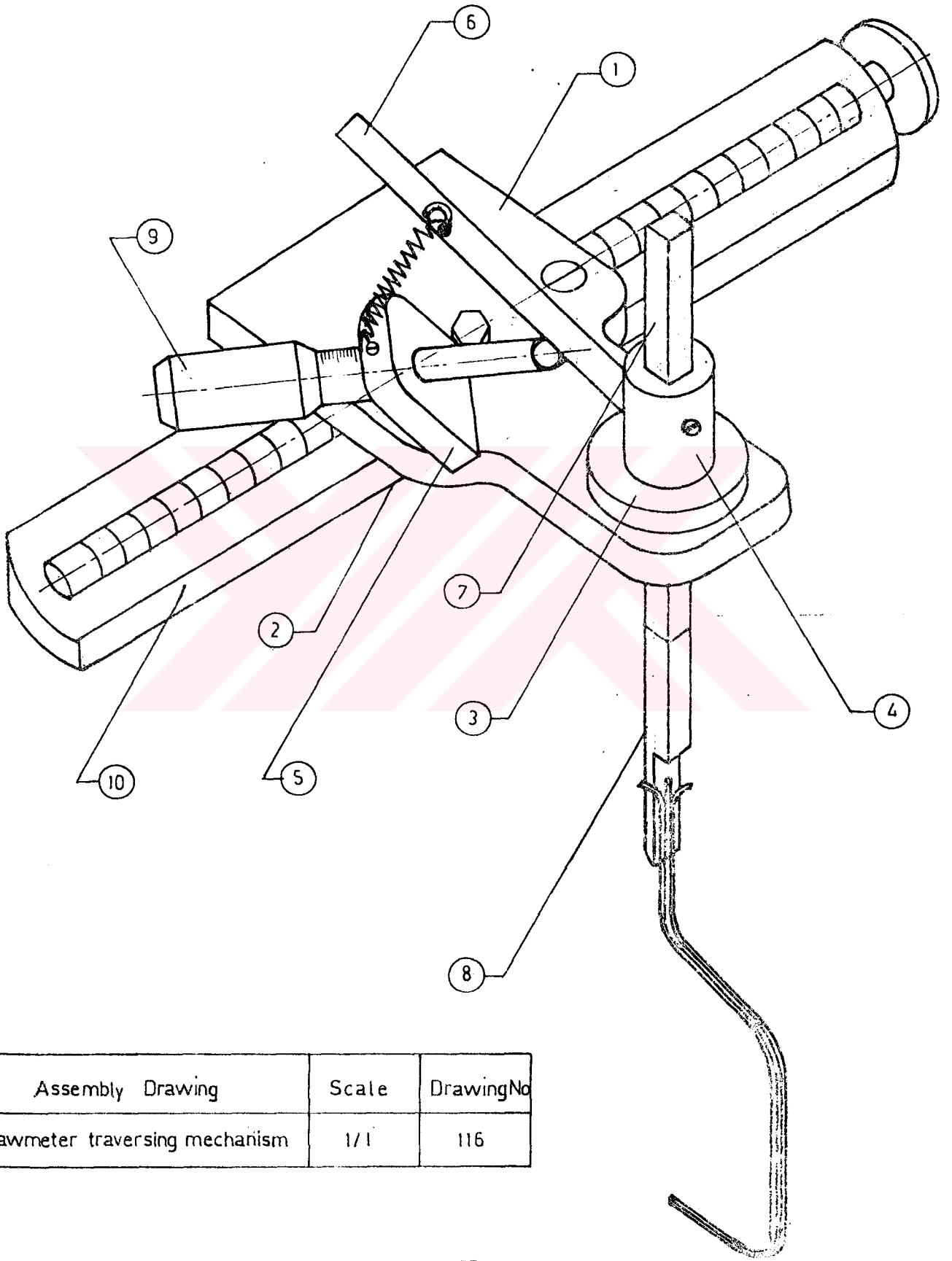

Assembly Drawing	Scale	DrawingNo
Yawmeter traversing mechanism	1/1	116

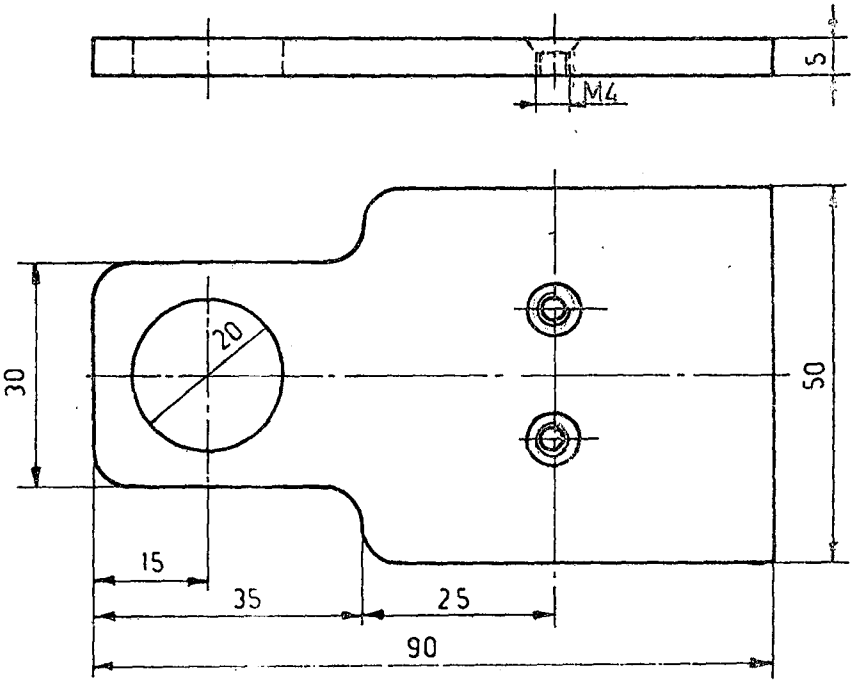
5
M4
30
20
50
15
35
25
90

1

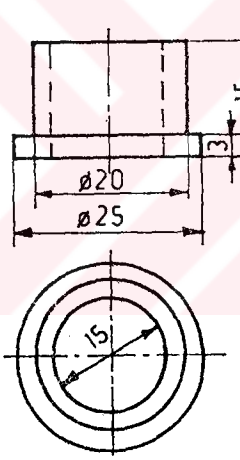
15
3
ø20
ø25
15

3

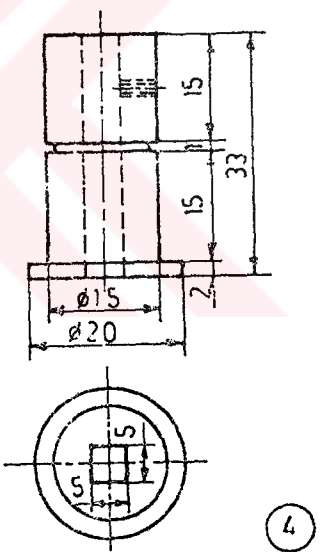
15
33
15
2
ø15
ø20
5
5

4

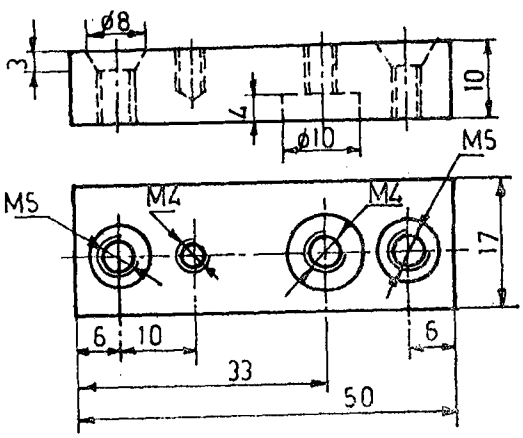
ø8
3
10
4
ø10
M5
M5
M4
M4
17
6
10
6
33
50

2

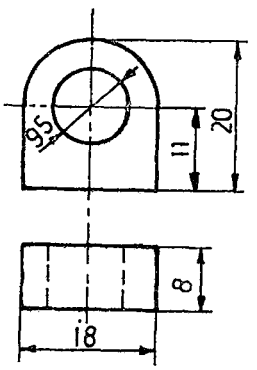
95
11
20
8
18

5

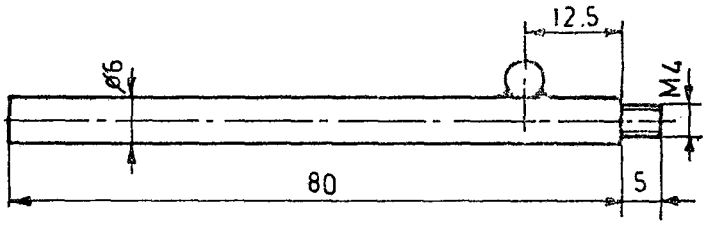
12.5
ø6
M4
80
5

6

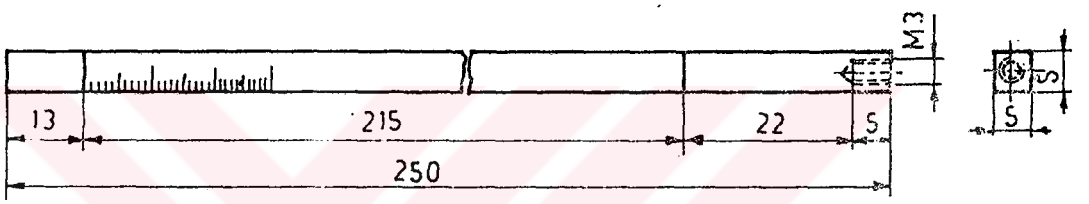
M3
S
S
13
215
22
5
250

7

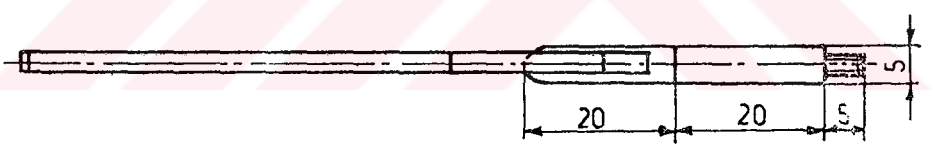
5
20
20
5

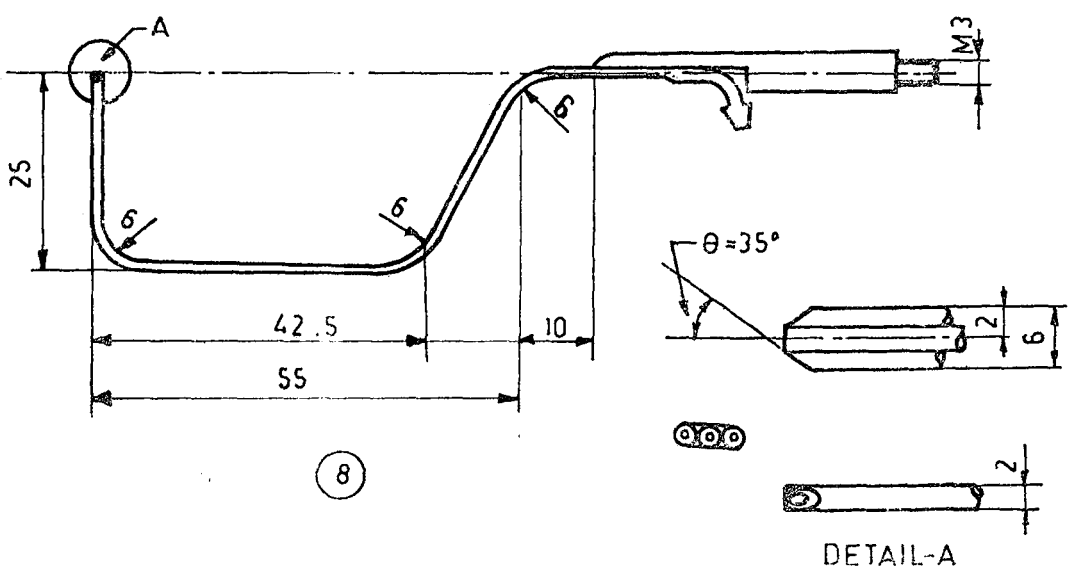
A
M3
25
6
6
6
θ=35°
42.5
10
55
2
6
2
DETAIL-A

8

PITOT TRAVERSING MECHANISM				Drawing No 117
Part No	Part Name	Material	Quantity	Scale
1	Bottom plate	Brass	1	1/1
2	Mechanism carrier	Brass	1	1/1
3	Supports	Brass	1	1/1
4	Tube carrier	Brass	1	1/1
5	Endless screw	Brass	1	1/1
6	Pitot tube	Brass	1	
7	Upper plate	Copper	1	

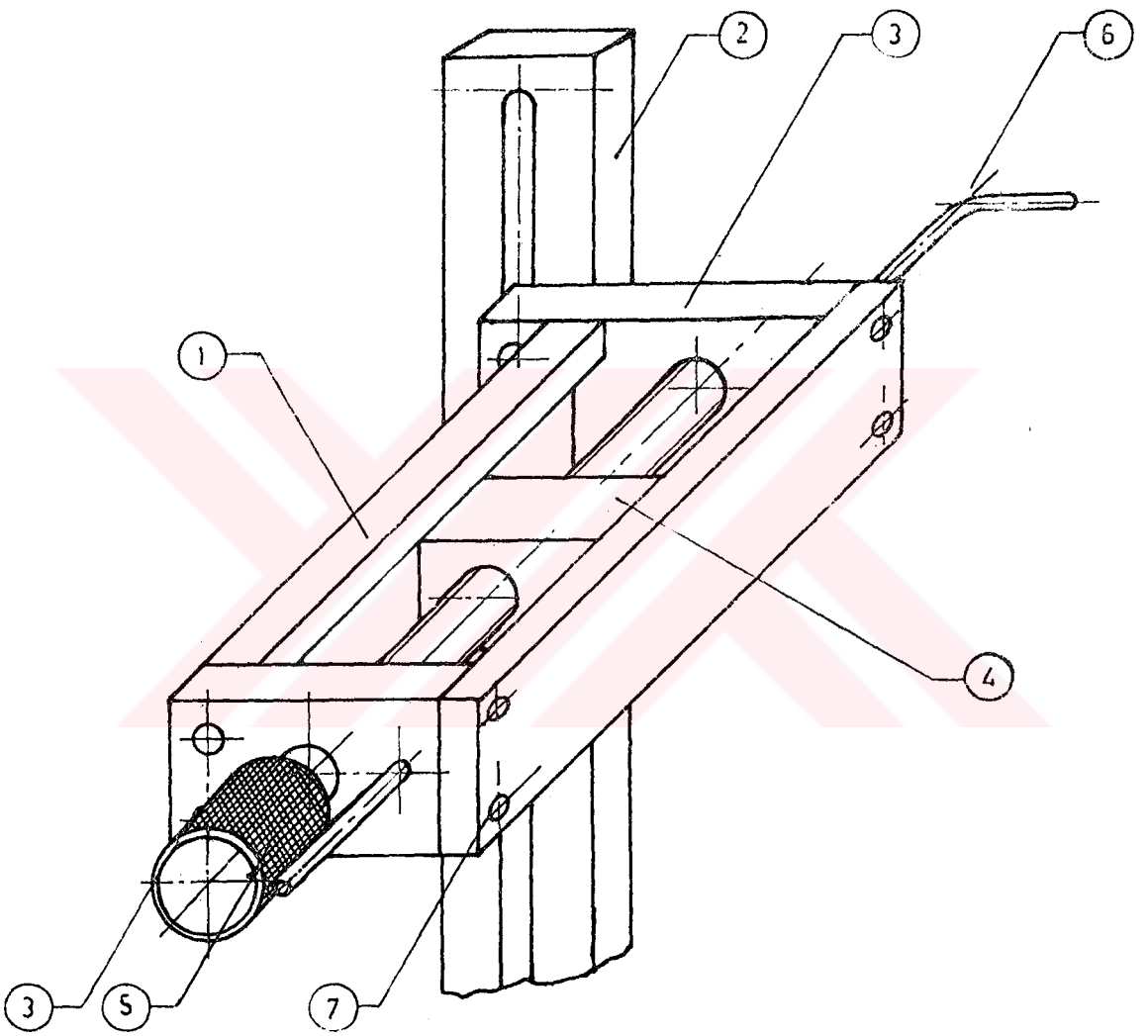

Assembly Drawing	Scale	Drawing No
Pitot traversing mechanism	1/1	117

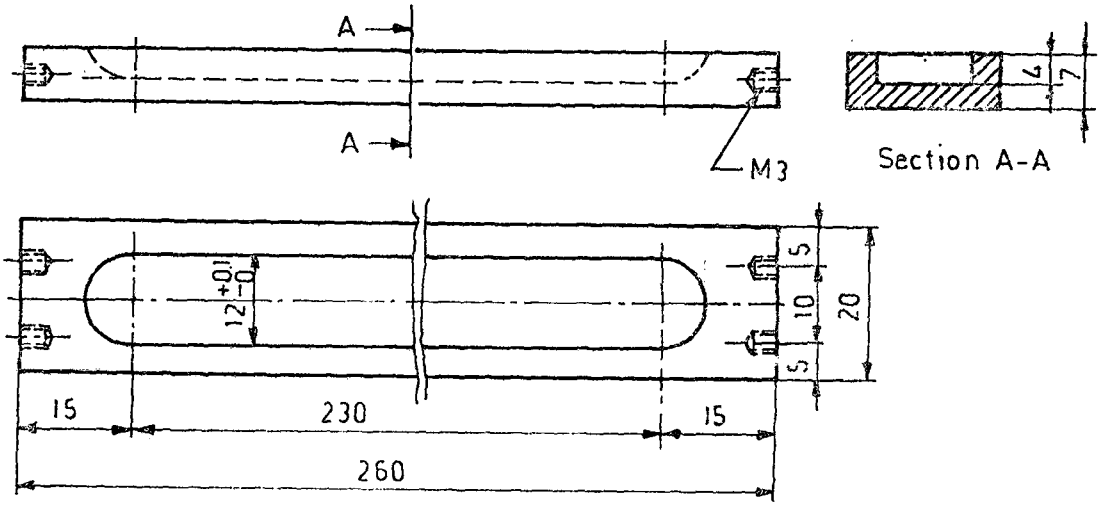
A
A
M3
Section A-A
4
7
12 +0.1 -0
5
10
5
20
15
230
15
260

①

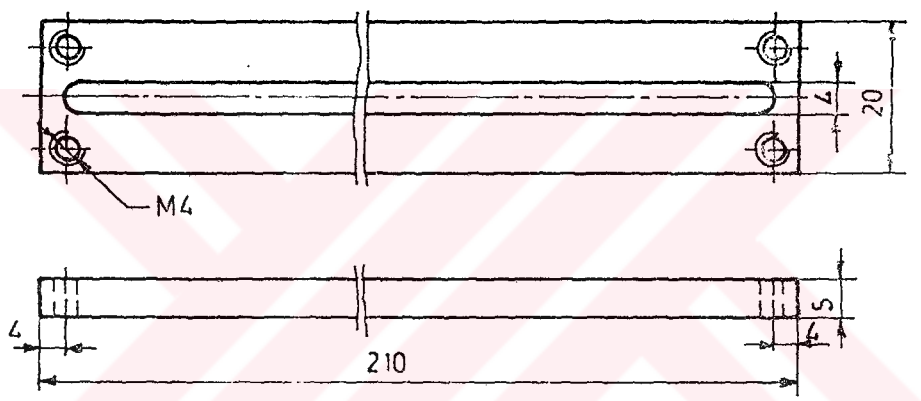
4
20
M4
5
4
4
210

②

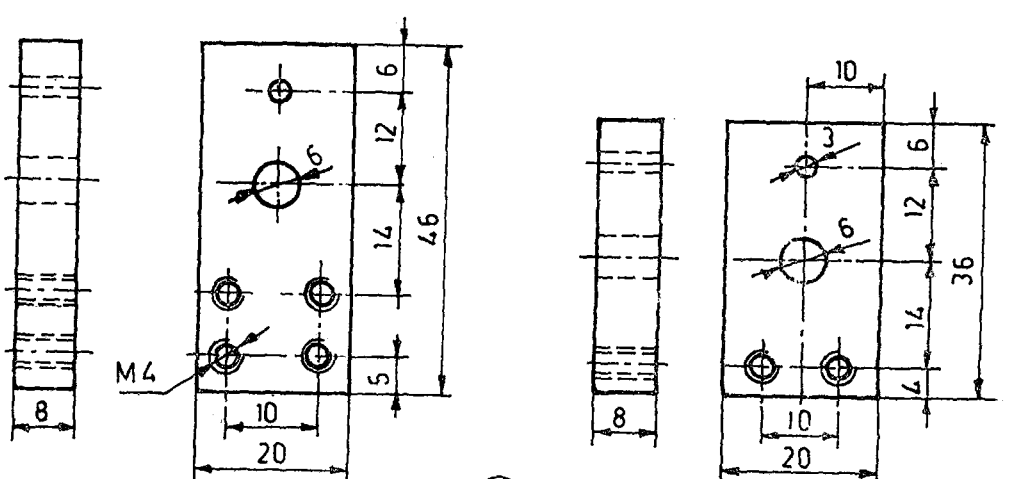
6
12
14
46
5
M4
10
20
8
10
6
12
14
36
4
10
20
8

③

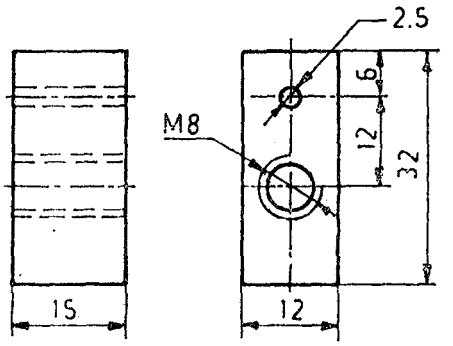

④

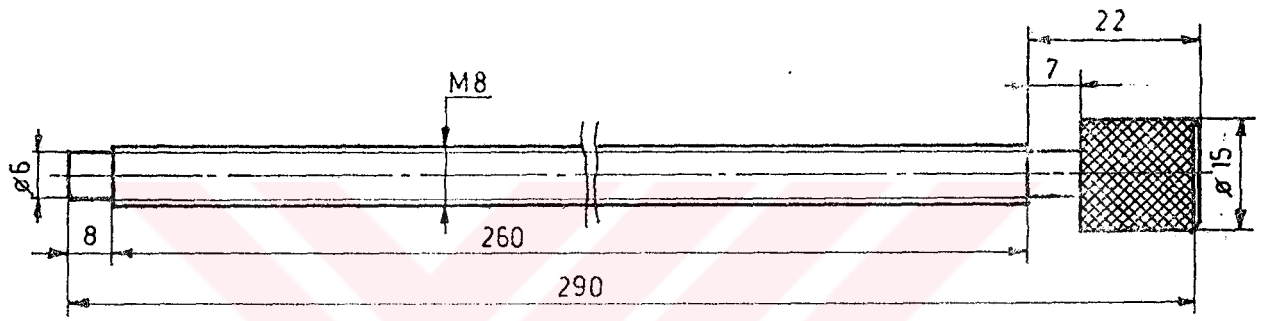

⑤

PITOT COMB TRAVERSING MECHANISM				Drawing No 118
Part No	Part Name	Material	Quantity	Scale
1	Wall tapping 1	Brass	1	1/1
2	Wall tapping 2	Brass	1	1/1
3	Comb carier	Brass	1	1/1
4	Connecting part	Brass plate	1	1/1
5	Pitot comb	Copper	1	1/1
6	Traversing rod	Steel	1	1/1
7	Fixing stud	Steel	2	1/1

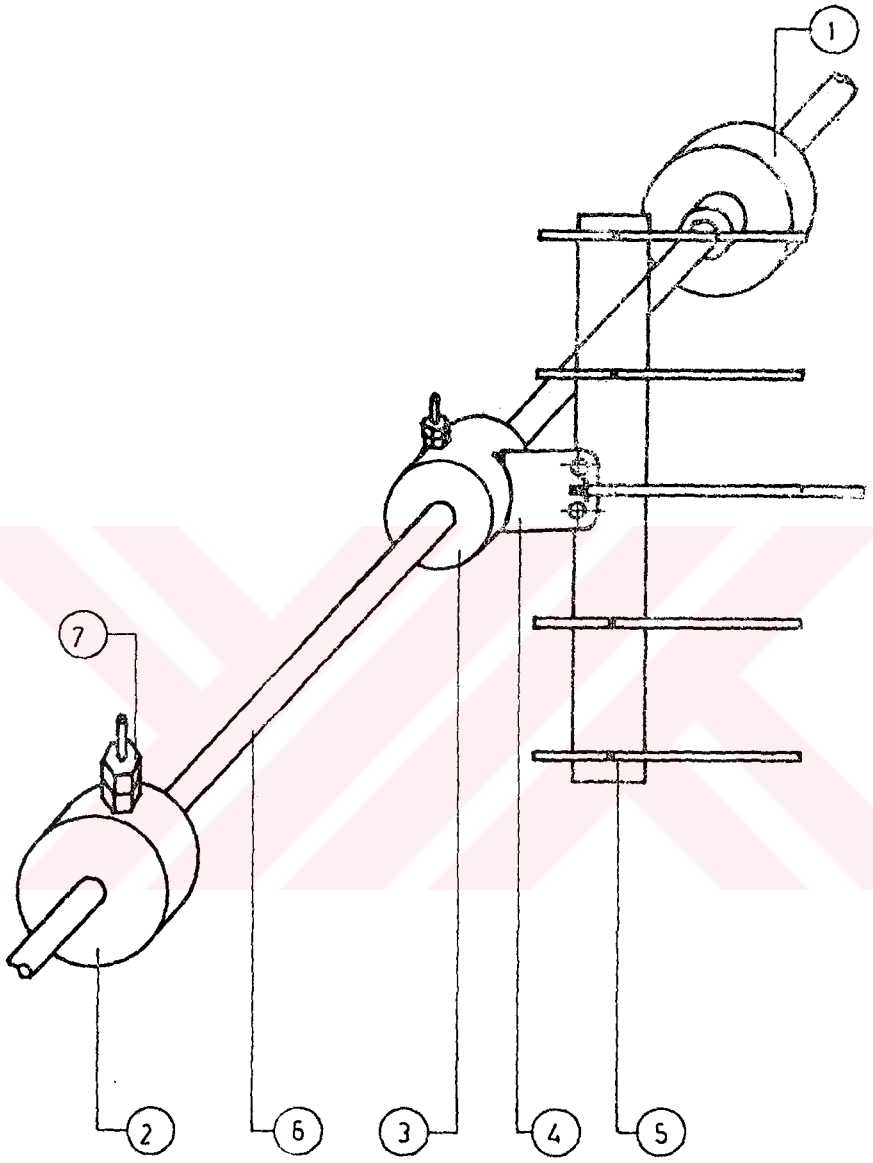

Assembly Drawing	Scale	DrawingNo
Pitot comb traversing mechanism	1/2	118

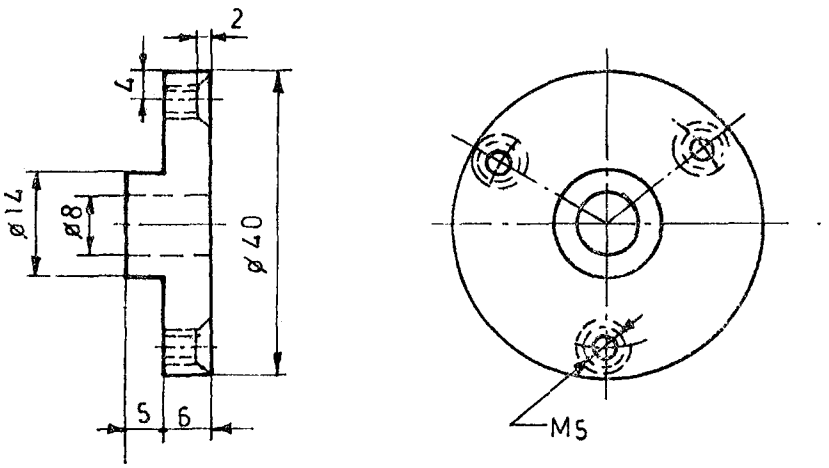

①

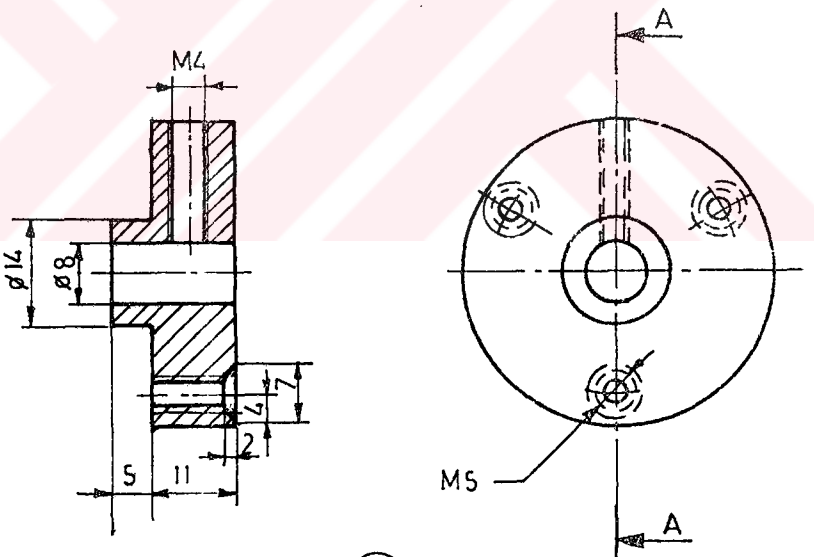

②

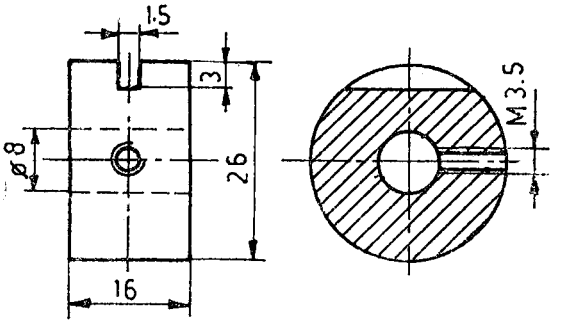

(3)

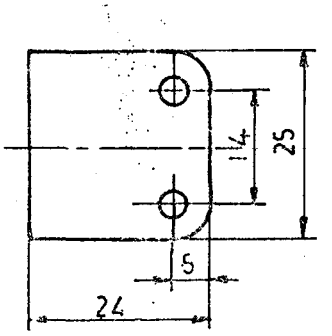

(4)

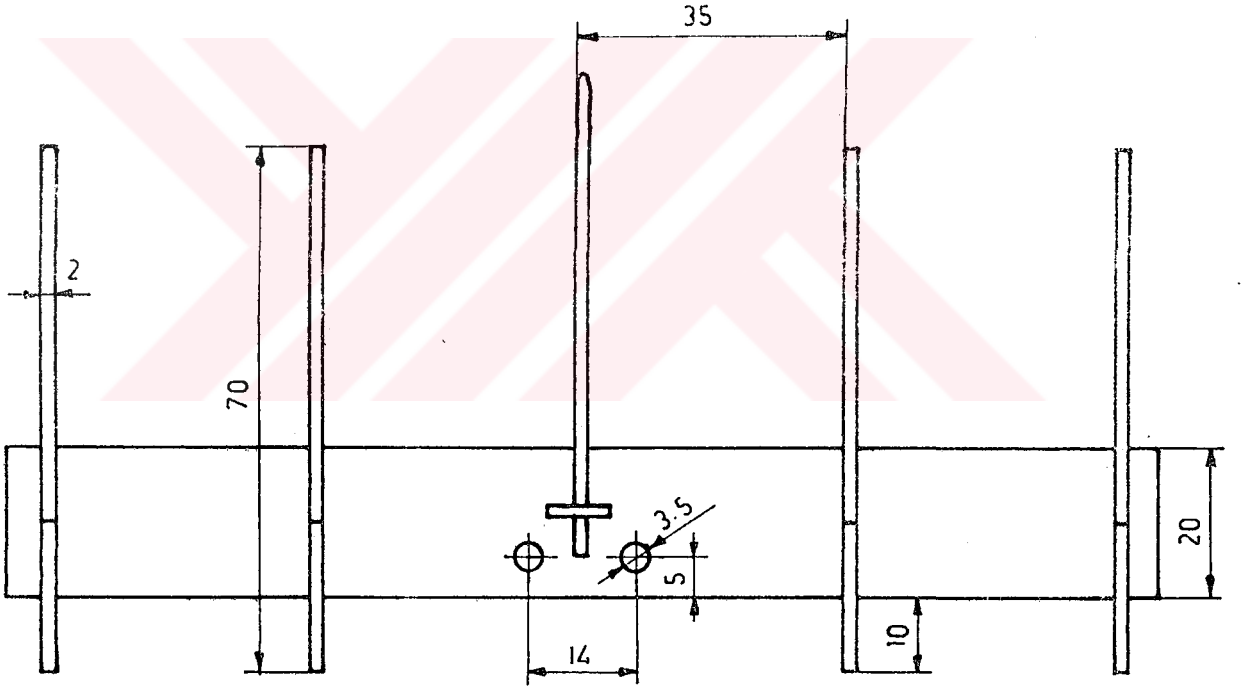

Thickness : 1.5

(5)

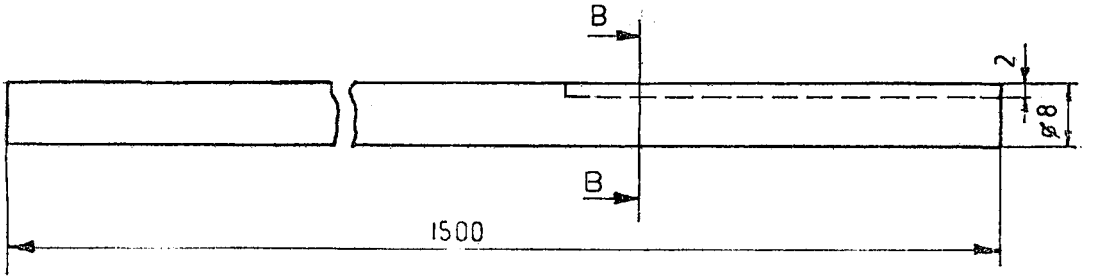

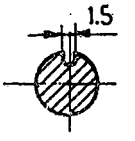

Section B-B

(6)